공학박사학위논문

Design and Analysis of Lattice-Tunable Phononic Crystals for Broadband Acoustic Stopband Control

광대역 주파수 차단을 제어하기 위한
격자 조율형 포노닉 크리스탈의 설계와 해석

2014년 2월

서울대학교 대학원

기계항공공학부

유 성 민

광대역 주파수 차단을 제어하기 위한 격자 조율형 포노닉 크리스탈의 설계와 해석

Design and Analysis of Lattice-Tunable Phononic Crystals for Broadband Acoustic Stopband Control

지도교수 김 윤 영

이 논문을 공학박사 학위논문으로 제출함

2013 년 11 월

서울대학교 대학원

기계항공공학부

유 성 민

유성민의 공학박사 학위논문을 인준함

2013 년 12 월

위 원 장 : 강 연 준

부위원장 : 김 윤 영

위 원 : 신 상 준

위 원 : 김 진 오

위 원 : 이 중 석

Abstract

Design and Analysis of Lattice-Tunable Phononic Crystals for Broadband Acoustic Stopband Control

Sungmin Yoo
School of Mechanical and Aerospace Engineering
The Graduate School
Seoul National University

A new type of tunable phononic crystals is proposed. The proposed phononic crystals can form acoustic stopbands of a wide frequency range by using two different physical phenomena of the Brag gap and local resonances. Since the frequency band of the stopband is inversely proportional to the lattice size, a method to increase the lattice size up to by a factor of 2 is proposed, covering quite low frequency range. To make a tunable stopband below the Bragg gap without increase in overall crystals size, the concept of an acoustically-resonant phononic crystal system is used, which utilize acoustic resonances. The system resembles a Helmholtz resonator so that the resulting stopband is independent of the lattice periodicity of the phononic crystal system. The finite element simulations for two-dimensional infinite and finite periodic structures are carried out to investigate various dynamic characteristics of the proposed tunable phononic crystals. The transmission analysis with finite periodic structures is used to investigate wave stop phenomena that may not be seen directly from their dispersion diagrams.

Individual stopbands of phononic crystals may not be sufficiently wide to cover a large frequency range and also passbands between stopbands are inevitable even if a wide frequency range is realized by stopband tuning. This physical restriction may be avoided if a finite periodic or semi-periodic phononic crystal structure is properly engineered. The proposed finite phononic crystal structure can be constructed either by tuning the structure as a whole or finding the proper configurations of each of the unit cell forming the structure separately by an iterative optimization algorithm. By these two methods, a large frequency range of stopped or significantly-reduced transmission is realized. All these findings are confirmed by a number of numerical simulations.

Key words: Tunable Phononic Crystals, Broadband Frequency, Stopband Control, Resonance Gap, Structure Design

Student Number: 2008-30860

Table of contents

List of Tables

List of Figures

Chapter 1.

Introduction

1.1 Motivation

Life in modern civilization is sieged by so many noise generated from various engineered machineries. In general, vibrations originated from machineries are converted to acoustic waveform and it is transferred through the air and then finally stimulates hearing organs of living things. The fact that exposure to noise in long term causes bad influences not only to physical health organs but also to psychological health have been studied so far and settled as a common sense. An environment of low-level noise would give us huge benefits of health and working productivity. Responding to unwanted noise, many efforts and researches to avoid noise have been carried out. One major way is to reduce generating noise from the origin of vibration. Another way is to apply physical treatment to propagating wave, such as attenuation of acoustic waves by viscosity and fraction or physical isolation of propagating waves. Recently noise cancellation is also spotlighted as an attenuation method. Using porous material or noise cancellation provides fine noise attenuation but traditional noise barrier is more appropriate to large-scale outdoor noise because of the cost problem. For evidence, we can easily observe many noise barrier structures in our urban life especially near the traffic site. Although its goodness, a conventional noise barrier prevents not only acoustic wave propagation but also other physical transfers such as optical light, air flow and mass transfers. It also has natural restriction that preventable frequency of acoustic wave is strongly determined by its material property—attenuation for a

low frequency acoustic wave demands massive structure than high frequency, which is a consequence of the mass density law.

Along the few decades recently, phononic crystals have received growing spotlights as an alternative noise barrier that is capable to overcome conventional one. Phononic crystals usually mean a structure that higher impedance materials, so-called inclusion or scatterer, are embedded periodically in the host material. The periodicity of inclusions makes phononic crystals pretending a homogeneous material for specific and finite frequency range, which is determined by dimensions of the periodicity mainly. A system that metal cylindrical rods are periodically arranged in the air is a typical example of phononic crystals for acoustic system. Using this simple acoustic structure, it is proved numerically and experimentally that phononic crystals has a capability to attenuation noise successfully[1,2]. The periodically arranged inclusions develop sound attenuation as a result of the destructive interference of the scattered acoustic wave by these obstacles[2], which is so-called bandgap or stopband. Kushwaha *et al.* [3,4] introduced the presence and characteristics of the acoustic bandgap in early time and Pennec *et al.* [5] synthesized about phononic crystals elaborately. Some particular phenomena originated from the bandgap were also studied such as excitation of evanescent waves[6-8] and localization of waves[9,10]. Applications utilizing bandgap are proposed for wave-guides[10-15] and filters[16].

A major advantage of phononic crystals as a noise barrier rather than the traditional one is that frequency of the stopband can be controlled by tailoring the distance between the inclusions, lattice size or constant. It represents that the restriction originated from material property for the traditional problems can be overcome by design of phononic crystals structure. Another major advantage is ability to flow air, light and transfer matter because acoustic phononic crystals are basically based on the assumption that inclusions are embedded in fluidic matters. Additional merit of the phononic crystals is that it has possibility to sublimate noise barrier into sculpture[17] or interior decoration. Traditional phononic crystals

however, have also own major disadvantage that stopband is over a narrow frequency band and the extremely large barrier will be required to attenuate low frequency noise considering relationship between the lattice size and operating frequency band. To complement this limitation, locally resonance sonic material, or phononic crystal was originated[18] due to their ability to form additional stopband decoupled from the periodicity. However, these stopbands cover a narrow attenuation range and the locally resonance phononic crystals is not suitable for use alone as a barrier for broadband noise. Therefore, utilizing both stopbands from the periodicity and local resonance is desirable to the noise barrier at the same time.

Considering usefulness of the bandgap, there is no doubt that enlarging bandgap have become an interesting research branch in phononic crystals. Since the bandgap exists for narrow range, it is desirable that bandgap is as wide as possible for noise barrier. Some researchers approached from concept of the crystal symmetry, which is came from crystallography, to find a way to enlarge bandgap theoretically[19-21]. According to them, reducing the lattice symmetry can enlarge bandgap, and moreover new gaps can be created. They added additional scatterers between existing scatterers to decrease the lattice symmetry by various methods. Wang *et al.*[22] investigated relation between shape, including angle, of the scatterers and that of the lattice. The result said that width of the bandgap is maximized when the symmetry of each scatterer is identical to the first Brillouin zone of the lattice; e.g., square scatterers in square lattices. This fact gives us very important and basic insight to enlarge the bandgap. Goffaux *et al.*[23] also showed that correlation between the angle of the square inclusion and the bandgap. According to the reference, increasing the rotational angle of the square rods with respect to lattice orientation enlarges bandgap. Meanwhile, the research also presented basic tuning concept for bandgap and recent work[15] that inherited this concept not only verified experimentally but also utilized to tunable acoustic waveguide. Another large branch on enlarging bandgap is design of the scatterer. Many researchers imported optimization techniques to design inclusions to

improve the bandgap[24-28]. Sigmund *et al.*[25] introduced systematic design procedure using topology optimization using gradient based updating algorithm in early times. Halkjær *et al.*[26] designed periodic plate structure that maximizes bandgap for bending waves in a Mindlin plate using topology optimization and they also verified their design experimentally. Optimization using topological generic algorithm was carried out theoretically by Bilal *et al.*[27]. They presented several optimized unit-cell layouts for bandgap considering out-of-plane, in-plane and combined out-of-plane and in-plane elastic wave propagation.

In many researches introduced so far, the branch of phononic crystal is deeply studied and many researchers have improved its narrowness of the bandgap or enlarged its tunability. Their works, however, carried out upon assumption of fixed lattice, which is the most influential determinant for the stopband. Once a lattice size is fixed, frequency band of the stopband will be determined according to its dimension. Some works[29-31] have been studied deformation of lattice for a new tunable method. Kim et al.[31] attained lattice perturbation by shear deformation of whole structure. They showed significant change of the bandgap in spite of little change of the periodicity. Elongation of lattice size was tried by two different approaches. Park et al. [30] stretched the whole structure and lattice size was regulated as a consequence of longitudinal deformation of both host material and inclusions. Although their excellent results, these two methods have common problem—basically deformable range is restricted by host material. Meanwhile, Cicek et al.[29] realized uniaxial elongation of periodicity using adjustment of intervals between inclusions. They tested various type of adjustment and reported tunable characteristics. This method is relatively free from the restriction that mentioned above. However, increase of the intervals inevitably causes elongation of the whole structure, so the intervals cannot be freely elongated. Unless huge change of the periodicity, tunable range of the bandgap will be restricted in convectional level determined by its lattice size.

Meanwhile, there are also many efforts to investigate locally resonant

phononic crystals to overcome physical limitation of pure bandgap, the Bragg gap, originated from periodicity of the scatterers. In general, frequency of stopband from local resonance is independent to the scatterer's interval but follows geometries of the scatterer itself due to the Helmholtz resonance and standing wave's cavity mode. Therefore, low-frequency bandgap—lower than the lowest Bragg gap can be realized by resonant structure of the inclusion, which is so-called locally resonant phononic crystals (LRPC). Many researches report that one-dimensional phononic crystals containing structure like Helmholtz resonator[32-34]. And also Hu *et al.* presented two-dimensional LRPC whose inclusion is C-shaped acting Helmholtz resonator [35]. Wang *et al.* [33] and Hu *at al.*[35] showed dispersion relation of the one-dimensional and two-dimensional LRPC, respectively. Chalmers et al. presented numerical and experimental verification of C-shaped LRPC mentioned theoretically by Hu et al.[36]. Another variation of the C-shaped LRPC was proposed and investigated by Cui et al. [37], which has multiple slit comparing the original C-shaped. Elford *et al.* proposed a new multiple coaxial C-shaped resonant sonic crystals. Multiple C-shaped scatterers in different sizes are embedded sequentially in the bigger scatterer and their slits are opened to the same direction. These multiple cavities resonate at different frequencies, and then consequentially, multiple additional stopbands are formed under the first Bragg gap. Romero-García *et al.* [38] used porous material as a C-shaped scatterer to design a tunable wideband bandgap acoustic filter. After two years later with two additional authors, they considered effects of elastic resonance of the horseshoe-shaped scatterer acting a cavity to resonant to find additional bandgap. Most recently, Li et al. investigated 2D and 3D dual-orifice resonant phononic crystals[39]. Two orifices for the resonator are both connected to the same central cavity symmetrically; Stopband of the proposed phononic crystals is $\sqrt{2}$ times higher than the single-orifice, convectional, resonant phononic crystals. Hou proposed ingenious type of scatterer[40]. He showed combination of I-beam-shaped scatterers makes resonant cavity and verified sensitive relation between

resonant bandgap and geometric parameters of scatterer theoretically. This gives us very fresh intuition that well-designed scatterer can create resonant cavity even if the unit scatterer itself is not a cavity-like shape.

As mentioned in the literature review, the locally resonance phononic crystals deserve spotlight and sufficiently qualified for alternative stopband. However, it has own disadvantages such as narrowness and isolation from the Bragg gap. To maximize benefits of the phononic crystals as a noise barrier, synergy between the two different stopbands must be considered. Nevertheless, there has been a tendency to consider them separately.

Considering literature studies previously discussed in this chapter, the aim of this thesis can be summarized as follows

1. Breakthrough the tunable stopband limitation as a consequence of lattice periodicity
2. Consider the synergy of two different stopbands—originated from periodicity and resonance, respectively.
3. Realize engineered phononic crystal structure whose stopband is extremely broad comparing to the convectional phononic crystals

To achieve above claims, this thesis will propose a new tunable phononic crystals and investigate acoustical features of this new phononic crystals. Chapter 2 of this thesis gives basic theories and analysis tools for understanding the phononic crystals and further chapters. Numerical methods are presented for the analysis of both infinite and finite models of 2D periodic structure. Chapter 3 introduces the concept of locally resonant phononic crystals and identifies its acoustic features using both analytic and numerical methods. Chapter 4 details new tunable phononic crystals and presents acoustic information obtained by all possible tools discussed in chapter 2 and 3. Reaching the chapter 4, it is possible to claim that the 1st and 2nd aims are accomplished. Chapter 5 discusses the design method for the engineered phononic crystal structure to attain 3rd aim. Two different methods originated from different perspective are prepared to solve the broadband noise.

The first method is utilizing all information obtained until the chapter 5. The second method is based on iterative optimization algorithm and useful to extremely wide band of noise rather than the first method.

Chapter 2.

Phononic Crystals

2.1 Overview

Phononic Crystals (PCs) are infinitely periodic structures consist of host material and inclusions whose mechanical properties are different to each other. Mechanical waves propagate mostly along the host material and are scattered by inclusions. Repetition of inclusions makes sound attenuation effects as a consequence of the destructive interference of the scattered waves. This well-known blocking effect is so-called Bragg gap or bandgap. In acoustics, frequency band of Bragg gap is influenced mainly by material properties of host, which determines wave speed, and periodicity of inclusions. If the wave speed and the periodicity are known, relatively exact position of Bragg gap in frequency will be obtained, and vice versa. This is main advantage of PCs.

In this chapter, the first recalls basic theories of classic acoustics because this thesis deals acoustic PCs. The chapter continues introducing some fundamental concepts to analysis periodic structures such as reciprocal lattice, Brillouin zones. Then, numerical analysis of single unit cell is carried out by finite element method (FEM) compatible to infinitely periodic structure. Finally, methods and results for calculating power transmission through the PCs structure are provided to verify whether single unit cell applied periodic condition can represent entire infinitely periodic structure.

2.2 Acoustic Waves in Homogeneous Fluid Materials

Before discussing about acoustic waves in periodic structure, it is necessary to remind basic acoustics theories. An acoustic wave may be defined as vibrational waves in which a physical quantity (*e.g.*, energy or pressure) propagates in a host fluid (*e.g.*, air or water), without net transport of the fluid. As the molecules of a fluid are displaced from their equilibrium state, internal elastic force causes, which is restoring force to enable vibrations that transmit acoustic waves. In general, pressure oscillation by external excitation breaks the equilibrium state of the molecules, then it makes acoustic waves may propagate passing pressure on to the next molecules. Therefore, it is possible to describe acoustic wave as small fluctuation of pressure *p(x, t)* in a compressible ideal fluid. Three major equations are applied to model the acoustic wave for pressure-wise, which are the equation of state, the equation of continuity and the equation of motion (Euler's equation). Finally the linear wave equation in terms of pressure is derived as a Helmholtz equation form.

2.2.1 Equation of State

According to reference[41], the isentropic relation between the total pressure P and the instantaneous density ρ under the adiabatic condition can be described

$$P = P_0 + \left(\frac{\partial P}{\partial \rho}\right)_{\rho_0} (\rho - \rho_0) + \frac{1}{2}\left(\frac{\partial^2 P}{\partial \rho^2}\right)_{\rho_0} (\rho - \rho_0)^2 + \cdots \tag{2.1}$$

where P_0 and ρ_0 are mean pressure and mean density of equilibrium state, respectively.

If the fluctuations are very small, equation (2.1) can be linearized

$$P - P_0 \approx \left(\frac{\partial P}{\partial \rho}\right)_{\rho_0} (\rho - \rho_0) \tag{2.2}$$

By applying the adiabatic bulk modulus B,

$$B = \rho_0 \left(\partial P / \partial \rho \right)_{\rho_0} \tag{2.3}$$

Equation (2.2) can be rewritten as

$$P - P_0 \approx B\left(\rho - \rho_0 \right) / \rho_0 \tag{2.4}$$

Practical pressure generating the acoustic waves is pressure difference from equilibrium pressure. Using the acoustic pressure p, difference between the total pressure and the equilibrium pressure, is profitable to describe acoustic wave equation. The acoustic pressure p can be defined as

$$p = P - P_0 \tag{2.5}$$

and condensation s is also useful to simplify acoustic equations in after works.

$$s = \frac{\rho}{\rho_0} - 1 \tag{2.6}$$

As a result of above, instantaneous density rho can be represented as

$$\rho = \rho_0 \left(1 + s \right) \tag{2.7}$$

Now, equation (2.4) is rearranged simply using the acoustic pressure and condensation as

$$p \approx Bs \tag{2.8}$$

2.2.2 Equation of Continuity

To relate the motion of fluid with its fluctuation, a functional connection between particle velocity $\vec{u}$ and the density ρ is necessary. The law of mass conservation is very useful to derive the equation of continuity. It states that the net rate of mass flow into the volume through its surface is must equal to the rate of mass increasing within the volume. Referring to Figure 2.1, the net flux of mass into the infinitesimal control volume resulting from flow in the x direction can be written as

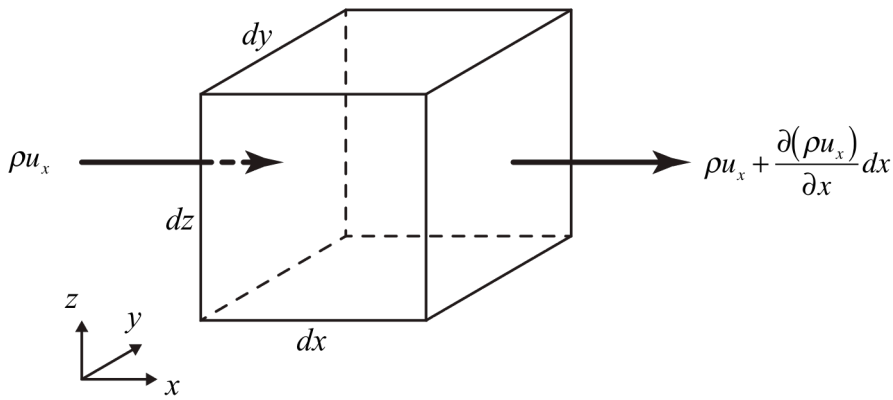

Figure 2.1 An element spatially fixed volume of fluid showing the rate of mass flow into and out of the volume resulting from fluid flowing in the *x* direction.

$$\left[\rho u_x - \left(\rho u_x + \frac{\partial(\rho u_x)}{\partial x} dx\right)\right] dydz = -\frac{\partial(\rho u_x)}{\partial x} dV \tag{2.9}$$

Likewise for the *y* and *z* direction,

$$\left[\rho u_y - \left(\rho u_y + \frac{\partial(\rho u_y)}{\partial y} dy\right)\right] dxdz = -\frac{\partial(\rho u_y)}{\partial y} dV \tag{2.10}$$

$$\left[\rho u_z - \left(\rho u_z + \frac{\partial(\rho u_z)}{\partial z} dz\right)\right] dxdy = -\frac{\partial(\rho u_z)}{\partial z} dV \tag{2.11}$$

where u_x, u_y and u_z are each directional velocity component in velocity vector $\vec{u}$, respectively, and infinitesimal volume $dV = dx \cdot dy \cdot dz$.

Equations from (2.9) to (2.11) can be gathered as the total influx and rewritten for vector form,

$$-\left[\frac{\partial(\rho u_x)}{\partial x} + \frac{\partial(\rho u_y)}{\partial y} + \frac{\partial(\rho u_z)}{\partial z}\right] dV = -\nabla \cdot \left(\rho \vec{u}\right) dV \tag{2.12}$$

The rate of mass increasing within the volume can be represented as density

change by time, $(\partial\rho/\partial t)dV$. And it must be equal to the total net influx,

$$\frac{\partial \rho}{\partial t} + \nabla \cdot \left(\rho \vec{u}\right) = 0 \tag{2.13}$$

wherein the gradient symbol represents

$$\nabla = \vec{i}\frac{\partial}{\partial x} + \vec{j}\frac{\partial}{\partial y} + \vec{k}\frac{\partial}{\partial z}$$

Equation (2.13) is well known the equation of continuity. It represents relation of two acoustic parameters, density and velocity, with time successfully. It can be simplified using equation (2.7) as

$$\rho_0 \frac{\partial s}{\partial t} + \nabla \cdot \left(\rho_0 \vec{u}\right) = 0 \tag{2.14}$$

wherein equilibrium density ρ_0 is not function of time and space, then it becomes

$$\frac{\partial s}{\partial t} + \nabla \cdot \vec{u} = 0 \tag{2.15}$$

the simplified linear continuity equation.

2.2.3 Equation of Motion

The last equation is relation between force by pressure and mass of fluid, which comes from Newton's second law. The motion of fluid element *dV* containing a mass *dm* will be accelerated by net force $d\vec{f}$, which satisfies Newton's second law as $d\vec{f} = (dm)\vec{a}$. The net force applying to normal plane resulting from pressure in the *x* direction can be written as

$$df_x = \left[P - \left(P + \frac{\partial P}{\partial x}dx\right)\right]dydz = -\frac{\partial P}{\partial x}dV \tag{2.16}$$

Same manner to other directions,

$$df_y = \left[P - \left(P + \frac{\partial P}{\partial y} dy \right) \right] dxdz = -\frac{\partial P}{\partial y} dV \tag{2.17}$$

$$df_z = \left[P - \left(P + \frac{\partial P}{\partial z} dz \right) \right] dxdy = -\frac{\partial P}{\partial z} dV \tag{2.18}$$

Combination of these forces neglecting gravitational force can be derived in vector form.

$$d\vec{f} = -\nabla P dV \tag{2.19}$$

Next step is obtaining an appropriate expression for the acceleration of the fluid element. According to reference [41], the acceleration is

$$\vec{a} = \lim_{dt \to 0} \frac{\vec{u}\left(x + u_x dt, y + u_y dt, z + u_z dt, t + dt\right) - \vec{u}\left(x, y, z, t\right)}{dt} \tag{2.20}$$

or

$$\vec{a} = \frac{\partial \vec{u}}{\partial t} + u_x \frac{\partial \vec{u}}{\partial x} + u_y \frac{\partial \vec{u}}{\partial x} + u_z \frac{\partial \vec{u}}{\partial x} \tag{2.21}$$

simplifying as vector form,

$$\vec{a} = \frac{\partial \vec{u}}{\partial t} + \left(\vec{u} \cdot \nabla\right)\vec{u} \tag{2.22}$$

where

$$\left(\vec{u} \cdot \nabla\right)\vec{u} \equiv u_x \frac{\partial}{\partial x} + u_y \frac{\partial}{\partial x} + u_z \frac{\partial}{\partial x}$$

Inserting the mass dm of the element, ρdV, to Newton's second law, $d\vec{f} = \left(dm\right)\vec{a}$ results

$$-\nabla P = \rho \left[\frac{\partial \vec{u}}{\partial t} + \left(\vec{u} \cdot \nabla\right)\vec{u} \right] \tag{2.23}$$

This is nonlinear Euler's equation of inviscid motion. Since particle speeds are typically of the order of 10^{-3} m s^{-1}, the second nonlinear term of the right hand side,

$\left(\vec{u}\cdot\nabla\right)\vec{u}$, can be neglected[41]. However, it may no be neglected in models of turbulent fluid dynamics noise sources such as jet engine exhausts.

Applying assumption of linearity to equation (2.15),

$$-\nabla P = \rho\frac{\partial\vec{u}}{\partial t} \tag{2.24}$$

the linear Euler's equation is derived, which valid for acoustic processes of small amplitude of motion.

2.2.4 Linear Wave Equation

The linearized equations (2.2), (2.7) and (2.16) can be combined to derive a single differential equation with respect to one dependent variable, pressure *p*. This is achieved by first applying the divergence to the linearized Euler equation (2.24) as

$$-\nabla^2 P = \nabla\cdot\left(\rho\frac{\partial\vec{u}}{\partial t}\right) \tag{2.25}$$

where $\nabla^2 \equiv \nabla\cdot\nabla$ is the Laplacian. Gradient $\nabla^2 P$ can be replaced by $\nabla^2 p$ because P_0 is weak function of space. And replacing ρ to ρ_0,

$$-\nabla^2 p = \nabla\cdot\left(\rho_0\frac{\partial\vec{u}}{\partial t}\right) \tag{2.26}$$

Substituting time differentiation of equation (2.14) to equation (2.26) becomes

$$\nabla^2 p - \rho_0\frac{\partial^2 s}{\partial t^2} = 0 \tag{2.27}$$

Since condensation *s* can be replaced as p/B from equation (2.8), finally the linear wave equation is derived as follow with thermodynamics speed of wave defined as $c^2 = B/\rho_0$.

$$\nabla^2 p - \frac{1}{c^2}\frac{\partial^2 p}{\partial t^2} = 0 \tag{2.28}$$

A time harmonic plane sound pressure field may be defined as

$$p = |\tilde{p}| e^{i(\omega t - \vec{k}\cdot\vec{r})} = \tilde{p} e^{i\omega t} \tag{2.29}$$

where $\tilde{p}$ is spatial distribution of complex amplitude of pressure, ω is angular frequency, $\vec{k}$ is the propagating vector and $\vec{r}$ is a position vector.

Substituting equation (2.29) to equation (2.28),

$$\nabla^2 \tilde{p} + (\omega/c)^2 \tilde{p} = 0 \tag{2.30}$$

the typical Helmholtz equation is derived finally. This equation is very useful because the equation is the partial differential equation with respect to spatial pressure amplitude only.

2.3 Finite Element Method for Acoustic System

The Finite Element Method (FEM) is a numerical technique to find approximate solutions for differential equations that describe a wide range of physical field problems. FEM starts from a basic concept that assemblage of many analytically describable simple elements can describe complex structure even if the structure is too complex to solve analytically. FEM discretizes arbitrary and continuous geometry into small but many elementary shapes such as triangle, rectangle and square of which govern equation is well known analytically. As the govern equation of the acoustic system is typical differential equation, Equation (2.28), the FEM is appropriate to obtain pressure field or eigen-mode/eigen-frequency of complicated phononic crystal structure including the unit-cell. Unlike the multiple-scattering method (MST) and the plain wave expansion (PWE), the FEM gives easy and systematic analysis for complicated shape of scatterer with varying geometry.

The govern equation for acoustic system, Equation (2.28), is applied to the

subdomain of each single element. In FEM formulation, all values such as pressure are dealt explicitly and discretely at nodes only and shape function approximates continuous pressure values inside the element for solving differential equation by using member node's value[42].

Acoustic system is to be considered in a volume V and its surrounding surface S. A functional for an acoustic system having uniform mass density can be written as,

$$\Pi = \int \left(\frac{p_{,x}^2 + p_{,y}^2 + p_{,z}^2}{2} + \frac{1}{c^2} p\ddot{p} \right) dV + \rho \int \ddot{u}_n p \, dS \tag{2.31}$$

In FEM formulation as mentioned before, pressure p within an element is interpolated by shape function, [**N**], and element degree of freedom, nodal pressure $\{\mathbf{P}_e\}$, as follow form.

$$p = [\mathbf{N}]\{\mathbf{P}_e\} \tag{2.32}$$

$$\ddot{p} = [\mathbf{N}]\{\ddot{\mathbf{P}}_e\} \tag{2.33}$$

Then pressure based mass, stiffness and load matrices for discretized element are formed respectively as

$$[\mathbf{M}] = \frac{1}{c^2} \sum \int [\mathbf{N}]^T [\mathbf{N}] dV \tag{2.34}$$

$$[\mathbf{K}] = \sum \int \left([\mathbf{N}_{,x}]^T [\mathbf{N}_{,x}] + [\mathbf{N}_{,y}]^T [\mathbf{N}_{,y}] + [\mathbf{N}_{,z}]^T [\mathbf{N}_{,z}] \right) dV \tag{2.35}$$

$$\{\mathbf{R}\} = \rho \sum \int [\mathbf{N}]^T \ddot{u}_n dS \tag{2.36}$$

Using Equations (2.34) to (2.36), the functional Equation (2.31) can be derived as matrix form:

$$\Pi = \{\mathbf{P}\}^T [\mathbf{M}]\{\ddot{\mathbf{P}}\} + \frac{1}{2}\{\mathbf{P}\}^T [\mathbf{K}]\{\mathbf{P}\} + \{\mathbf{P}\}^T \{\mathbf{R}\} \tag{2.37}$$

where $\{\mathbf{P}\}$ is the global nodal pressure. To finish FEM formulation, the stationary

condition $\{\partial\Pi/\partial\mathbf{P}\}=\{\mathbf{0}\}$ is applied to Equation (2.37) then

$$[\mathbf{M}]\{\ddot{\mathbf{P}}\}+[\mathbf{K}]\{\mathbf{P}\}=-\{\mathbf{R}\} \tag{2.38}$$

To obtain dispersion relation of the phononic crystals by FEM, eigen-frequency analysis is necessary. Eigen-frequency can be calculated under assumption that forcing matrix becomes zero and pressure becomes $p=\tilde{p}\sin\omega t$. After inserting $\{\mathbf{R}\}=\{\mathbf{0}\}$ and $\{\mathbf{P}\}=\{\tilde{\mathbf{P}}\}\sin\omega t$ into Equation (2.38), then the following FEM matrix formulation for eigen-frequency analysis can be obtained.

$$\left([\mathbf{K}]-\omega^2[\mathbf{M}]\right)\{\tilde{\mathbf{P}}\}=\{\mathbf{0}\} \tag{2.39}$$

Harmonic analysis for acoustic problem is not so much different from Equation (2.39). The only two differences are that unknown for harmonic analysis is $\{\tilde{\mathbf{P}}\}$ not ω and $\{\mathbf{R}\}\neq\{\mathbf{0}\}$.

There are two main different boundary conditions for acoustic FEM used in this thesis. One is the sound-hard boundary and another one is radiation boundary conditions. These two boundary conditions are used to simulate boundary between acoustic fluid and rigid and infinitely outgoing boundary without reflecting, respectively. Normal component of the particle velocity is vanished on a sound-hard boundary. For a zero dipole source, it can be written as Neumann condition form, which means that the normal derivative of the pressure at the boundary vanishes as

$$\frac{\partial p}{\partial n}=0 \tag{2.40}$$

And the radiation boundary condition for incoming plane wave, $p_i e^{-i\mathbf{k}\cdot\mathbf{r}}$, can be derived[43]:

$$\mathbf{n}\cdot\left(\frac{1}{\rho}\nabla p\right)+i\frac{k}{\rho}p+\frac{i}{2k}\Delta_{\mathrm{T}}p=\left(\frac{i}{2k}\Delta_{\mathrm{T}}p_i+\left(ik-i\left(\mathbf{k}\cdot\mathbf{n}\right)\right)\frac{p_i}{\rho}\right)e^{-i\left(\mathbf{k}\cdot\mathbf{r}\right)} \tag{2.41}$$

where n is the normal vector of the boundary. Vector k is defined as $\mathbf{k}=k\mathbf{n}$, where

$k = \omega/c$, and p_i is magnitude of incoming pressure. The Δ_T denotes the Laplace operator in the tangent plane at the particular point. If there is no incoming wave, Equation (2.41) can be simplified as

$$\mathbf{n} \cdot \left(\frac{1}{\rho} \nabla p \right) + i \frac{k}{\rho} p = 0 \tag{2.42}$$

then finally transformed as impedance matching boundary condition.

$$\mathbf{n} \cdot \left(\frac{1}{\rho} \nabla p \right) + \frac{i\omega p}{Z} = 0 \tag{2.43}$$

where acoustic impedance $Z = \rho c$ for analysis domain.

2.4 Acoustic Dispersion Diagram Construction

As mentioned from the beginning of this chapter, the phononic crystals structure is basically regarded infinitely periodic—inclusions are arranged infinitely. Analyzing the genuine infinite problem is not an efficient way to understand phononic crystals under perspective for wave propagation. The Brillouin zone can be useful way to solve this problem. The first Brillouin zone is a uniquely defined primitive cell in reciprocal lattice to represent whole infinite structure[44]. The Bloch wave description of waves in the Brillouin zone represents whole wave behaviors in the infinite structure. In other words, eigen-frequency analysis of a single unit-cell along its reciprocal vector is equivalent to the entire phononic crystal. Standard method is to find existing eigen-frequency corresponding to the Bloch wave-vector. Gathering of the information constructs dispersion diagram, which shows relation between wave-vector k and angular frequency ω. If some eigen-frequency exists for a Bloch wave-vector, it means that the acoustic wave of the eigen-frequency propagates as same direction as that wave-vector. On the contrary if there are no eigen-frequency for a Bloch wave-vector, it represents that

corresponding wave is not able to exist in the phononic crystal along that direction. That is so-called the bandgap or stopband.

Dispersion diagrams can also be obtained using the FEM and commercial FEM software COMSOL Multiphysics™ provides good solution for it. The unit cell, seen in Figure 2.2, is used as a FEM model to construct dispersion diagram. The structure is originally supposed to be infinite then unit-cell applied periodic boundary condition for the two directions x and y. By Floquet-Bloch theorem, the relation for the pressure distribution p for nodes on the boundary of the unit-cell can be expressed as

$$p\left(x+a_1+a_2\right)=p(x)\exp\left[i\left(k_x+k_y\right)\right] \tag{2.44}$$

where x is the position vector in the unit-cell, a_1 and a_2 are the basis vectors for the doubly periodic structure. The k_x and k_y are each directional component of the Bloch wave vector.

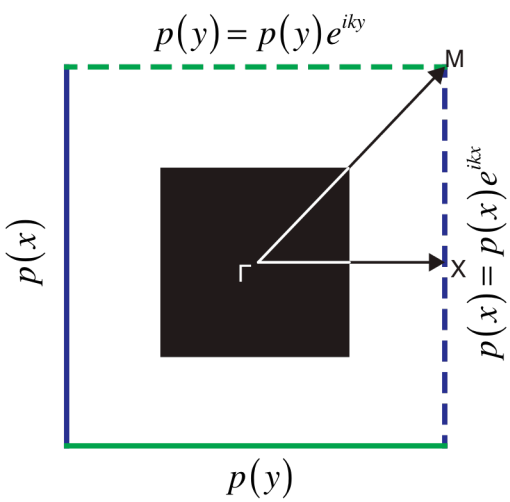

Figure 2.2 Single unit cell of an infinite phononic crystals with periodic boundary conditions.

Before apply periodic condition to the edge of the unit-cell, the sound hard boundary condition, Neumann boundary condition, must be applied to the edge

first. Because the inflow through one of the boundaries is as same as the outflow through the pair when the boundaries are periodic. The next step is applying phase relation to the pair boundary. This phase relation represents the wavenumber of the incident wave in the periodic structure. The pressure values at all edges of the analysis domain are relocated by the periodic boundary conditions to the pair edges. Three representative directions, principal symmetry directions, of the Bloch wave vector in the first Brillouin zone are ΓX, XM and ΓM. The each notation represents horizontal, vertical and diagonal incident wave, respectively. To obtain dispersion diagram, phase relation applied to the pair edge follows the next rules. For the ΓX direction, k_x varied from 0 to π, keeping k_y=0; XM direction k_y varied from 0 to π, keeping k_x=π; and in the ΓM direction k_x and k_y varied from 0 to π.

Now, an infinite phononic crystal composed of rigid square cylinder in air, with lattice parameter a, and size of the square scatterer is 0.5a×0.5a. All geometric parameters are described by lattice parameter, size, a, see Figure 2.2. Figure 2.3 shows the first ten bands for analysis model proposed in Figure 2.2. Frequency is normalized by $\omega a/2\pi c$, where ω is angular frequency and c is speed of sound, which is commonly used in phononic crystal branch.

The gray shaded area in Figure 2.3 indicates partial bandgap, or Bragg gap. Sequential naming for the stopband starts from bottom to upward in frequency axis. The lowest stopband calls the first Bragg gap, next is the second Bragg gap, and so on. Bragg gap is limited in ΓM direction; therefore it means that horizontally incident acoustic wave cannot propagate of which frequency is within the gray area. The dispersion remains linear trend $c = \omega/k$ in the low-frequency range. It means that the phononic crystal behaves like an isotropic homogenous material at that frequency band. The propagating wave cannot notice the small inclusion due to the long-wavelength limit. Meanwhile, dispersion curves in upper frequency band of the first Bragg gap are quite different to lower ones. Many interesting and particular phenomena such as zero group velocity and inverse group velocity occur in this region because wavelength of the incident wave is short enough to reveal

the scattering effects. These effects are subjects of another major research branches of the phononic crystals.

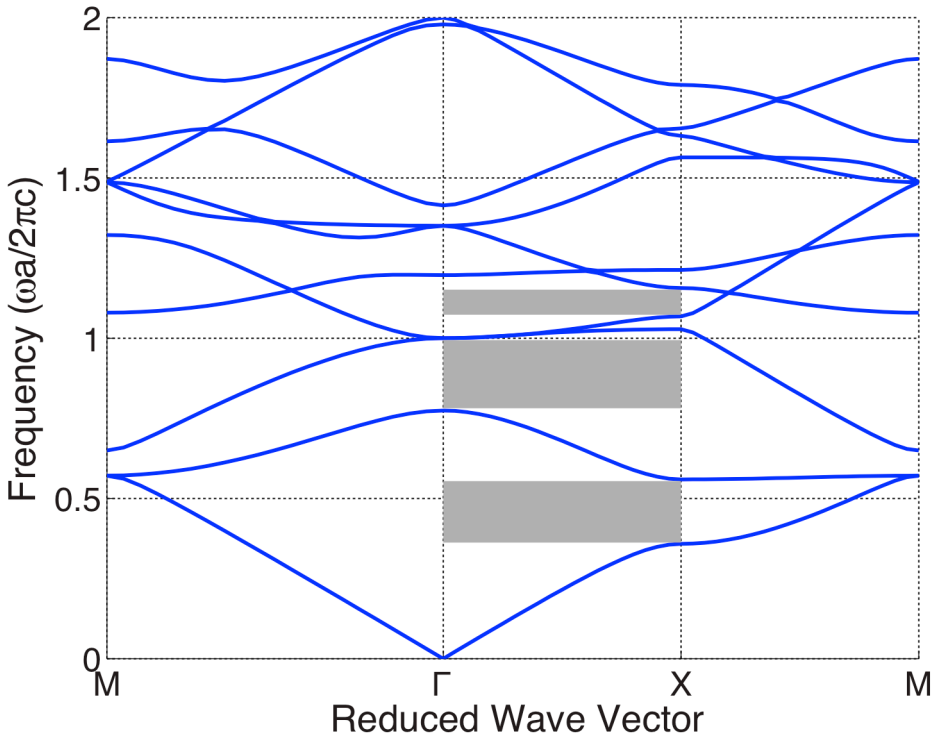

Figure 2.3 Dispersion diagram for a phononic crystals introduced in Figure 2.2. Shaded area indicates partial stopband.

2.5 Transmission Calculation of Phononic Crystal Structure

A time harmonic FEM analysis was carried to calculate the pressure field of the actual finite phononic crystals. Since the practical installation of the phononic crystal structure in the real world differs from ideal infinite phononic crystals, analysis of finitely arranged inclusions is more useful in engineer's perspective. Many researches have reported that finite phononic crystal structure behaves as

infinite of that if the number of unit-cell is more than six, in general. Transmission of acoustic wave, therefore, obtained by harmonic FEM is very useful to crosscheck with dispersion diagram analysis, assumed as infinite structure, whether the acoustic wave corresponding to the bandgap attenuates actually. In this thesis, analysis model has 8 unit-cells as a standard.

The finite element method has been utilized to calculate the pressure field behind a phononic crystal and to generate a pressure map of the system at fixed frequency. A two-dimensional phononic crystal system in a square lattice has been described in Figure 2.4. This phononic crystal structure consists of eight unit-cell introduced in previous section, which composed of rigid square scatterer in air, with lattice parameter a, and size of the square scatterer is 0.5a×0.5a. Harmonic incident wave for selected frequency to survey a response comes from left edge of the structure and goes out through the right edge. Radiation boundary condition, Equation (2.41), is applied to the both edges and p_i = 1 Pa (N/m2) is applied to the left side only to simulate the incident wave. The sound-hard boundary conditions have been applied to boundary between air and rigid scatterer. As a result, subdomains of the scatterers become non-solving domain and it reduces computational cost. To emulate y-directional infinite periodicity, the periodic boundary conditions with Neumann type are applied to the upper and exterior edges. For the numerical simulation, we used quadratic Lagrange triangular elements approximately 150,000 to solve the overall analysis domain. The number

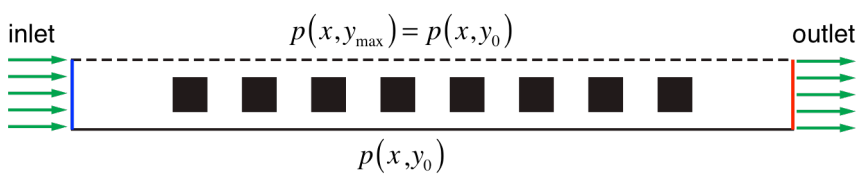

Figure 2.4 Conceptual definition for finite element method to calculate transmitted power spectrum of the phononic crystals. Eight unit cells are arranged. Periodic condition is applied to emulate infinite periodicity to y-direction.

of elements was decided to guarantee that edge of the largest unit element is shorter than the 1/4 wavelength of the incident wave.

By solving for a parametric sweeping frequency, a frequency spectrum displaying the attenuation properties of the phononic crystal can be constructed. Transmitted power for selected frequency f can be calculated by following definition

$$P(f) = \frac{W_{\text{out}}(f)}{W_{\text{in}}(f)} \tag{2.45}$$

where

$$W_{\text{out}}(f) = \int_{\Omega} \frac{p(f) \cdot p^{*}(f)}{2\rho c} \tag{2.46}$$

$$W_{\text{in}}(f) = \int_{\text{A}} \frac{p(f) \cdot p^{*}(f)}{2\rho c} \tag{2.47}$$

The Greek symbol alpha, A and omega, Ω indicate the inlet and outlet of the structure, respectively. The symbol p represents pressure and p^{*} is complex conjugate of the p. The calculated transmitted power spectrum is plotted in Figure 2.5 with corresponding dispersion diagram. Since the direction of the excitation wave applied to the transmission analysis is identical to the ΓX direction, dispersion diagram for ΓX is plotted. The gray shaded area in Figure 2.4 indicates stopband from the dispersion diagram. On the whole, the finite element computed transmission spectrum is in good agreement with the dispersion diagram. From the dispersion diagram, the first Bragg gap is formed from normalized frequency $\omega a/2\pi c$ = 0.358 to 0.559, as well as it can be observed in transmission spectrum. The second Bragg gap is formed at frequency band 0.774–1.00. Center frequency of the second Bragg gap, 0.887 is almost twice as the first Bragg gap, 0.456. It satisfies the Bragg law $n\lambda = 2a\sin\theta$ for the second Bragg gap, *i.e.* when n=2 and θ=90°, where $\lambda = 2\pi c/\omega$. The practical center frequency of the fist Bragg gap in Hertz unit can be calculated from the normalized frequency and some examples are

served in Table 2.1.

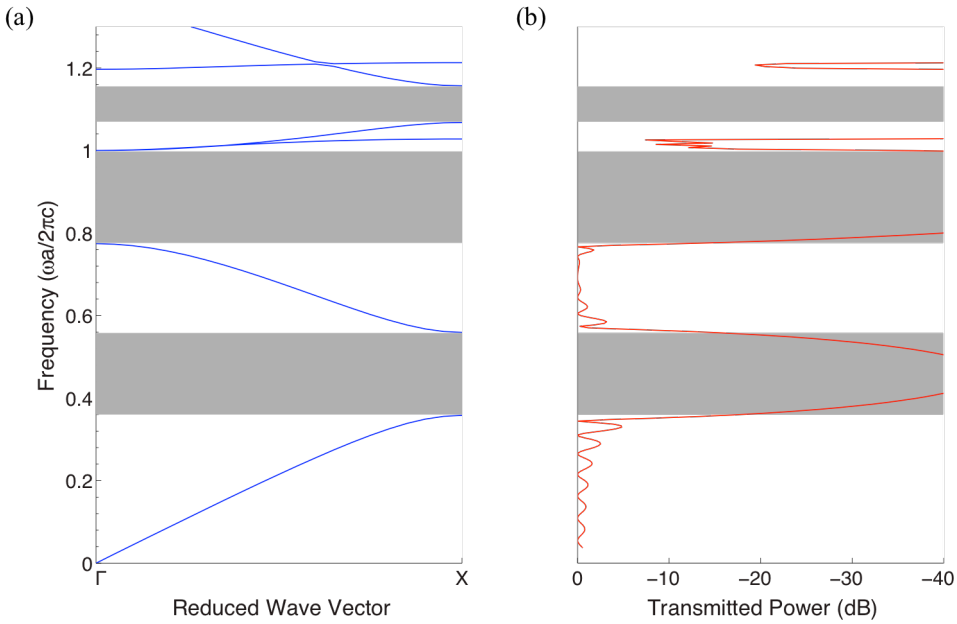

Figure 2.5 A Comparison of dispersion diagram in the ΓX direction, (a), against the transmission analysis, (b). Shaded area indicates stopband.

Table 2.1 Practical frequency examples for representative examples.

Host material	*c* (m/s)	*a* (mm)	First Bragg gap (kHz)
normalized	1	1	0.358 – 0.559
air	343	127	0.967 – 1.510
air	343	12.7	9.668 – 15.10
air	343	2	61.39 – 95.87
water	1490	2	266.7 – 416.5
water	1490	1	453.4 – 833.0
water	1490	127	4.200 – 6.558

2.6 Summary

In this chapter, basic knowledge and analysis tools for understanding phononic crystals are recovered. Finite element method of acoustic system can be utilized to obtain not only dispersion diagram but also transmission spectrum of the 2D phononic crystals. Dispersion diagram is constructed from 2D infinitely periodic model and it informs stopbands. By applying periodic boundary conditions to the edges of the domain and applying a phase shift, one unit cell can represents the whole infinite system; it saves computational cost. Basically, stopbands revealed in the transmission spectrum is almost same to dispersion diagram. However transmission spectrum provides additional information—attenuation intensity of the stopband. One can regard the transmission analysis is much better than the dispersion diagram method. The scale of finite element model for transmission analysis is much larger than the dispersion diagram's and it should be solved many times as number of the frequencies. Therefore, both methods are not an alternative relation but complementary method. These two methods will be useful in following chapters.

Chapter 3.

Locally Resonant Phononic Crystals (LRPC)

3.1 Overview

In previous chapter, phononic crystals attenuate acoustic waves in frequency of the Bragg gap, successfully. The frequency of the Bragg gap is strongly dependent on periodicity of inclusions rather than any other parameters. This characteristic is major advantage of the phononic crystals but also weak point that the first Bragg gap is the lowest attenuable frequency band. It means that the large dimension of unit cell is required to make frequency of bandgap lower. To overcome this limitation, many researches[38-40,45-49] suggested locally resonant phononic crystals (LRPC) that local resonances arise from cavity-like inclusion. This cavity-like inclusion makes not only local resonance but also the Bragg gap simultaneously. Local resonance disturbing the wave propagation may exist lower than the first Bragg gap according to geometry of LRPC acting resonator. Mechanism of local resonance of LRPC is totally separated from the Bragg gaps'. Looking at the large frame, it may say that the resonance frequency of LRPC follows the rules of the Helmholtz resonator [39,46].

Two major subjects are discussed in this chapter. First, studies about pure Helmholtz resonator and its modification are carried out to obtain analytic equations for its resonance frequency. Next, numerical tests, band diagrams and transmission tests, are presented to claim that estimation of resonance frequency of LRPC using analytic equation originated from Helmholtz resonator is fairly valid.

3.2 Helmholtz Resonator

3.2.1 One-Degree-of-Freedom Mass-Spring Model

Helmholtz resonator consists of a cavity, which may contain fluid surrounded by rigid wall, and neck, which is narrow relatively to cavity (see Figure 3.1). One-degree-of-freedom (DOF) mass-spring model presents good explanation of the Helmholtz resonator. To understand Helmholtz resonator as an 1-DOF mass-spring model, let the neck is assumed as an airtight piston floating on fluid filled a fixed volume. The neck is regarded as a single piston having effective mass if the fluid in the neck is incompressible. Meanwhile, the cavity acts as a spring. The cavity has relatively sufficient space filled with fluid that is able to be compressible. When the neck is pressured inward to cavity by excitation pressure, volume of the cavity is compressed then pressure inside the cavity increases than equilibrium state. After removal of the excitation pressure, cavity tries to push back the neck. These considering are valid when an acoustic wave whose wavelength is sufficiently larger than the dimension of the whole resonator to neglect the spatial differences of the pressure distribution within the cavity and the neck.

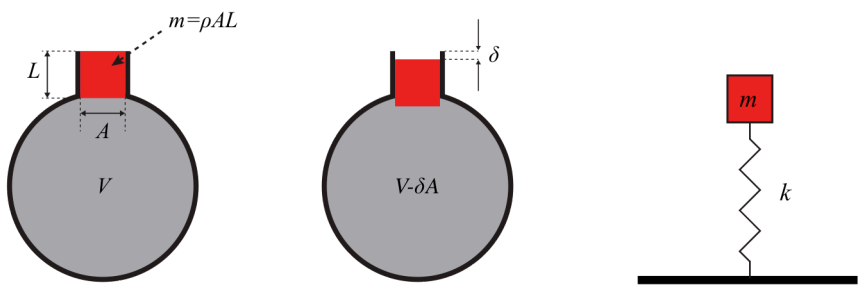

Figure 3.1 Schematic of a Helmholtz resonator with a spring-mass comparison.

The total effective mass of the neck is

$$m = \rho AL \tag{3.1}$$

where ρ is the density of the fluid, A and L are the cross-section area and length of the neck, respectively.

Pushing distance δ by the neck occurs volumetric change of the cavity as

$$\Delta V = -A\delta \tag{3.2}$$

resulting in a condensation

$$\frac{\Delta\rho}{\rho} = -\frac{\Delta V}{V} = \frac{A\delta}{V} \tag{3.3}$$

where V is the volume of the cavity. Then the pressure relation considering condensation is

$$p = \rho_0 c^2 \, \Delta\rho/\rho = \rho_0 c^2 \, A\delta/V \tag{3.4}$$

where ρ_0 is the density of fluid in the cavity. This pressure equally works to the entire area of the cavity including cross-area of the neck. Any other area except the neck cannot moves as restricted by rigid wall but the neck is free to push back by applied force. The restoring force is

$$f = pA = \rho_0 c^2 \, A^2\delta/V \tag{3.5}$$

and the effective stiffness k from mass-spring system is ($f = k\delta$)

$$k = \rho_0 c^2 \, A^2/V \tag{3.6}$$

The govern equation of 1-DOF mass-spring system without damping is well known as

$$m\ddot{\delta} + k\delta = |F| e^{i\omega t} \tag{3.7}$$

where $|F|$ is the amplitude and ω the is angular frequency of externally applied harmonic force, respectively, and t is time. Natural frequency of the system is

$$\omega_0 = \sqrt{\frac{k}{m}} = c\sqrt{\frac{A}{LV}} \tag{3.8}$$

and resonance occurs when an angular frequency of oscillation equals $\omega = \omega_0$.

Although Equation (3.8) is a function of simple geometric parameters such as A, L and V only, resonance frequency shows very good agreement with actual Helmholtz resonators. Verification of this characteristic is presented in the next section.

3.2.2 Numerical Verification: Shape of Cavity

Eigen-frequency and eigen-mode analysis are carried out in this section to check how valid equation (3.8) is. Figure 3.2 shows three test models whose A, L and V are same values but shape of V is different. Analysis domain is 127mm by 127 mm and resonator is positioned center of the domain. Parameters for the neck of all three examples are perfectly same as A = 1 mm, L = 31.75 mm. Quantity of V, area of the cavity in this 2-D problem, is same as $V = 0.001$ m^2 but different shape, circular, squared and diamond-like, respectively.

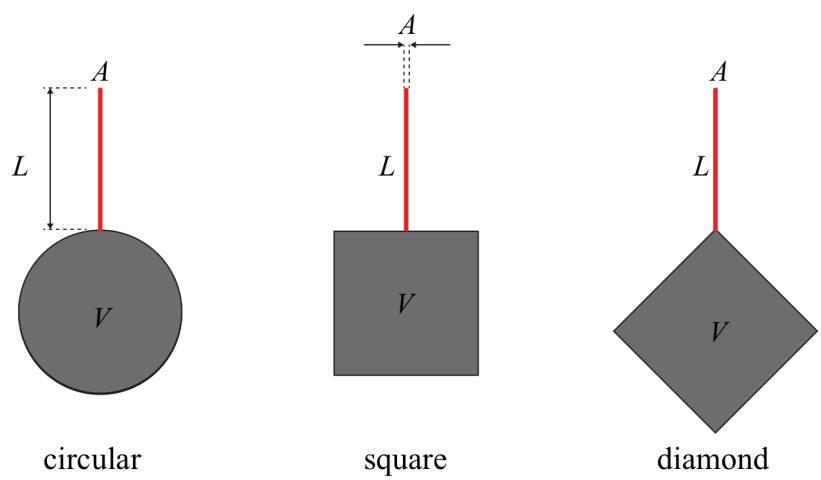

Figure 3.2 Three different types of cavity to verify influence of cavity shape on the resonance frequency. All conditions are equal except the shape of cavity.

Table 3.1 lists the resonance frequencies of each case, that are the analytic calculation from Equation (3.8) and numerical eigen-frequency of circular, squared and diamond-like cavity. All resonance frequencies of the test models are close to the analytic one with errors less than 2%.

Table 3.1 Resonance frequencies for several different types of cavity.

	Frequency (Hz)
Equation 3.8	305.1
Circular	303.7
Square	303.3
Diamond	299.9

3.2.3 Numerical Verification: Parametric Study

In this sub-section, subject to investigate is the squared cavity resonator in Figure 3.2 because latter part of this thesis mentions only squared cavity continuously. All geometric parameters and frequency are normalized as lattice size a and $\omega a/2\pi c$, respectively.

Problem setup is constructed as Figure 3.3. Investigation parameters are L, A and X independently. Parameter X indicates distance from the original position. Only one parameter varies but the others are fixed. Resonance frequency against L, length of the neck, is shown in Figure 3.4. Solid line represents resonance frequency obtained from Equation (3.8) and discrete marks indicate numerical one. The numerical data shows good agreement with the square root function of $1/L$ for $L > 0.2a$. For range of $0 < L < 0.2a$, it means that the resonant structure is far from the ideal Helmholtz resonator.

Figure 3.5 presents results of changing A, cross-section of the neck, as same manner as Figure 3.4. The numerical results agree well with the solid line, the

square root function of the A within A < 0.01a. A large A also means that the neck is so wide as to be no longer the ideal Helmholtz resonator.

Result for the parameter X is posted in figure 3.6. Resonance frequency calculated from Equation (3.8) is plotted as a horizontal line because there are no terms for the position of the neck in the equation. Although there is a tendency that resonance frequency decreases as increasing X, influence from the position of the neck is not as critical as other two parameters. Considering geometric limitation of X, $X_{\max.} \simeq 0.118a$, position of the neck may be neglected.

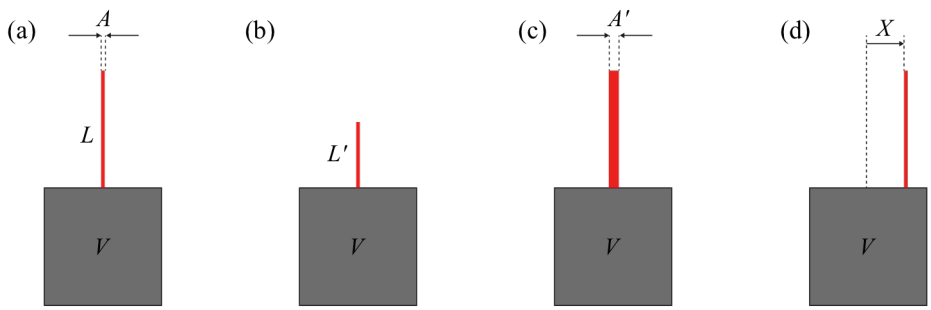

Figure 3.3 Schematics for parametric study. Investigation targets are (a) original layout, (b) length, (c) cross-section area, and (d) position of the neck.

3.2.4 Summary

Based on the facts that have been presented so far, it is reasoned that the major determinants of the resonance frequency are quantities of each parameters in the classic equation for Helmholtz resonator, Equation (3.8), rather than its geometry. It means that the designing parameters of the resonator structure may be abridged as just three quantities, L, A and V. Several parametric studies using FEM are carried out to verify analytic estimation of the resonance frequency. As a result, resonance frequency of the resonant structure is in good agreement with analytically estimated one under condition that its geometry is resembled to the ideal Helmholtz resonator.

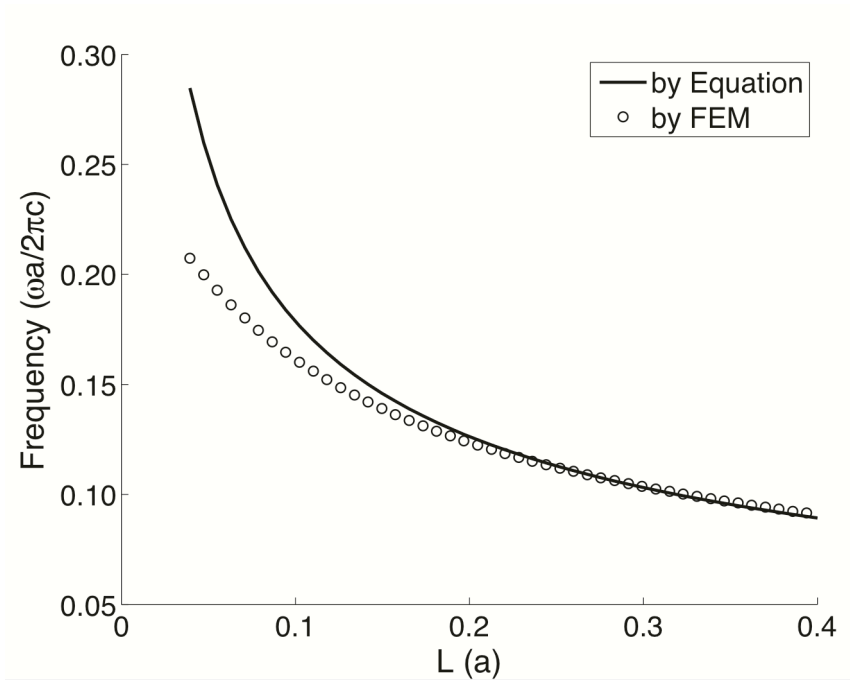

Figure 3.4 A comparison of the resonance frequency computed by eigen-frequency analysis using FEM and by analytic equation originated from the Helmholtz resonator with respect to varying L.

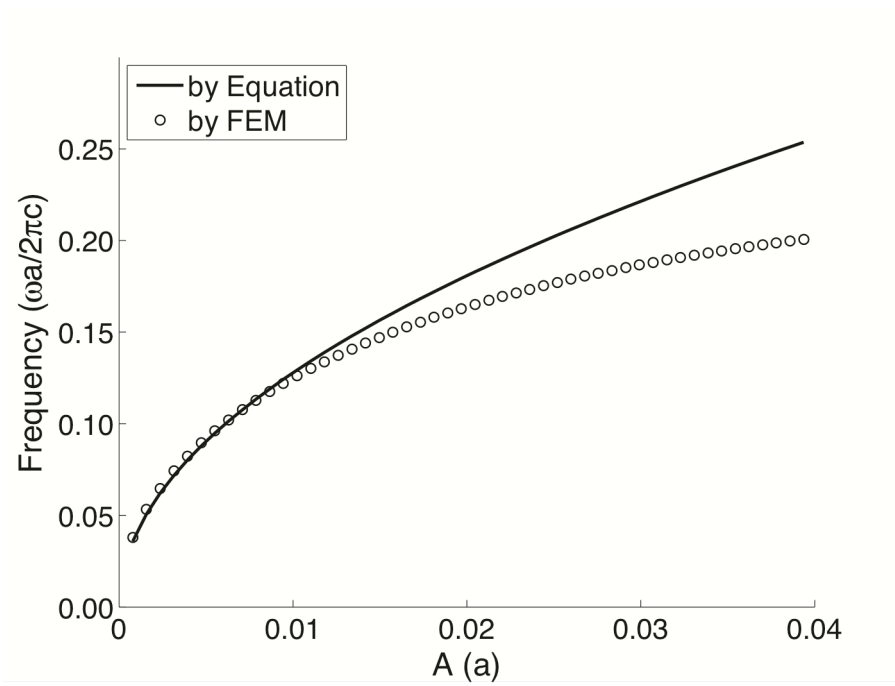

Figure 3.5 A comparison of the resonance frequency computed by eigen-frequency analysis using FEM and by analytic equation with respect to varying A.

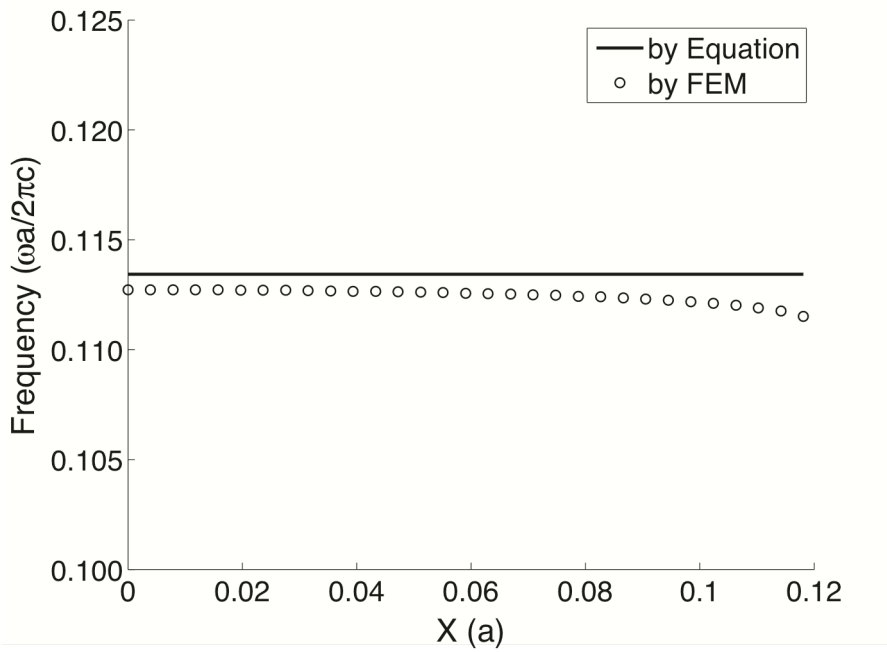

Figure 3.6 A comparison of the resonance frequency computed by eigen-frequency analysis using FEM and by analytic equation with respect tovarying X.

3.3 Modified Helmholtz Resonator (Multiple Slits)

In the last section, single-slit Helmholtz resonator was discussed both analytically and numerically. The main explanation using 1-D spring mass model is that a neck, slit, acting a mass oscillates at its natural frequency, or resonance frequency. The natural frequency of the spring mass system is determined by mass and stiffness. By this relation, a natural frequency of the system whose mass is different to another should be also different when the stiffness is same at all. Then, it is natural to question that multiple resonances occur if the mutually different necks are connected to the same cavity. In conclusion, there are no multiple resonances even if the multiple necks are applied. Only one resonance frequency exists consequently on effective mass, which is summated mass of necks connected the same cavity.

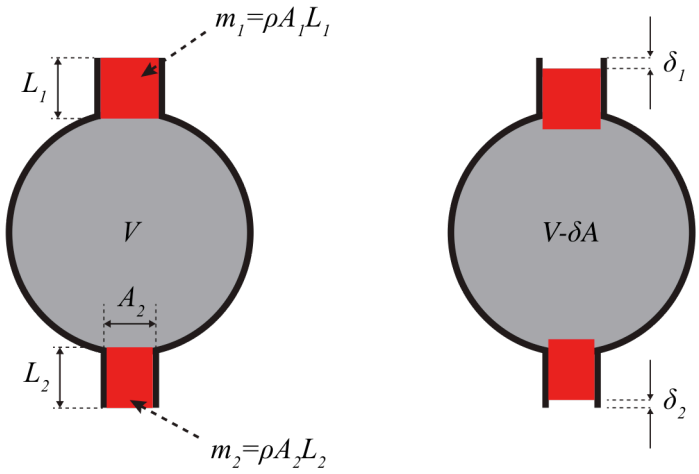

Figure 3.7 Schematic diagram of a dual slit resonator.

3.3.1 Analytic Approach

Figure 3.7 illustrates model of two-neck cavity structure. Parameters of neck, A and L are different to each other as $A_1 \neq A_2$, $L_1 \neq L_2$. Two different necks construct each effective mass, m_1 and m_2 whose displacements are δ_1 and δ_2, respectively. Volumetric change of cavity caused by both δ_1 and δ_2 is

$$-\frac{\Delta V}{V} = \frac{A_1\delta_1 + A_2\delta_2}{V} \tag{3.9}$$

and inserting to equation (3.4), outward pressure of the cavity is derived as

$$P_{in} = \rho c^2\left(-\frac{\Delta V}{V}\right) = \rho c^2\left(\frac{A_1\delta_1 + A_2\delta_2}{V}\right) \tag{3.10}$$

The pressure P_{in} equally affects to the entire cavity. Of course, the effective masses m_1 and m_2 are also affected by it through the area A_1 and A_2. Appling same procedure discussed in section 3.2.1, govern equation of each mass is written as

$$m_1\ddot{\delta}_1 + P_{in}A_1 = A_1P_{out}e^{i\omega t} \tag{3.11}$$

$$m_2\ddot{\delta}_2 + P_{in}A_2 = A_2P_{out}e^{i\omega t} \tag{3.12}$$

where P_{out} is the externally applied harmonic force. These two equations can be rewritten as

$$\rho L_1 \ddot{\delta}_1 + \rho c^2 \left(\frac{A_1\delta_1 + A_2\delta_2}{V} \right) = P_{out} e^{i\omega t} \tag{3.13}$$

$$\rho L_2 \ddot{\delta}_2 + \rho c^2 \left(\frac{A_1\delta_1 + A_2\delta_2}{V} \right) = P_{out} e^{i\omega t} \tag{3.14}$$

Ignoring the spatial effect of the P_{out}, relation between m_1 and m_2 can be derived as

$$\rho L_1 \ddot{\delta}_1 + \rho c^2 \left(\frac{A_1\delta_1 + A_2\delta_2}{V} \right) = \rho L_2 \ddot{\delta}_2 + \rho c^2 \left(\frac{A_1\delta_1 + A_2\delta_2}{V} \right) \tag{3.15}$$

From Equation (3.15) it follows that

$$L_1 \ddot{\delta}_1 = L_2 \ddot{\delta}_2 \tag{3.16}$$

Assuming all of the initial conditions are zero, Equation (3.16) results following

$$L_1 \delta_1 = L_2 \delta_2 \tag{3.17}$$

Inserting equation (3.17) to Equation (3.13) and (3.14), then

$$\rho L_1 \ddot{\delta}_1 + \frac{\rho c^2}{V} \left(A_1 + A_2 \frac{L_1}{L_2} \right) \delta_1 = P_{out} e^{i\omega t} \tag{3.18}$$

$$\rho L_2 \ddot{\delta}_2 + \frac{\rho c^2}{V} \left(A_1 \frac{L_2}{L_1} + A_2 \right) \delta_2 = P_{out} e^{i\omega t} \tag{3.19}$$

The each natural frequency of the necks can be obtained from Equation as

$$\omega_1 = c \sqrt{\frac{A_1 + A_2 \frac{L_1}{L_2}}{L_1 V}} \tag{3.20}$$

$$\omega_2 = c \sqrt{\frac{\frac{L_2}{L_1} A_1 + A_2}{L_2 V}} \tag{3.21}$$

Final forms of equation (3.20) and (3.21) are perfectly coincident as

$$\omega_1 = \omega_2 = \frac{c}{\sqrt{V}}\sqrt{\frac{A_1}{L_1}+\frac{A_2}{L_2}} \tag{3.22}$$

Working the same procedures for multiple necks, Equation (3.22) can be extended simply as

$$\omega = \frac{c}{\sqrt{V}}\sqrt{\frac{A_1}{L_1}+\frac{A_2}{L_2}+\cdots+\frac{A_n}{L_n}} \tag{3.23}$$

where the n is number of necks.

In case of all parameters of the necks are same, the resonance frequency is derived as simple form

$$\omega = c\sqrt{\frac{nA}{LV}} \tag{3.24}$$

Both Equation (3.23) and (3.24) have meaning that adding neck to the Helmholtz resonator increases its resonance frequency regardless of position of the neck.

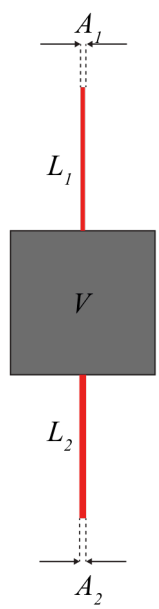

Figure 3.8 Conceptual geometry of the dual slit resonator for eigen-frequency analysis using finite element method.

3.3.2 Numerical Verification

To verify the equations discussed previous sub-section, numerical eigen-frequency analyses for resonator-like structures are carried out as similar as section 3.2. Firstly, coincidence between resonance frequency of analytic model and numerical one is examined for some parameter sets. Secondly, parametric study is carried out with respect to varying A. Lastly, effectiveness of position of the necks, not included in Equation (3.23), is checked.

Figure 3.8 is definition of the test problem. Two necks whose parameters are different to each other are connected to the same cavity. Table 3.2 shows testing parameter sets and its results. Analytic resonance frequency, f_a, is calculated from Equation (3.23), while numerical one, f_n, is obtained from eigen-frequency analysis.

As shown in Table 3.2, numerical eigen-frequency of the system is well fit for analytic one. There are no additional natural frequencies of each necks but only one exists as derived as Equation (3.23).

Table 3.2 Parameter set of test problem for Figure 3.10.

Set	L_1 (mm)	L_2 (mm)	A_1 (mm)	A_2 (mm)	V (mm^2)	f_a (Hz)	f_n (Hz)
1	31.75	31.75	1	1	1008.1	431.5	435.3
2	31.75	31.75	1	0.5	1008.1	373.1	379.3
3	21.75	41.75	1	1	1008.1	454.6	452.3
4	21.75	41.75	1	0.5	1008.1	413.6	409.3

3.4 Locally Resonant Phononic Crystals (LRPC)

Until now, single structure of the resonator-like structure is discussed only. Applying the infinitely periodic condition to the resonator-like structure, the periodic structure has both characteristics of resonator and phononic crystals, because rigid wall surrounding the cavity may act as an inclusion of the phononic crystals, in opposite viewpoint, the inclusion of the phononic crystals may form a

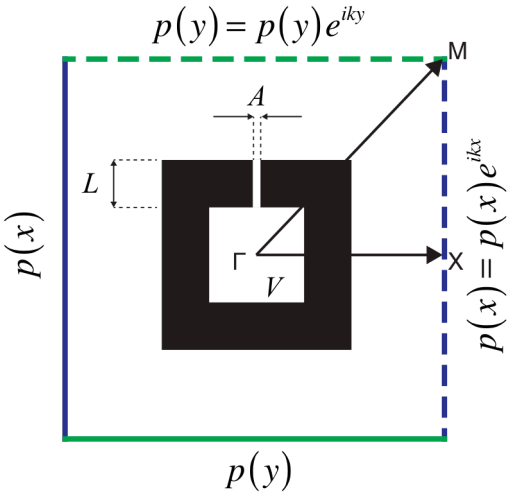

Figure 3.9 Unit cell of an acoustically resonance phononic crystals with periodic boundary conditions described.

cavity of the resonator. From a whole structural standpoint, a resonance occurs inside the cavity locally, which is small part of the structure. For this reason, the infinitely periodic resonator-like structure may be named as Locally Resonant Phononic Crystals (LRPC).

In this section, two major analyses from the phononic crystals' perspective that we discussed in the Chapter 2 are applied to the LRPC. One thing is for diagram of the dispersion relation and another thing is for verifying transmission. Same numerical procedures shown in the section 2.4 and 2.5 are carried out in this section.

3.4.1 Dispersion Diagram of the LRPC

A periodic acoustic structure, LRPC, is defined as Figure 3.9. This structure is almost same as Figure 2.2 except two things. A square cavity is embedded in the square inclusion. And a neck, acoustic channel, connects cavity and host material. The periodic boundary conditions have been employed as we discussed in the

section 2.4.

Numerical investigation of eigen-frequency of the LRPC varying the wave vector in the first Brillouin zone is plotted in Figure 3.10. Looking at the diagram of the dispersion relation, it is obvious that a full bandgap, from 0.1475 to 0.1526, is added under the first Bragg gap located at 0.3571–0.541 that already observed in Figure 2.3 as 0.358–0.559. This full bandgap is caused resonance of the cavity, and for this reason it is called the resonance gap distinguishing from the Bragg gap. Obvious proof of this bandgap can be observed in next sub-section, which discusses transmission of the LRPC.

The frequency-wise location of the resonance gap can be estimated by Equation (3.8). Using practical parameters L=31.75 mm, A=1 mm and V=1008.1 mm^2 as described in Figure 3.9, an analytic resonance frequency, $f_a = 2\pi\omega_a$, is computed as 408.8 Hz. The resonance gap is located at 391 Hz to 412 Hz, and then f_a locates well within the resonance gap.

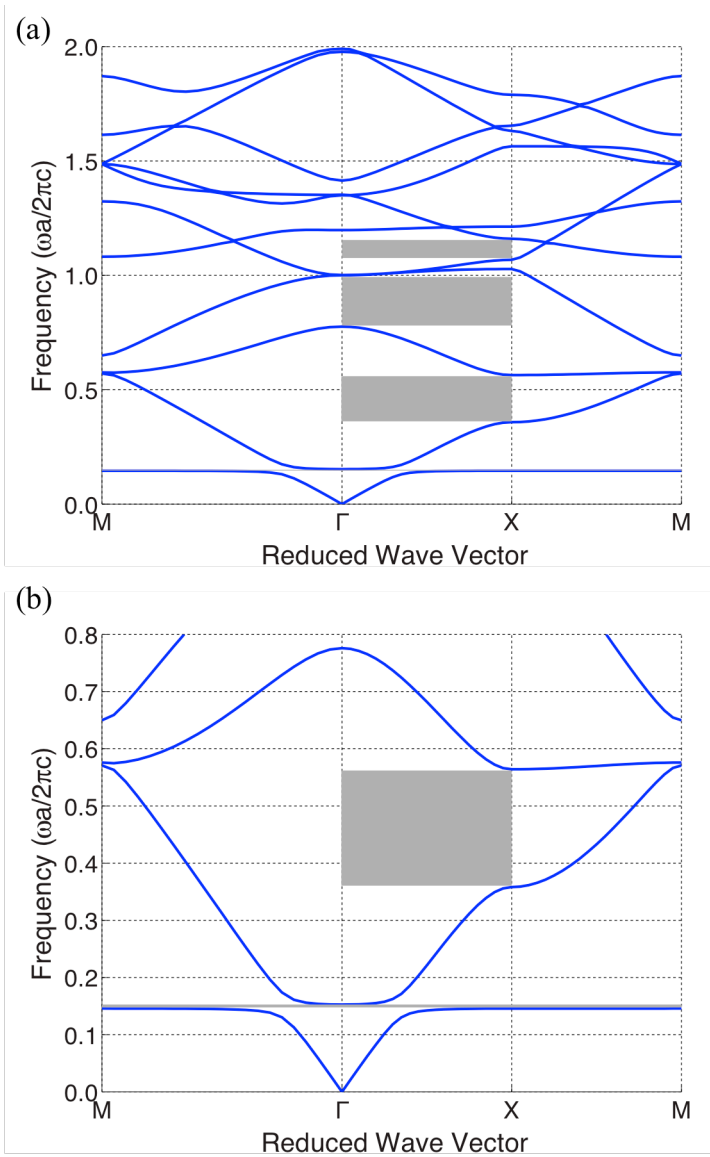

Figure 3.10 Dispersion diagram for a locally resonant phononic crystals described in Figure 3.9. (a) Full dispersion diagram for the first ten bands, (b) zoomed view for frequency range of 0–0.7405. Shaded area indicates stopband.

3.4.2 Transmission of the LRPC

Same procedures discussed in the section 2.5 are presented in this sub-section as well. One thing is checking whether the resonance gap revealed in the band dispersion actually blocks the acoustic wave using transmission analysis. Another thing is influence of the number of the unit LRPC on actual transmission.

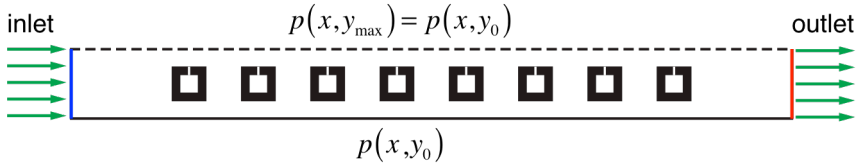

Figure 3.11 Schematic definition for finite element method to calculate transmitted power spectrum of the locally resonant phononic crystals. Periodic condition is applied to emulate infinite periodicity to y-direction.

Using module of the Pressure Acoustics within the commercial FEM package, COMSOL Multiphysics, a time-harmonic analyses are carried out for obtaining pressure field and power transmission of the acoustic wave. Figure 3.11 shows the FEM definition for transmission analysis. To save the computational costs, single row of the structure is solved with y-directional periodic condition. The periodic boundary conditions are applied to upper and lower edge of the analysis domain. This modeling is equivalent to the infinitely periodic structure along the y-direction. An acoustic wave source comes from the left and propagates through the finitely arranged LRPC region. A radiation boundary condition is applied to the very right of the analysis domain to eliminate wave reflection, *i.e.* the infinite space virtually continues after the boundary. The rigid inclusion of the LRPC acting scatterer is realized by blank area enclosed with acoustic hard wall boundaries. The only difference between Figure 2.4, pure phononic crystals system, and this new system is existence of resonant cavity with connecting neck.

Figure 3.12 shows the pressure field of the system at three frequencies representing resonance gap, passband and the Bragg gap. According to band diagram of the LRPC, see Figure 3.10 (b), $f_1 = 0.15$, $f_2 = 0.28$ and $f_3 = 0.5$ belong to the resonance gap, passband and the Bragg gap, respectively. All of excited waves propagate as if the system is a homogenous material; excited waves maintain its wave-pattern as a plane wave.

Looking at Figure 3.12 (a), it is obvious that amplitudes of pressure in the cavities are extremely larger than any other region and waves are no longer to

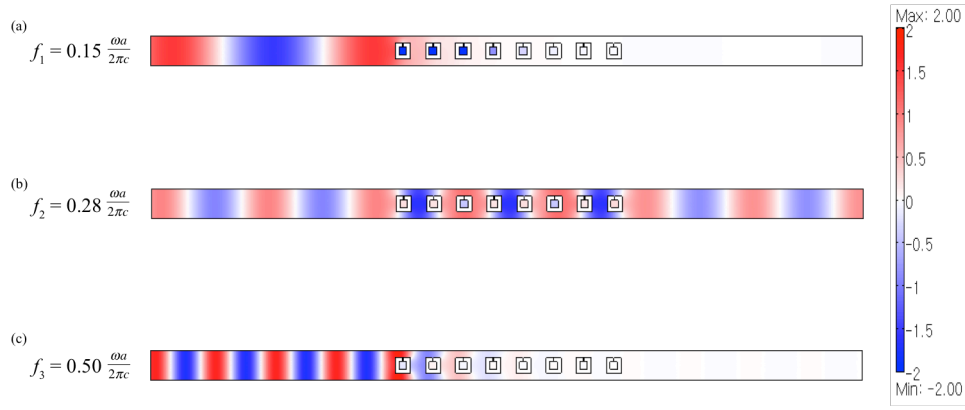

Figure 3.12 Pressure field of locally resonant phononic crystal structure for three representatives of each band. (a) resonance gap, (b) typical passband, (c) the Bragg gap. Pressure scales of three results are in common. Value exceeded the legend is expressed as maximum color.

propagate through the LRPC region, *i.e.* the acoustic waves are trapped in the cavity due to the resonance of the neck. This is reason that named Locally Resonant Phononic Crystals because acoustic pressure resonates at local region, cavity. Meanwhile, the acoustic wave at frequency corresponding to the Bragg gap decays gradually passing through the LRPC region. The resonance gap and the Bragg gap not only originated from the different mechanism, resonance or destructive scattering, but also appear in totally different pressure patterns.

Extending the previous analysis, spectral transmission of Figure 3.12 is plotted in Figure 3.13 with corresponding band diagram. Direction of applied wave in Figure 3.12 corresponds to the reciprocal wave vector Γ-X. Gray-shaded areas represent the stopbands including Bragg gap and the resonance gap; the lowest gray-shaded area is for resonance gap in both subplots in Figure 3.13. The overall figure of the low transmission regions are well fit for its band diagram including the resonance gap. Comparing to the Bragg gap, transmitted power of the resonance gap is much less, *i.e.* acoustic waves are blocked efficiently by resonance gap rather than the Bragg gap.

Influence of finite number of the LRPC on the transmission is also collected in Figure 3.14. The left low transmission region, 0.1475 to 0.1526, is for resonance

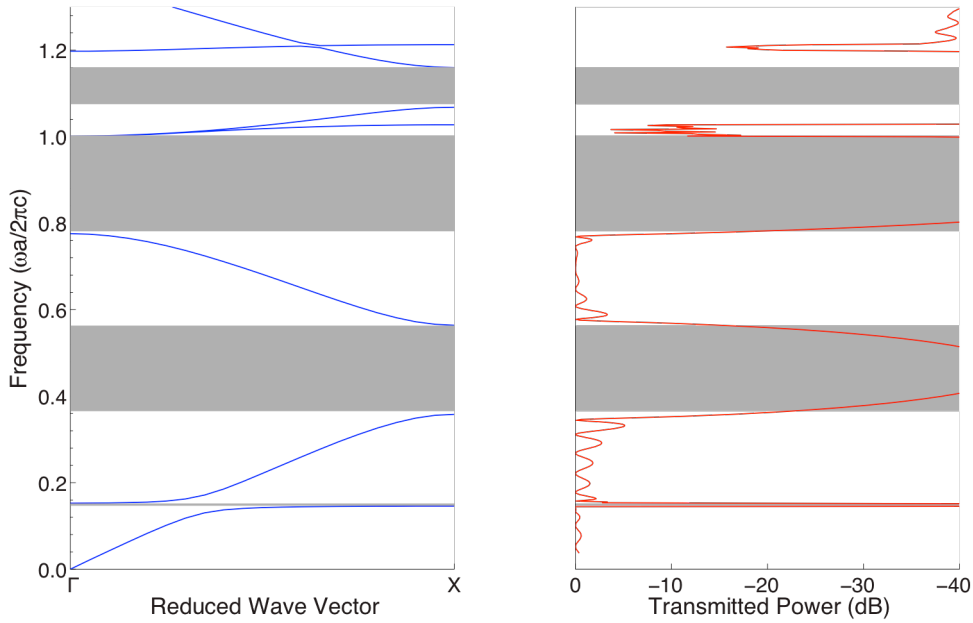

Figure 3.13 A Comparison of dispersion diagram in the ΓX direction, (a), against the transmission analysis, (b). Shaded area indicates stopband.

gap and the right one, 0.3571–0.541, is for the Bragg gap. Unlike the Bragg gap, the resonance gap is manifested even with solitary-LRPC system because the resonance gap is fundamentally not caused by infinite periodicity but cavity resonance. This is another advantage of the resonance gap against to the Bragg gap. Of course, the more LRPC exists, the less acoustic wave transmits for the resonance gap.

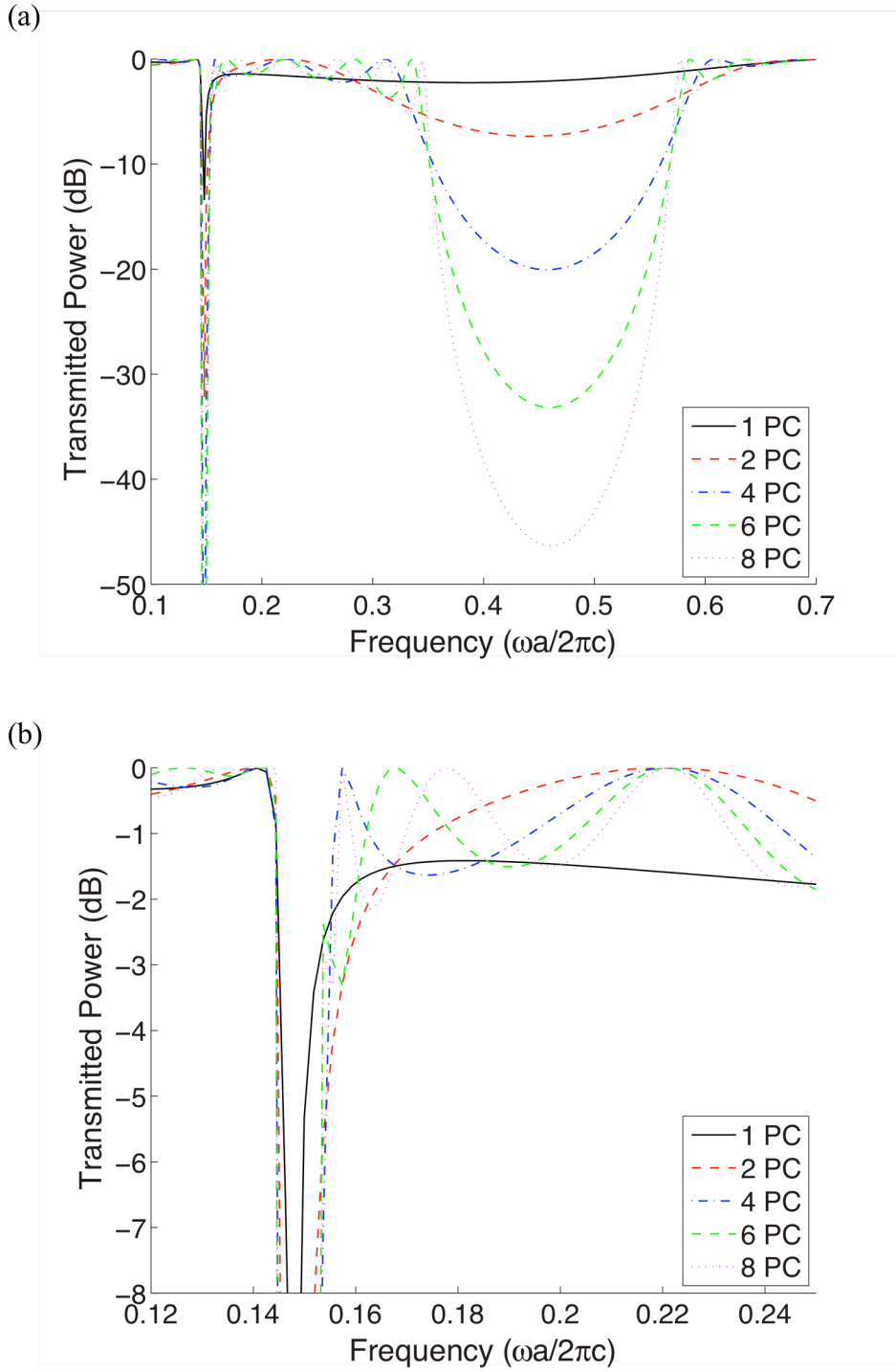

Figure 3.14 A comparison of power transmission spectrum of the locally resonant phononic crystal structure against the number of unit cell. (b) is the zoomed view for the resonance gap.

3.5 Summary

Based on the facts that have been clarified so far, the factor governing the resonance frequency of the LRPC are quantities of the cross-section of the neck, A, the length of the neck, L, and the volume of the cavity, V. Also the resonance frequency of the LRPC can be easily estimated by simplified equation derived from spring-mass-model. Resonance of the LRPC is well observed in the band diagram as additional bandgap. And also transmission of the LRPC agrees with the band diagram. Based on parametric studies, it is possible to conclude that the resonance gap behaves independently to the Bragg gap. From this characteristic, bandgap lower than the Bragg gap is achieved successfully importing locally resonant concept to the phononic crystals.

Chapter 4.

Lattice-Tunable Phononic Crystals (LTPC)

4.1 Overview

During the previous two chapters, basic acoustic characteristics and analyzing techniques for the phononic crystals and locally resonant phononic crystals (LRPC) were presented in order to found after works. Eventually, in this chapter, main subject of this thesis is introduced. The novel phononic crystals having particular tuning method are able to manipulate not only the resonance gap but also the Bragg gap at the same time. Also, the Bragg gap of the proposed phononic crystals can be tuned for wide range due to lattice transferring, plus, the resonance gap is connected with the Bragg gap within the tunable range.

This chapter starts from introducing a new design layout of the phononic crystals. Then, routine analyses about phononic crystals are carried out for the new one. Simply modified tuning schemes based on the original one are proposed and analyzed.

4.2 Design Motivation

Three principal goals for a new tuning method are considered as followings

1. Huge tunable range
2. Consistency
3. Dynamic tunability

In order to achieve the first goal, huge tuning range, two ways can be considered. One thing is enlarging tunability of the Bragg gap. Another is adding locally resonant inclusion that resonance gap in place other than the Bragg gap. The convectional tunable phononic crystals [15,23,47,50,51] applied the Bragg gap are restricted in fixed lattice size. Recalling the Bragg law, see Equation (4.1), it is obvious that the tunable range of the phononic crystals is decided by the lattice size fundamentally; although somewhat large tunable range of the Bragg gap can be achieved by inclusion-wise change, it cannot break the limitation of the self-periodicity because the periodicity, lattice size, rules the Bragg gap dominantly as discussed in the chapter 2.

$$2d = n\lambda \tag{4.1}$$

The easy way to overcome this limitation and make tunable range large is dramatic variation of the lattice size, which is d in Equation (4.1) and it determines wavelength of the Bragg scattering, λ. Some researches have already reported variation of the lattice as a tuning method [29-31]. Various typical methodology to deform the lattice were tried such as elongation[30], compression[29], shear deformation by external force[31]. However, they utilized variation of the lattice as an alternative method of the convectional inclusion-wise tuning method and did not consider that large variation of the lattice can shift the Bragg gap large. Defending their situation, their tuning methodology contains an inevitable aspect that host material is solid, which cannot deform dramatically. On the other hand, fortunately, host material of the acoustic phononic crystals is generally fluid type. It means that deforming inclusion may affect directly and dramatically to its periodicity, lattice size, disregarding the host structure. This inspires the new tuning method, the main subject of this thesis. After all, in aspect of enlarging tunable range of the Bragg gap, an inclusion-wise transition causing a lattice variation is adopted as a basic concept of the new tuning scheme.

Another solution to achieve the first goal, huge tuning range, is adding tunable

resonance gaps that the Bragg gap cannot cover. This approach is especially useful for low frequency band under the first Bragg gap, the lowest one, because the resonance gap works independently of the Bragg gap and then it can be tuned for the different range of the bandgap. As already discussed in the chapter 3, the resonance gap appeared in the form of additional bandgap to the Bragg gap. There are two major considerations attributable to different governing factors from the Bragg gap. First, the resonance gap behaves as resonant mechanism, which means extra tuning scheme may be necessary to tune the resonance gap. An undesirable situation is that a tuning method for resonance gap is totally different to the Bragg gap's. Surely, a unified tuning scheme for both the resonance gap and the Bragg gap is efficient in aspect of realization. Second, a bandwidth of the resonance gap is relatively narrow to the Bragg gap, especially at the frequency band lower than the first Bragg gap, because the resonance is fundamentally valid only for a specific frequency, such as natural frequency. Some efforts have been tried out for enlarging the resonance gap[46,52]. Elford *et al.* [46] designed a multiple C-shape resonators that all resonators are embedded in the same inclusion at once. Their strategy for enlarging the resonance gap is overlapping the individual resonance peaks of each resonator. Although successful effects for enlarging, the resonance gap was not perfectly overlapped especially in the low frequency band. Their design has inherent limited margin to overlap all resonances under frequency band of the Bragg gap by few resonator and adding multiple resonators in one inclusion is not good tunable figure. Therefore, in this research, this approach is drastically dropped in spite of its goodness. Instead, this research peruses a widely tunable resonance gap that individuals are relatively narrow but broadly movable by simple way; it is bound up in the next second goal, consistency.

Consistency, the second goal, means that both the Bragg gap and the resonance gap are tuned by unified tuning method. As already discussed above, the Bragg gap and the resonance gap behave independently by different mechanisms; therefore individual tuning schemes specialized in each gap mechanism may be necessary. In

aspect of engineering, dualized tuning method is not efficient to design and control. A unified tuning method that both gaps are tuned consistently together is desirable. It benefits reducing complexity of designing and tuning.

Dynamic tunability, the third and last goal, is also important consideration. A totally fixed PC, which has no means of external handling for stopband, is restrictive to shut out broadband acoustic waves because the stopband is also fixed for the given PC. If a unit stopband can be shifted seamlessly in wide range despite of its narrow bandwidth, it is possible to claim that the PC can attenuate all frequencies in its tunable range. Of course, this approach may need extra processes to tailor the stopband for target frequency; but it is profitable to overcome physical limitation of the PC itself such as narrow bandwidth of the resonance gap and large passband between the Bragg gaps. Moreover, on-demand dynamic tunability becomes an essential basis for achieving the active control of PC.

Considering all three goals, a new tuning methodology was developed to achieve that using only one tuning parameter can tailor both the Bragg gap and the resonance gap for seamless wide frequency range.

4.3 Design Layouts and Tuning Procedure

Now, a new tuning methodology, dually tunable phononic crystals (LTPC), is presented in this section. The LTPC consists of two tuning parameters, α and β. The 2α is perfectly coincident to lattice size of PC. Therefore the α determines frequency band of the Bragg gap macroscopically. Assuming practical application of the LTPC, the α will be determined after target frequency band to exclude is selected and once fixed α is not be allowed to change. The parameter α, therefore, can be regarded as a static and passive tuning parameter. Another tuning parameter β determines geometry of inclusions inside the LTPC, which changes both the Bragg gap and the resonance gap and its tunable range is seamless with respect to β. The LTPC is designed to achieve that the β becomes a dynamic tuning parameter.

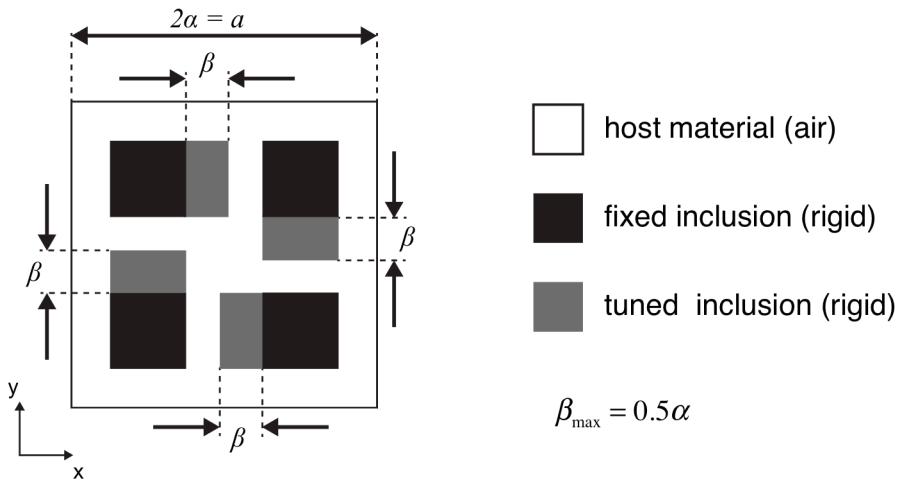

Figure 4.1 Design layout of Lattice-Tunable Phononic Crystals (LTPC).

Figure 4.1 shows a design layout of the LTPC. Parameters α and β are same as above paragraph. All the rest of geometries can be describable by α, and then the LTPC is geometric similarity with respect to α. For this reason, it is convenient that β is also described by α. A LTPC consists of four independent sub-inclusions. A lattice size of undeformed sub-inclusions is one-half of the LTPC's, 0.5α. The inclusions can be elongated unidirectionally as much as β and their directions are rotational symmetric. The maximum β is 0.5α, and then inclusions are fully elongated and reach neighboring inclusion. Four fully elongated sub-inclusions can form a new super-inclusion.

Inclusion layouts corresponding to some representative β are illustrated in Figure 4.2. Lattice size of the LTPC of Figure 4.2 (d) is two times that of (a). Therefore it is possible to expect that the Bragg gaps of (d) shifts down as one-half of (a); see Equation (4.1) and detailed numerical results will be presented in the next section. Although a cavity, air occupation, is formed in (d), it has no influence to acoustic analysis because it is perfectly isolated by rigid inclusions except some numerically trivial solutions negligible.

Figure 4.2 (c) is a special situation of (b) occurring resonance gap. When the inclusions are elongated very closely to neighboring inclusion, air occupation area

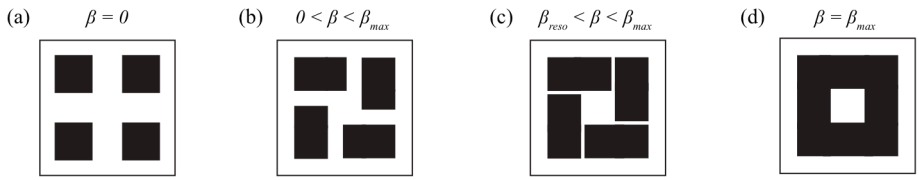

Figure 4.2 Representative layouts corresponding tuning parameter β.

connecting central cavity to the host material is sufficiently narrow to become a neck of the resonator. Four necks are identical and connected with one cavity, and then the resonance gap can be estimated by Equation (3.24). Estimation agrees well with numerical results; it will be presented in the next section.

4.4 Acoustic Analysis

In this section, routine analyses of PC are also carried out for the LTPC; both band diagrams and power transmission analyses with respect to varying β are presented. Since the resonance gap appears for specific condition of β, detailed studies of the resonance gap of the LTPC is also achieved.

4.4.1 Band Diagram of the LTPC

Convectional definition for the LTPC is depicted in Figure 4.3. The same as before, the acoustic eigen-frequency analysis for band diagram is performed; periodic boundary conditions varying by the wave vector in the first Brillouin zone are applied and dispersion diagram is obtained collecting eigen-frequency of that situation. Since the dispersion diagram for full wavevector is very complex and a plane wave whose direction belongs to Γ-X is assume to calculate a transmission of the LTPC, therefore, the only wavevectors within Γ-X are surveyed.

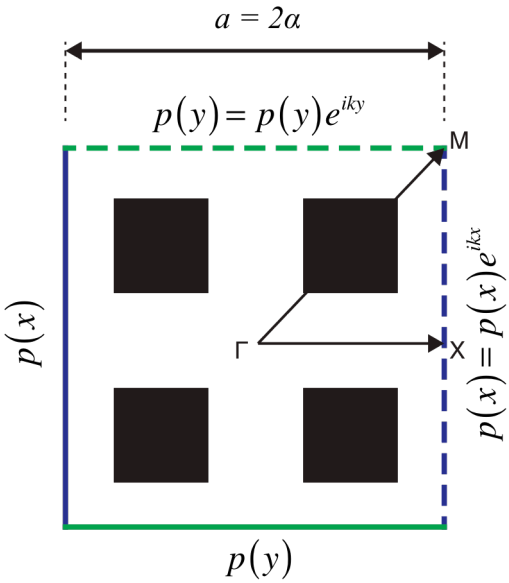

Figure 4.3 Single unit cell of an infinite phononic crystals with periodic boundary conditions.

Dispersion diagram for varying β is plotted in Figure 4.4. Four representative βs are selected as same as Figure 4.2 and each β stands for particular situation of the LTPC. The β=0, Figure 4.4 (a), is state that sub-inclusions are minimum as square and lattice size of inclusion influencing the Braggs gap is minimized as 63.5 mm. So the lowest Bragg gap is positioned in the highest frequency band comparing with any other states of the LTPC. This state takes charge of attenuating highest frequency band of acoustic waves. The β=0.5α=0.25a, Figure 4.4 (d), is state that sub-inclusions are maximized as rectangular form (0.5a ×0.25a) and a super-inclusion is fully developed by four sub-inclusions; the effective lattice size of LTPC renewed by the super-inclusion is also maximum, therefore, the Bragg gap is formed in the lowest frequency range. The β=0.13a, Figure 4.4 (b), represents transitional state between (a) and (d); and β=0.245a, Figure 4.4 (c), is one of the special case of (b), the resonance gap.

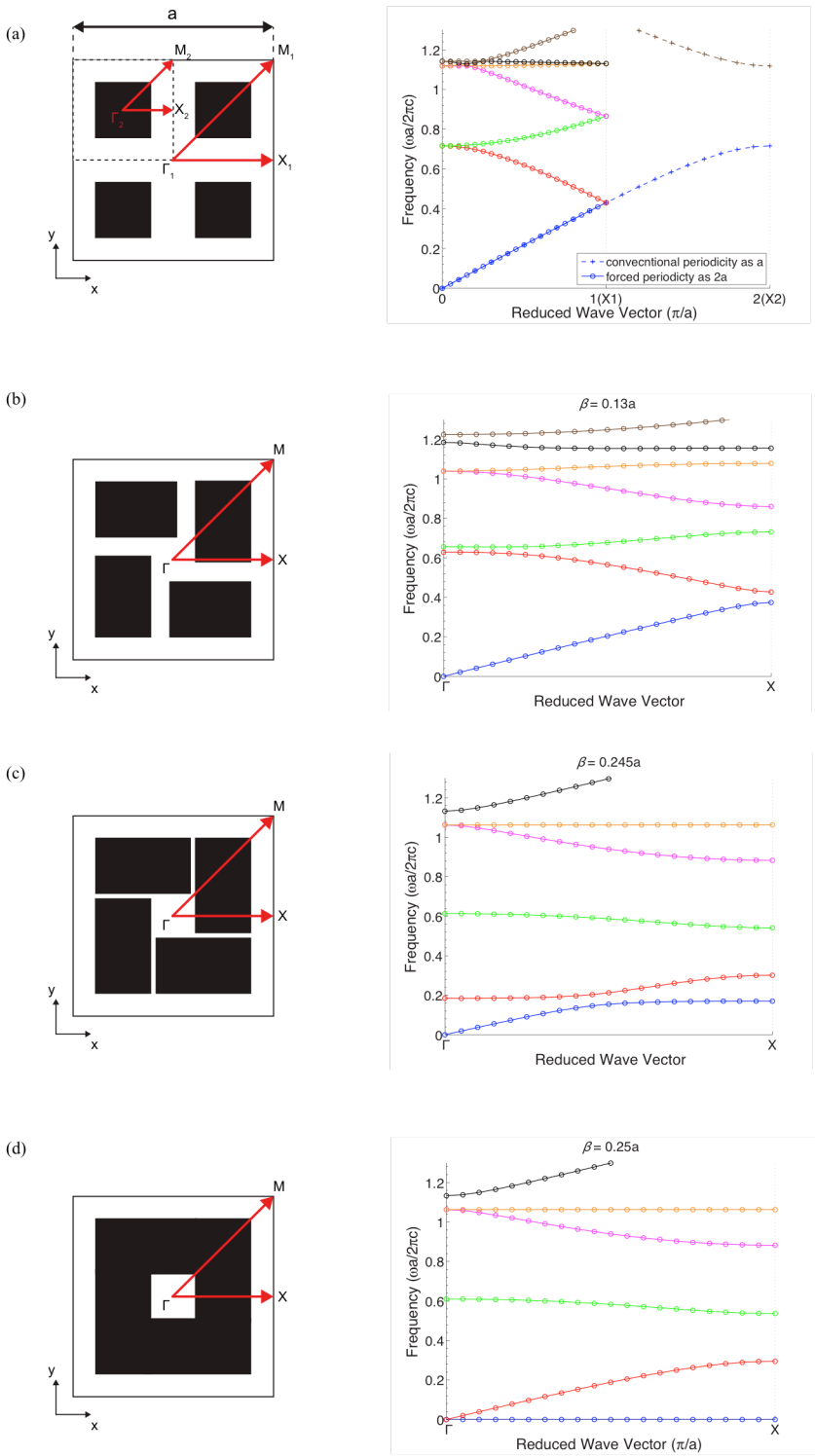

Figure 4.4 Geometric layouts (left) with corresponding dispersion diagram (right) for, (a) $\beta = 0$, (b) $\beta = 0.13$a, (c) $\beta = 0.245a$ mm (d) $\beta = 0.25a$.

Before discussing detailed exposition about sub-figures in Figure 4.4, the folded branch and the deaf branch have to be mentioned. Since geometry and lattice size of four inclusions in Figure 4.4 (a) are perfectly same to each other, the two particular braches are revealed. For easy understanding and comparing, both dispersion diagram for one-inclusion PC and four-inclusion PC are plotted in the same figure. The dashed line with + mark stands for the dispersion curve of the one-inclusion PC. Since the lattice size of the one-inclusion PC is one-half of the four-inclusion PC, its reduced wave vector is twice large than the four-inclusion PC. The solid line with O mark is dispersion curve of the four-inclusion PC. The blue line in the range of the reduced wave vector 0 to1 is a superposition of both dispersion curves for each PC. The green, magenta, black and orange solid line with O mark correspond the deaf mode; the orange solid line is almost covered by black one. The red one is a folded line of the blue dashed line that resulted by correct first Brillouin zone. The green and magenta lines seem like separated curves but these are originally the same deaf branch but folded. Same manner can be applied to pair of black and orange line. Particularly, the orange line remains horizontally flat branch even if the β changes, which means not-propagating branch, on the other hand, the black one varies dramatically along the β variation.

Since the green line and the magenta line are deaf branch, an acoustic wave belongs to those branches cannot propagate through the PC in spite of existing branch. Once inclusions deforms as $\beta>0$, however, similarity of inclusions is broken and deaf branches lose their deafness along the β increasing. Unfortunately, this phenomenon is not observable analyzing the band diagram only. For this reason, transmission analysis for finitely arranged PC structure is essential to the LTPC. This topic will be soon discussed in the next sub-section.

As plotted Figure 4.4 (b), the sub-inclusions are no more identical geometry for $\beta>0$, and then both x-directional and y-directional overlapped periodicity of sub-inclusions are invalid. Therefore deaf branches and folded branches are no more themselves. Folded branches such as red, magenta and black lines are

separated from its pair and behave independently along the β variation. Also, the former deaf branches now become the propagating branches, *i.e.* the passband. Meanwhile, transferring capability of the former deaf branch is not fully developed just after β=0 but increases gradually with β increasing. Repeatedly, it can be found evidently in the transmission analysis, which will be introduced in the next sub-section.

A slight gap between the first and second branch of the Figure 4.4 (c), blue and red line, is the resonance gap of the LTPC. Its location and bandwidth is much lower and much narrow than the first Bragg gap, respectively. For β increasing, it becomes lower and narrower, and finally vanishes; see figure 4.4(d). Basically, location of the resonance gap follows the Equation (3.24) for large β, which means neck of the resonator should be sufficient narrow to act as a Helmholtz resonator.

The final tuning stage of the LTPC is introduced in Figure 4.4 (d). Since four sub-inclusions are unified as one super-inclusion, a dispersion diagram is obtained as

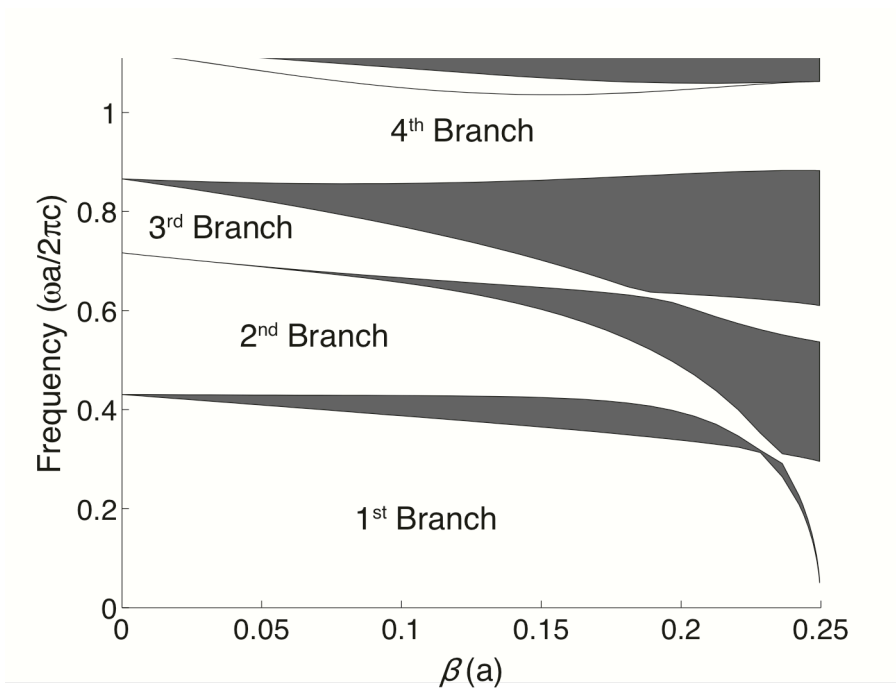

Figure 4.5 Gap map of the LTPC for entire tunable β. Gray shaded region indicates the stopband and White region represents passband.

typical form that is appropriate to its lattice size and inclusion. There is no more resonance gap because the cavity to resonate is isolated by rigid square-hollow square inclusion. The first branch, the blue solid line on the bottom of the Y-axis, is now become a numerically trivial solution generated by the isolated cavity.

Figure 4.5 shows the collection of the stopbands along the β variation. Gray shaded area represents stopband for specific β and blank regions are passband, *i.e.*, intervals between two branches of Figure 4.4 are replaced by gray region in Figure 4.5. There are no gray area for $\beta = 0$ because all branches are connected somehow in spite of the deaf or folded branch. Then, stopbands grow with increasing β. Particularly, the lowest gap region becomes zero again for $\beta = 0.2287a$, and then it turns to resonance gap. Detailed transition of this region will be discussed in the next section.

4.4.2 Transmission Spectra of the LTPC

As emphasized repeatedly in previous sub-section, the transmission analysis is a core and essential tool for understanding the LTPC. The dispersion diagram for the unit LTPC provides restrictive information, which is caused by methodological limitation. There is a huge passband for entire β, whose normalized frequencies are located from 0.8838 to 1.060, see Figure 4.5. Considering the dispersion diagrams only, therefore, the LTPC seems to be not useful. To take out the invisible stopband of the LTPC, the transmission scanning analysis is required.

Figure 4.6 shows the FEM definition of transmission analysis, (a), the transmitted power spectra (TPS) map, (b) and pressure field of three representatives, (c), respectively. For Figure 4.6 (b), power transmission is displayed in decibels. Black region signifies that a transmission of a specific β and frequency is blow the -40 dB, *i.e.*, non-propagating band; on the other hand, white one means that acoustic power is transmitted losslessly through the LTPC, *i.e.*, passband. Some periodic gray zones, passband but not transmitted perfectly, are

caused by thickness resonance from the finitely arranged PC structure. This thickness resonance occurs only for passband. As already mentioned in Chapter 2, therefore, slight fluctuation of the transmission is a proof that corresponding branch is a passband.

Three representative situations are studied and their results are plotted in Figure 4.6 (c). The point A, point B and point C stand for passband, the Bragg gap and the resonance gap, respectively. These three situations have totally different pattern of pressure field. For the point A, a plane wave propagates from left to right without decay and maintains its wave front; for the point B, a plane wave maintains its wave front but decays through the PC structure and finally there is no transmission after the structure. Pressure of the point C is quite different pattern from the others. Relatively very large magnitudes of pressure, plus or minus, are located in the cavity of the LTPC and plane wave decays very fast. This is a typical pressure pattern of the resonance gap. As introduced just before, the easiest way to distinguish an acoustic wave passing through the PC is watching pressure pattern of the wave inside the PC structure. Although there are other methods such as eigen-mode check for unit cell analysis, the method applied in Figure 4.6 (c) is not only the clearest but also most convenient way to discriminate; and it is physically correct for checking whether a wave propagates because actual harmonic wave is excited directly for the FEM.

Comparing Figure 4.6 (b) and Figure 4.5, overall, these two gap maps are very similar to each other except two the major disagreements. First and the most noticeable one is the region in the normalized frequency range of 0.7165–1.111 with the entire β. This region corresponds to the 3rd and 4th branch of the Figure 4.4, the green and magenta line respectively. Transmission of the region, therefore, should be the same as any other passband. From Figure 4.6 (b), however, there are some very low transmission areas for low β even though they correspond to the pass branch. The low transmission region still exists for very low β in spite of the asymmetric sub inclusions, *i.e.*, scattering effect of the formerly symmetric sub

inclusions still affects wave propagation. Although this band seems to be a stopband, it is a definite passband because obvious proof of the passband, frequency-wise transmission fluctuation, is observed for most β range. Additionally, unlike most passband nor stopband, transmission ratio of the 3rd and 4th branch varies with β, from under -40 dB to 0 dB. This behavior of the Bragg-gap-like passband cannot be predictable by dispersion diagram. Acoustic blocking performance of the LTPC should be evaluated by the transmission analysis not by dispersion diagram. Also a tuning programming shall be planned using the transmission map, Figure 4.6 (b). From this result, therefore, the LTPC can be used to attenuate the acoustic wave in a frequency range of 0.7165–1.111 though passband branches exist in dispersion diagrams. As a result, the LTPC guarantees that there is at least one β to prevent propagation of an arbitrary acoustic wave in a frequency range of 0.0926~1.111. For example, appropriate β for blocking normalized frequency 0.9257 is $0<\beta<0.0394a$. Unfortunately, there is no unitary β for attenuating total frequency zone at once, but combination of some DTPCs whose β is different can broaden the stopband of the LTPC structure; this subject will be discussed in next chapter.

Second and the minor difference is bandgap region between the 1st and 2nd branch, whose β and frequency are ranged of about 0.079–0.22a and 0.322–0.404, respectively. According to Figure 4.5, this region is a definite Bragg gap but transmission pattern is quite different to other bandgaps. For the LTPC, in general, transmission of the stopband, both the Bragg gap and the resonance gap, is below than -40 dB and independent on β. But the transmission of this region is not low as much as other typical stopband and it seems to be relevant to β. Exactly speaking, a bandwidth of the gap varies with its β and a transmission ratio is determined by the bandwidth. This phenomenon, unfortunately, is hard to explain and it exceeds covering range of this thesis. Form an aspect of application, this gap region can be covered perfectly by the other β such as $0.2362a< \beta< \beta_{max}$. So this region has no merit for practical usage.

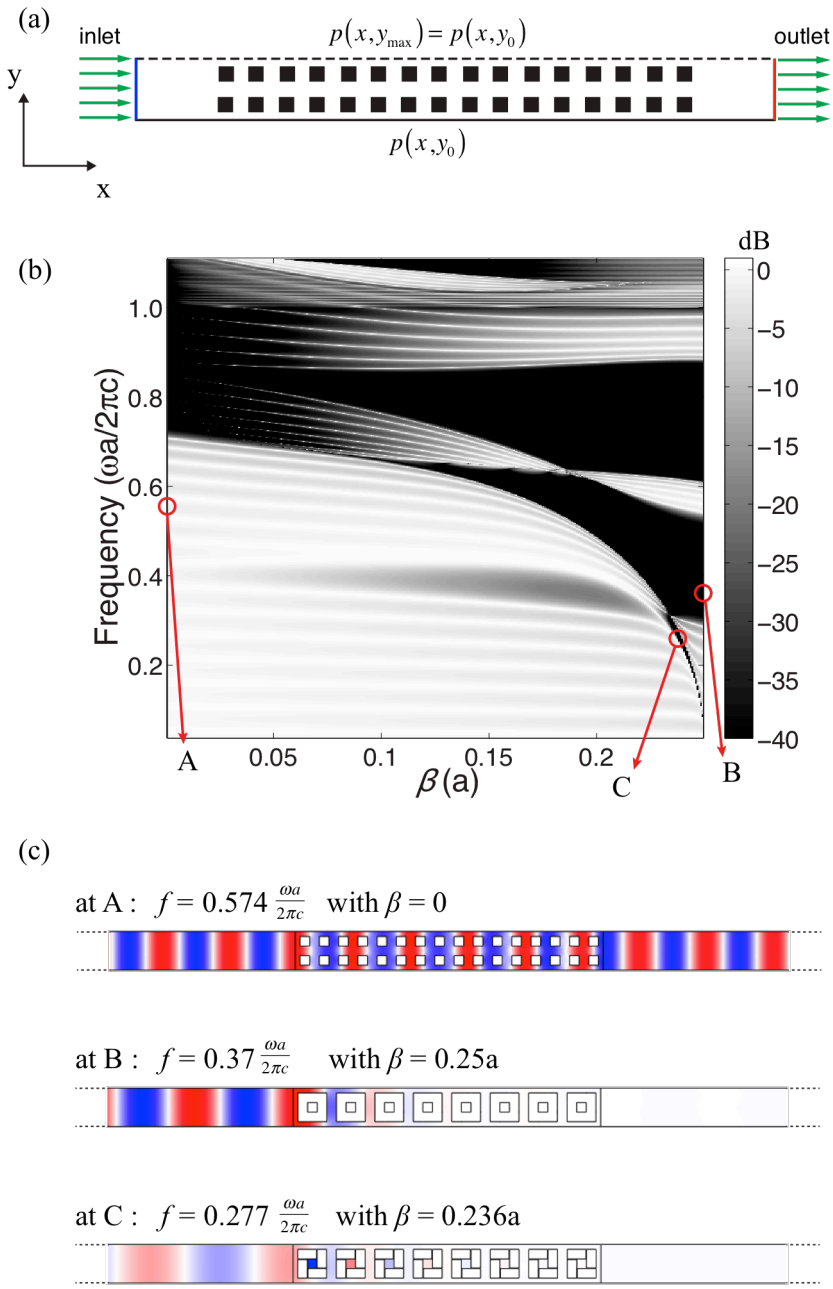

Figure 4.6 Finite element analysis to obtain the transmission map of the LTPC for entire tunable range of β. (a) problem definition, (b) obtained transmission map, (c) pressure field for three interesting points.

4.4.3 Detailed Transition Analyses on the Resonance Gap Region

Transitional patterns of both dispersion curve and transmission accompanied by varying β are particular phenomena of the LTPC. In two limit case—β=0 and $\beta=\beta_{max}$, there are only typical Bragg gaps. Dispersion curves, however, are deformed continuously by varying β. During the transition of dispersion curves, the resonance gap is revealed and vanished for specific range of β. In this sub section, more detail studies about generation and degeneration of the resonance gap will be presented. A comparison of transmission map and analytic estimation for the resonance gap will also be discussed.

Figure 4.7 shows six representative βs and their dispersion diagrams near the generation and degeneration of the resonance gap. And four capital alphabets inside the figure are frequency selected to survey transmission of some different βs and their results are plotted in Figure 4.8. The β=0.2047a, Figure 4.7 (a), indicates transitional state just before the generation of the resonance gap. The frequency A and B are selected for checking pressure pattern of their assigned gap, the Bragg gap. Interestingly, these gaps are regarded as the Bragg gap, nevertheless pressure pattern are quietly different to each other. Pressure localizations at cavities are definitely observed at frequency A but slightly at B. Frequency A, therefore, belongs to not only the Bragg gap but also the resonance gap. Using Equation (3.24) with n=4, an estimated resonance frequency is 0.5417 and this is close to frequency A. Although frequency A, 0.4813, is not perfectly matched to the estimated one, 0.5417, it is possible to claim that frequency A exists within a range of the resonance gap. This is because the cavity resonance is formed as a stopband having finite bandwidth for the phononic crystals and the actual resonance gap tends to be located lower than the estimated one for small β, which means that the LTPC is away from ideal condition of the Helmholtz resonator. The error between estimation and actual one tends to increase extremely for decreasing β. This irregularity, mismatch between the estimation and the actual resonance gap, will be discussed later of this sub-section. On the other hand, frequency B representing the

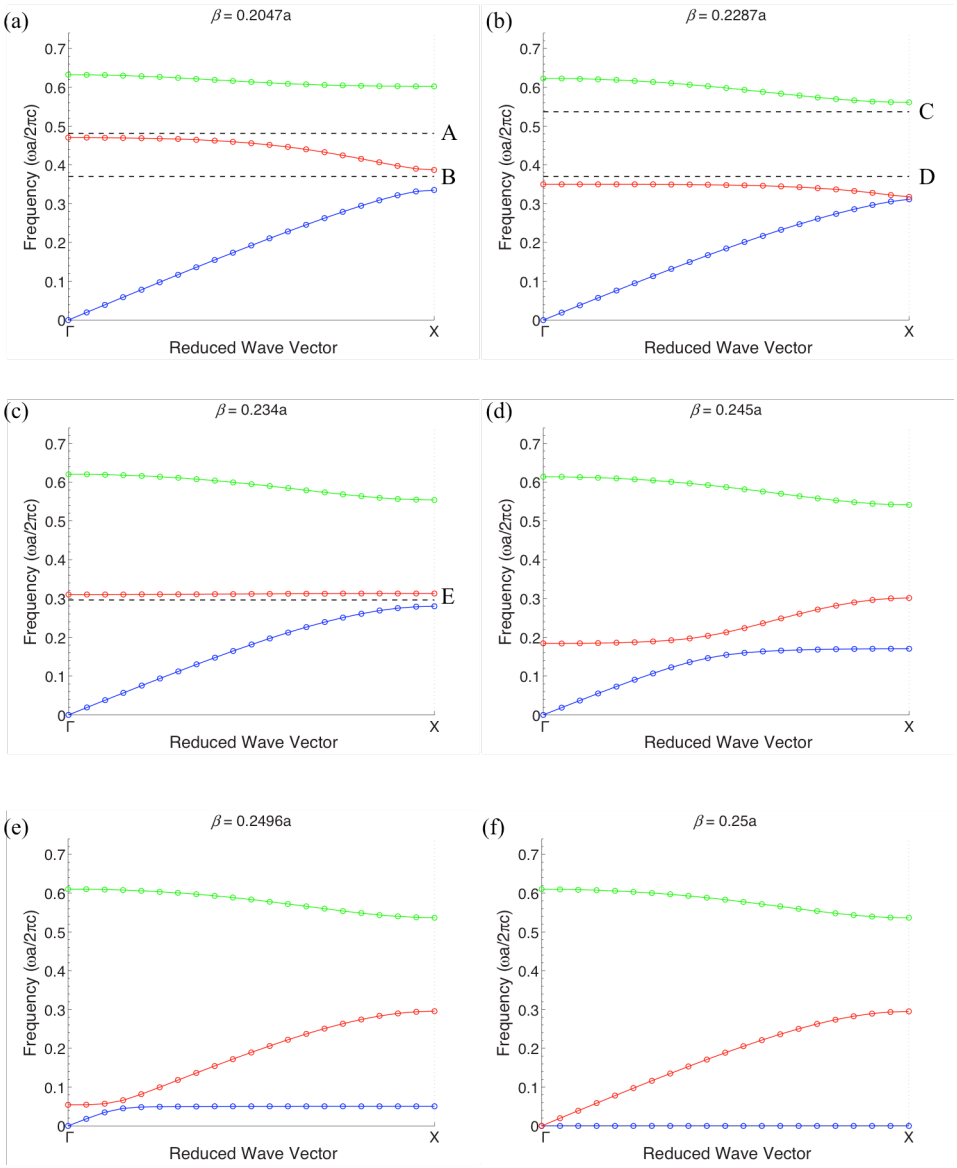

Figure 4.7 Dispersion diagrams for explaining characteristic of the resonance gap region.

1st stopband is not a resonance gap though some cavity localizations are found in the Figure 4.8. It is because that amplitude of the localized pressure in the first left cavity is not large enough to become a resonance, *i.e.*, the localized pressure does not act as an obstructer for wave propagation any more. Furthermore, even the amplitude of some other frequencies belong to the same stopband is smaller than the incident pressure.

Next, Figure 4.7 (b) indicates disappearance of the 1st stopband, *i.e.*, 1st and 2nd branches are attached to each other at the reduced wave vector $k=\pi/a$. For this situation, an estimated resonance frequency is 0.372 and frequency D, 0.370, is very close to it. As presented in Figure 4.8, pressure localization is observed in cavities and transmission pattern of the frequency D is similar to frequency A not B despite the same frequency. Meanwhile, the pressure pattern of frequency C, 0.537, is similar to frequency B, even though frequency C and D belong to the same stopband region. It means that this stopband region is naturally the Bragg gap and the resonance gap coexists within the Bragg gap. Then the resonance gap becomes a major factor of wave disturbance rather than the Bragg gap.

Figure 4.8 (c)–(e) show transition of the resonance gap. After the Figure 4.8 (c), the resonance gap becomes a solely dominant factor of the 1st stopband and its bandwidth decreases gradually with β shrinking; and it vanishes at the final stage, $\beta=\beta_{max}$. In the final stage, for the reminding, 1st branch is a set of numerically trivial solutions caused by isolated cavity.

A zoomed transmission map from Figure 4.6 (b) is presented in Figure 4.9, range of β is 0.2205–0.2488a and range of frequency is 0.037–0.370. Detailed

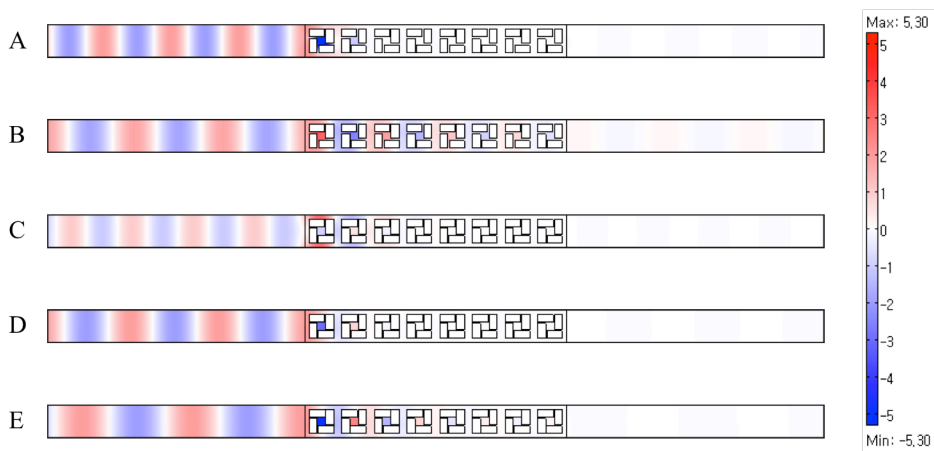

Figure 4.8 Pressure field of LTPC structure for frequency introduced in Figure 4.7. Pressure scales of all the results are in common.

transition of the resonance gap can be observed in Figure 4.9. Bandwidth shrinking of the resonance gap along the β increasing is also revealed clearly and it is much easier than the dispersion diagrams to understand a transitional characteristic of the resonance gap of the LTPC. The red-solid line represents analytic estimation by Equation (3.24) and it can be rewritten for this problem with respect to Hz form as

$$f_{est} = \frac{2c}{\pi}\sqrt{\frac{2(0.5\alpha - \beta)}{\alpha^3}} \tag{4.2}$$

This estimated normalized-frequency, f_{est}, successfully indicates the center of the resonance gap for large β. However, interval between the red line and the actual center of the resonance increases by decreasing β. Actually speaking, the estimation is no longer valid for β<0.245a because a resonator is no longer an ideal Helmholtz resonator in this range. To overcome this problem, the regression

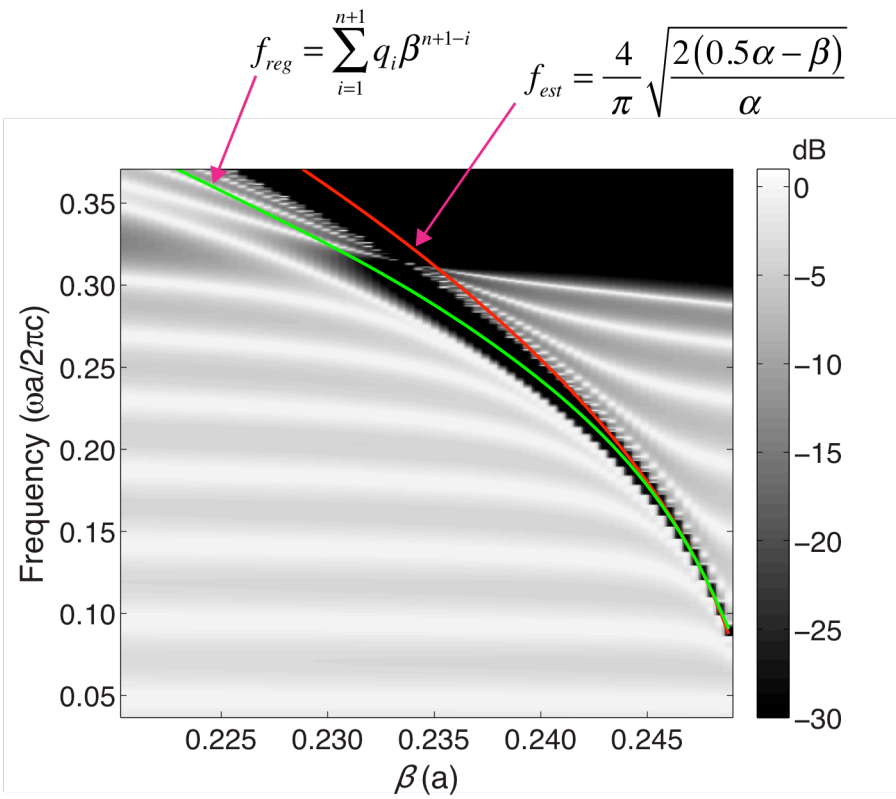

Figure 4.9 Zoom of the transmission map with two solid lines calculated by two different estimating equations.

analysis is needed to derive a new equation of numerical estimation based on actual transmission map. Polynomial form for regression analysis can be written as

$$f_{reg} = \sum_{i=1}^{n+1} q_i \beta^{n+1-i} \tag{4.3}$$

where q_i is the coefficient of regression and n is the degree of the polynomial and it is selected as 6 for this research. The polynomial curve whose n is less than 6 cannot reflect whole resonance gap. The nonlinear least square method[53] was used to calculate coefficient q_i. The calculated values are presented in Table 4.1 and completed new estimation curve is plotted as a green solid line in Figure 4.9. The new estimation line, of course, is coincident to centerline of the resonance gap. This numerical estimation curve is very useful to obtain a specific β for an arbitrary target resonance frequency, and it will be practically applied to design a LTPC structure in the next chapter.

Table 4.1 Coefficient of the regression equation.

Coefficient	Value
q_1	-2.0705×10^{9}
q_2	3.7681×10^{9}
q_3	-2.1870×10^{9}
q_4	6.7684×10^{8}
q_5	-1.1781×10^{8}
q_6	1.0934×10^{7}
q_7	-4.2277×10^{5}

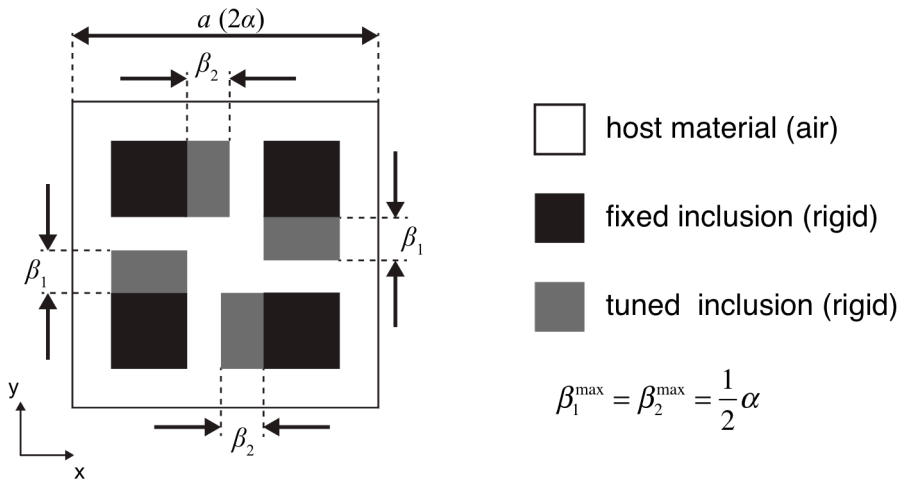

Figure 4.10 Separation of tuning parameter β into β_1 and β_2 for modification of tuning method.

4.5 Modification of Tuning Method

So far, simultaneous modification of all sub-inclusions has been discussed and its acoustic characteristic, emphasis on the transmission, was investigated. In this section, completely different transmission map will be obtained by simple modifications from the original tuning method. The new tuning method consists of two alterations. Four sub-inclusions now deforms separately by two independent groups with different sequences, and touching on it, the original tuning parameter β is also divided into β_1 and β_2 and they are in charge of tuning parameter of each deforming group, see Figure 4.10. Advantage of this modification is that totally different transmission response from the original one can be achieved only by different sequencing without overall mutation of tuning scheme.

Figure 4.11 shows two different modified tuning schemes. Basically, these two schemes are same but the only difference is sequence of deforming. Both ends of the modifications are same as the original one. There are two major motivations for this additional modification. One thing is enlarging the effective inclusion size and another is doubling the effective cavity size. For state III of both modification A and B, as a result, the effective area of combined sub-inclusions is three times

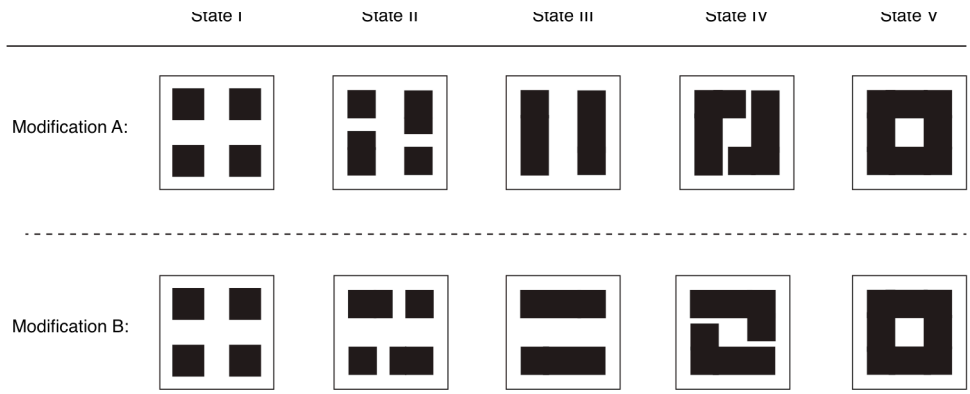

Figure 4.11 Scenarios of modified tuning method.

larger than the original one. Moreover, for modification B, the effective lattice size is already fully developed for horizontal direction. This makes huge difference of the transmission map between modification A and B. It will discuss later part of this section.

Secondly, doubling the effective cavity area can be achieved just like state IV. According to Equation (3.24), effective cavity area becomes double when the number of neck, n, is cut in half, then the resonance frequency will be dropped down as much as $1/\sqrt{2}$ against the original method for same β. And there is supplementary effect that bandwidth of the resonance gap is slightly enlarged.

The TPS maps of each modification are collected in Figure 4.12. For convenience, the TPS maps for both β_1 and β_2 are plotted at once as varying sequence of two tuning parameters. In case of modification A, β_1 increases first from 0 to 31.75 mm, and then β_2 increases as same amount as β_1 with the fully increased β_1; and vice versa for modification B. Although the only two differences are dualized deformation of inclusions and its sequence, transmission characteristics of each tuning methods are not only dissimilar to the original but also to each other. Same transmission pattern of deaf branch, transmission gradually increases with respect to β_2 increasing, can be also observed in both Figure 4.12 (a) and (b); and the transmission pattern is revealed in range of β_1 only. The deaf branch can be revealed when the periodicity of internal lattice is

duplicated as perpendicular direction of incident wave, *e.g.*, a vertically duplicated periodicity for a horizontally incident wave. Since the β_1 increasing breaks the duplication, the former deaf branch now becomes normal propagating branch gradually.

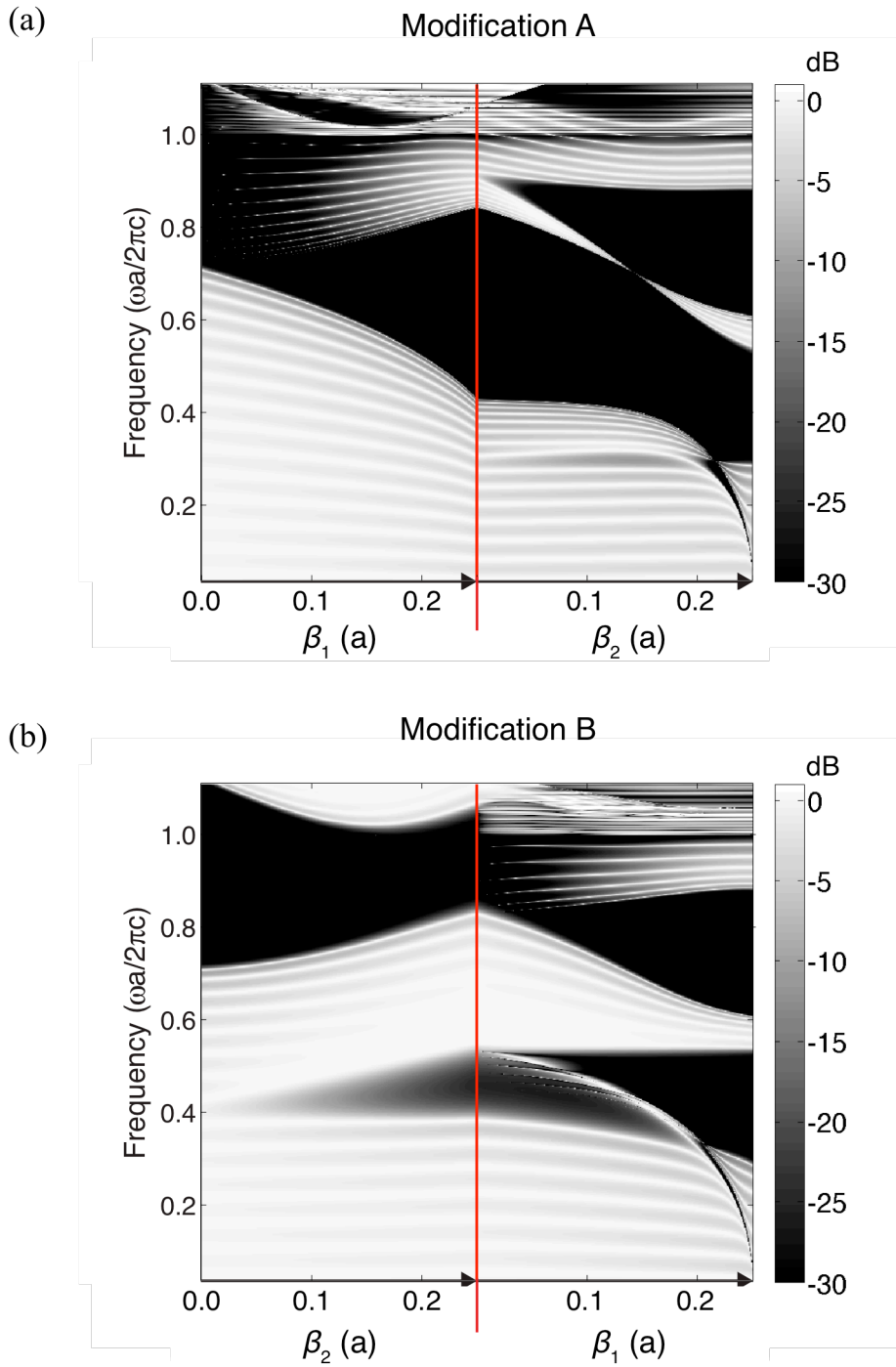

Figure 4.12 Transmission map of the modified tuning method. (a) modification A, (b) modification B. Red vertical line indicates Stage III.

4.6 Summary

In this chapter, a new tunable phononic crystal, LTPC, was proposed and numerically studied to understand its acoustic features. The new method is able to tune both the Bragg gap and the resonance gap by same tuning scheme, which deforms its four sub-inclusions by rotational symmetric and then it can make a lattice double and act as a resonator. Both dispersion diagram analysis and transmitted power spectra map were carried out and the results said

1. Tunable range of the Bragg gap in normalized frequency form, $\omega a/2\pi c$, is 0.296–1.111.
2. Tunable range of the resonance gap is theoretically 0–0.315 for the same superlattice. Its bandwidth, however, is relatively narrow than the Bragg gap, extremely narrow for low frequency.
3. Frequency-wise position of the resonance gap is just blow the first Bragg gap with overlapping region and also their β, tuning parameter, is almost in the same region, near the β_{max}.

Additionally, simply modified tuning schemes were also proposed and analyzed. Deformation of sub-inclusions was divided into two groups; and transition patterns of the transmission are very different from the original, according to different sequence of deformation. The division of the deformation provided doubled resonant cavity compare with the original. The resonance gap, therefore, could be formed in the lower frequency than the original in sprite of the same quantity of tuning parameter.

Chapter 5.

Design of Phononic Crystal System Using LTPC

5.1 Overview

All the phononic crystals (PC) discussed in previous chapters are under assumption of infinite periodicity. To realize stopband practically as a dispersion diagram informed, finitely at least 4–6 PCs are required. And there must be many passbands between stopbands unless the structure is filled with rigid material. This discontinuity of stopbands is the major restriction to utilize a PC for preventing broadband acoustic wave. To overcome this limitation, combination of several types of PC can be considered. The idea is very simple but sufficiently powerful because the stopband guarantees that an acoustic wave corresponding to the stopband cannot propagate through the structure. Total size of the PC structure, however, is determined by required individual PCs. This problem may be severe to the resonance gap because preventable bandwidth of the individual resonance gap is very narrow especially for a low frequency. On the other side of the resonance gap, a less number of unit cells can generate the effect of blocking wave than the Bragg gap. From a composite PC structure's perspective, this advantage may be reinforcement for narrowness of an individual resonance gap.

Everything mentioned so far in this overview section is connected to design of the PC structure consisting of the LTPC. The proposed LTPC is able to tune both the Bragg gap and the resonance gap using single tuning parameter, β. The PC structure, therefore, can be set up as sequential array of tuning parameters such as $\beta_1\beta_2\ldots\beta_n$ and this 1-D structure is infinitely arranged perpendicular to the longitudinal direction. The tuning parameter β now becomes a design variable and its combination becomes a design of the PC structure. Elements of the structure

may be selected by intuition originated from the acoustical information of the LTPC such as the dispersion diagram or transmission map. For the resonance gap, however, it is much hard to design a PC structure whose structural stopband is continuously overlapped by each narrow stopbands. To overcome difficulty of intuitive design, a numerical optimization may be helpful in designing.

This chapter consists of two major parts. Intuitive design using stopband information obtained from the previous chapter will be introduced first. This approach is able to take care of the most design problems considering the Bragg gap. As already mentioned before, however, there are some limits to design a PC structure aimed at combining resonance gaps. Next part, therefore, is applying design optimization to complement the intuitive design.

Table 5.1 Definition of Target Bands with respect to α=63.5mm

	Frequency (Hz)
Band I	250 – 1000
Band II	1000 – 2000
Band III	2000 – 3000

5.2 Design Objective and Selection of Target Band

Design objective of a new LTPC structure is to attenuate a multi-frequency acoustic wave. The target band will be defined to exceed the range of stopband of single-kind LTPC and designed structure must prevent waves of the entire frequencies inside the target band. The structure, therefore, must consist of more than two DTPCs.

Definition of the three target bands is introduced in Table 5.1 and Figure 5.1. To realized practical frequency band in Hertz range considering well-known 1/3

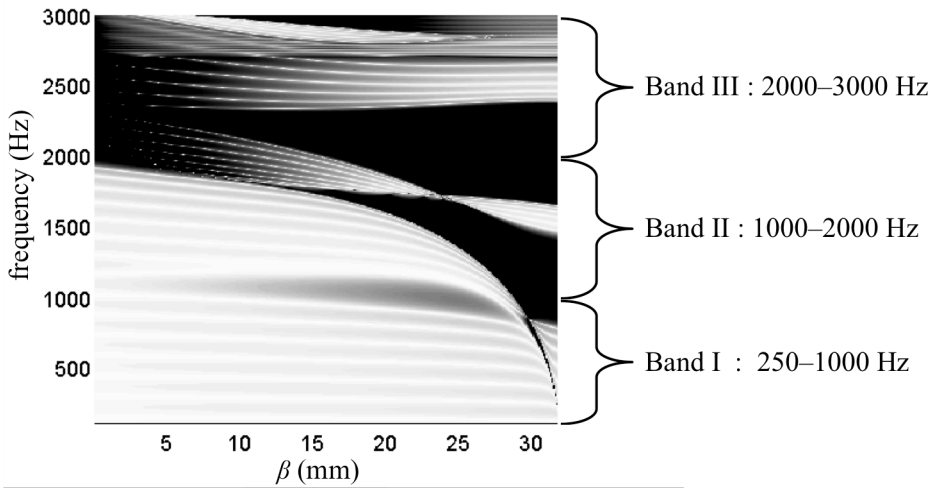

Figure 5.1 Definition of target band with transmission map of the original LTPC.

octave band 250–3000 Hz (instead of 3150 Hz), lattice size $a = 2\alpha = 127$ mm and speed of sound c = 343 m/s are selected hereafter. Practical frequency bands of several different cases for a and c are introduced in Table 5.2. The main portion of the Band I is the resonance gap and highest part of the Band I is overlapped by the lowest 1st Bragg gap region of $\beta=\beta_{max}$ ($0.25a$). Since the range of β for the resonance gap is very close to the β_{max}, these two regions are grouped into one, the Band I. As a bandwidth of the resonance gap is very narrow, designing a PC structure that is able to prevent the entire Band I is very hard to achieve. The Band I, therefore, will become a main issue of the designing. The Band II is equivalent to summation of the 1st and 2nd Bragg gap and a passband between them for $\beta=\beta_{max}$. A single-typed LTPC structure, therefore, cannot attenuate this target band, *i.e.*, there must be at least two different kind of the LTPC. The Band III, the last one, is identical to the entire 1st Bragg gap of $\beta=0$, so that there are no design issues when the target band is the Band III alone. The Band III is meaningful only when it is combined with the other bands.

Table 5.2 Practical frequency bands for representative examples.

Host material	c (m/s)	a (mm)	Band I (kHz)	Band II (kHz)	Band III (kHz)
normalized	1	1	0.092 – 0.370	0.370 – 0.740	0.740 – 1.110
air	343	127	0.250 – 1.000	1.000 – 2.000	2.000 – 3.000
air	343	12.7	2.500 – 10.00	10.00 – 20.00	20.00 – 30.00
air	343	2	15.88 – 63.50	63.50 – 127.0	127.0 – 190.5
water	1490	2	68.96 – 275.8	275.8 – 551.7	551.7 – 827.5
water	1490	1	137.9 – 551.7	551.7 – 1103	1103 – 1655
water	1490	127	1.086 – 4.344	4.344 –8.688	8.688 – 13.03

5.3 Structure Design using Acoustic Information of LTPC

Figure 5.2 shows a schematic diagram of the design problem. Any other conditions are totally same to the transmission analysis except the design part, sequential array of PCs. A design variable χ_i has a one-to-one correspondence with an individual LTPC and its tuning parameter β. Set of design variables are selected by a designer referring stopband feature of a corresponding β.

5.3.1 Design Target: Band I

The Band I is the lowest target band, 250–1000 Hz for α=63.5 mm, and its most part consists of the resonance gap. The remaining part, 850–1000 Hz, is lowest part

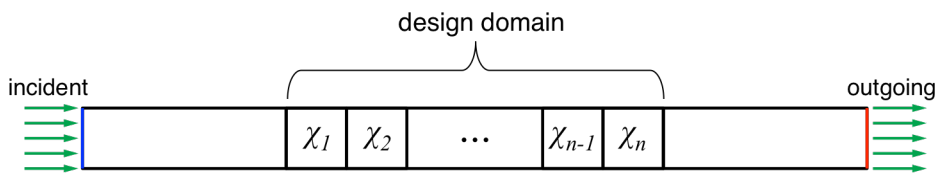

Figure 5.2 Schematic definition of design problem with design variables

of the first Bragg gap for $\beta \simeq \beta_{max}$ and its corresponding range of β is overlapped with the resonance gap's. It allows to, therefore, let the designer pay attention to the resonance gap region only.

Figure 5.3 shows selected design variables and its preventable bandwidth. The blue and vertical lines indicate β value, x-directionally, and bandwidth of its stopband, y-directionally. It is clear that the actual considering frequency band is covered by summation of y-directional projections of each blue line. This selection is based on numerical estimation Equation (4.3). From this estimation equation, at least 16 design variables are necessary to cover seamlessly the considering frequency band, 250–850 Hz, under the assumption that the resonance gap occurs for a single LTPC. Of course, this assumption is not appropriate but fairly valid to define the worst condition to design for the resonance gap. To realize the resonance gap normally, deployment of at least two PCs for each design variable is recommended, the more the better. In that case, however, whole structure will become too large, *e.g.*, over 4 meters for α=63.5 mm and n=16×2=32. So n=16 is fixed hereafter as standard number of the design variable to compare design methods.

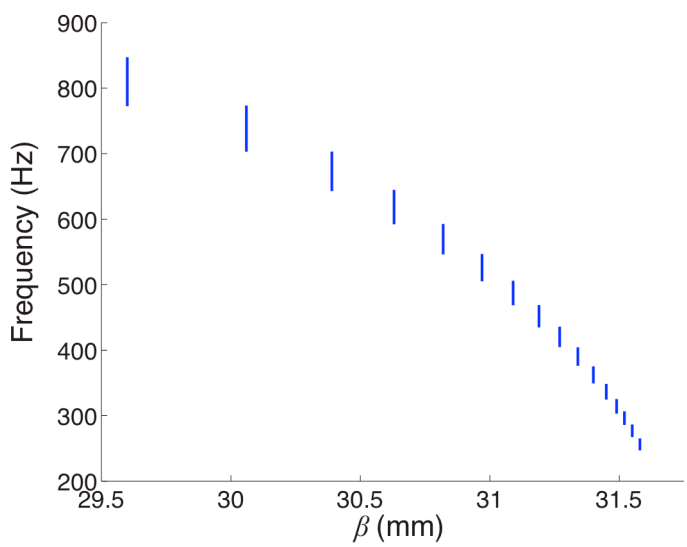

Figure 5.3 Selection of design variables to attenuate Band I and their coverable

Transmission spectrum for selected design variables is plotted in Figure 5.4 (b) and the design variables are indicated in Figure 5.4 (a), whose height corresponds its β value and numeric value above the square tip signifies its value. Since only one LTPC is assigned to each design variable, most frequency is well transferred; even transmission of 480 Hz is 0 dB, which means there are no transmission loss. Meanwhile, the range of 850–1000 is fully blocked because the Bragg gap is revealed successfully owing to many design variables resembling to β_{max}. From the Bragg gap's perspective, there are no significant difference in geometry of the inclusion between β_{max} and selected most design variables.

The result may inform a bad product but it also reports two important aspects to design for Band I. First, The Band I is extremely severe condition to design utilizing the resonance gap. Second, good design for other combined band including Band I such as Band I+II or Band I+II+III cannot be expected by using the same design method. This will be discussing in the next section.

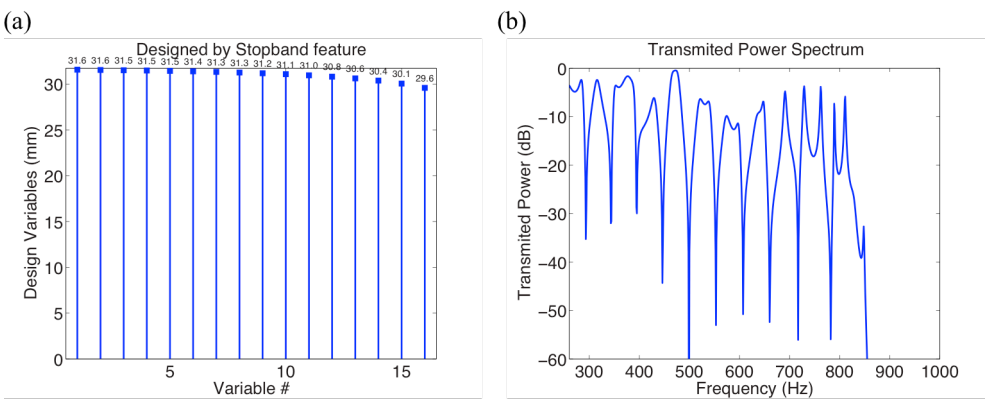

Figure 5.4 Result of stopband-based design for Band I. (a) selected design variables, (b) its transmission spectrum.

5.3.2 Design Target: Band II

Band II is in the range 1000–2000 Hz and the 1st and 2nd Bragg gap of β_{max} (31.75 mm) covers the most range of the Band II except 1400–1650 Hz. The frequency

range 1400–1650 is a typical passband for β_{max} but it turns to stopband when β=23.5 mm. Therefore, only two types of LTPC is needed to cover the Band II. Former part of the structure, β_1– β_8, consists of β=23.5 mm and later part, β_9– β_{16}, consists of β=31.75 mm.

Figure 5.5 shows selected design variables, (a), for Band II and its transmission spectrum, (b) in the same manner as Figure 5.4. Since the Band II is within the range of the Bragg gap, transmission loss is definite than the Band I. Most of transmissions within the Band II are under the -40dB, 1/10000; therefore it may conclude that the design for the Band II is successfully carried out. Designing of a target band including only the Bragg gap is much easier and more intuitive than including the resonance gap.

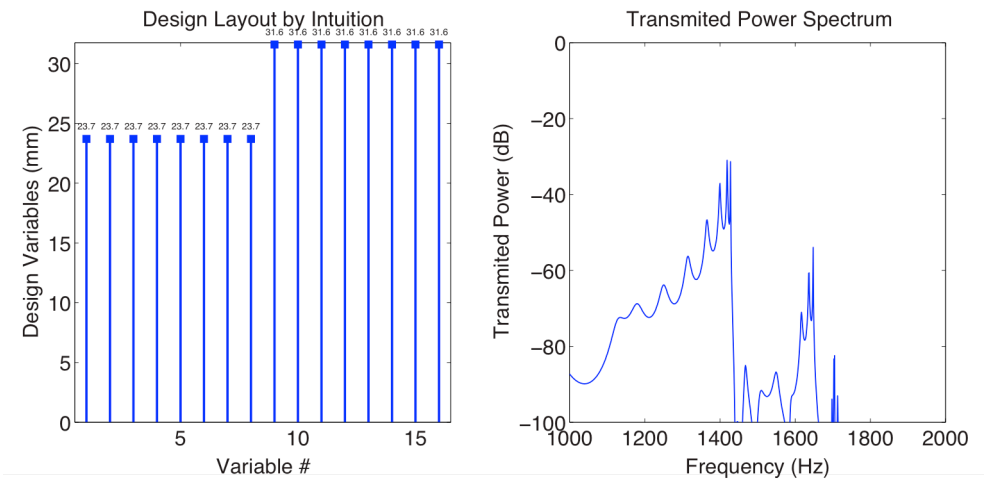

Figure 5.5 Result of stopband-based design for Band II. (a) selected design variables, (b) its transmission spectrum.

5.3.3 Design Target: Band II+III

Target frequency band is now expanded to higher region. Band III, 2000–3000 Hz, can be fully covered by β=0, whose 1st Bragg gap is 2000–3000. Therefore,

stopband for Band II+III can be easily achieved adding sufficient β=0 to reveal its 1st Bragg gap to the design for Band II.

Figure 5.6 shows selected design variables, (a), for Band II+III and its transmission spectrum, (b) in the same manner as Figure 5.4 and 5.5. Also the Band II+III is within the range of the Bragg hap, transmission loss is significant. Spectrum lines between Figure 5.5 (b) and 5.6 (b) are very similar to each other but their transmission magnitudes are very different; spectrum of the Band II+III is almost 30 dB lower than of the Band II's. Since the actual arranged number per design variable is smaller than the Band II, the effectiveness of the Bragg gap is weakened.

For example, in case of the Band II, number of β=23.5 was 8 but it is now 5 for the Band II+III.

Although some transmissions are increased than the Band II, the result may be enough to claim that the objective of the design is successfully accomplished unlike the case of Band I.

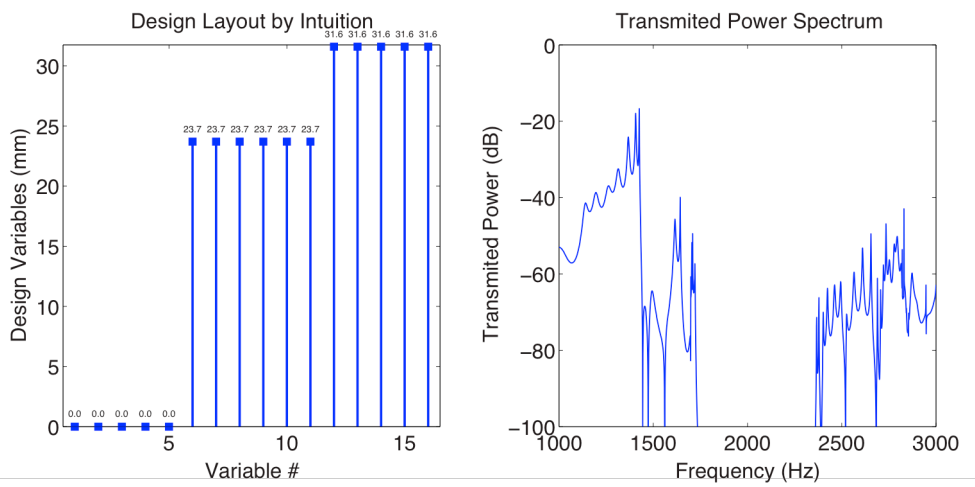

Figure 5.6 Result of stopband-based design for Band II+III. (a) selected design variables, (b) its transmission spectrum.

5.3.4 General Comments on Information-based Design Method

In this section, the information-based designs were carried out, which is based on stopband information that already obtained by dispersion diagrams and transmission analyses. Although the information-based design method could take care of the most design problem for the Bragg gap, a targeted frequency band containing the resonance gap region such as Band I was hard to design. Twice or triple large number of design variables than the original structure may solve this problem but this approach is undesirable because its size becomes also twice or triple. Unless this difficulty resolved, acoustic blocking structure utilizing the LTPC may become half-functional structure. Automatic design method, therefore, based on numerical algorithm to resolve the limitation of the information-based design is prepared as an alternative approach.

5.4 Structure Design using Optimization Algorithm

The numerical optimization is not far from the previous design problems. The only difference is that design variables are selected by numerical algorithm not a design person. All conditions except design subject, iterative optimizer, are totally equal to the information-based design.

5.4.1 Optimization Definition

An objective function is that a function used to evaluate design. For every possible design, the function returns a numeric value that indicates the evaluation of the design[54]. In a minimize problem, an optimizer tries design variables as low as possible in bound of satisfying its constraints. Design objective in this thesis is maximizing acoustic wave reduction for specific target band. Objective function, therefore, is defined as minimizing transmitted power of the acoustic wave and it

can be expressed as follows

$$\min\left(\sum_{f=f_l}^{f_u} P(\boldsymbol{\chi};f)\right) \tag{5.1}$$

where the objective function is considered in the frequency band between the lower frequency f_l and upper frequency f_u. The symbol $\boldsymbol{\chi}$ is the set of design variables defined as

$$\boldsymbol{\chi} = \{\chi_1 \quad \chi_2 \quad \cdots \quad \chi_n\} \tag{5.2}$$

with bound as

$$0 \le \chi_i \le \chi_{\max} \quad (i = 1, 2, \cdots, n) \tag{5.3}$$

There are no additional constraints except bound for the design variable and its upper limitation $\chi_{\max}$ is set to be 31.6 mm not $\beta_{\max}$ in order to void a instable meshing problem that caused by extremely narrow area.

The function P in the Equation 5.1 is transmitted power ratio between inlet and outlet of the structure. This function is perfectly same as used so far to calculate transmitted power spectrum in previous chapters and it can be rewritten for optimization form,

$$P(\boldsymbol{\chi};f) = \frac{W_{\text{out}}(\boldsymbol{\chi};f)}{W_{\text{in}}(\boldsymbol{\chi};f)} \tag{5.4}$$

where

$$W_{\text{out}}(\boldsymbol{\chi};f) = \int_{\Omega} \frac{p(\boldsymbol{\chi};f)\cdot p^*(\boldsymbol{\chi};f)}{2\rho c} \tag{5.5}$$

and

$$W_{\text{in}}(\boldsymbol{\chi};f) = \int_{\text{A}} \frac{p(\boldsymbol{\chi};f)\cdot p^*(\boldsymbol{\chi};f)}{2\rho c} \tag{5.6}$$

The Greek symbol alpha, A, and omega, Ω indicate integral line of the inlet and outlet, respectively. The symbol p represents pressure and p^* is complex conjugate

of the p. The density of air, ρ, is 1.21 m/s and the speed of sound, c, in air is 343 m/s.

The Sequential Quadratic Programming (SQP)[55] is selected as an optimizer for solving entire optimal design problems in this thesis. The SQP is well known iterative and gradient-based optimization algorithm. Sensitivities for updating each design variable are calculated numerically by the forward difference approximation method.

5.4.2 Optimization Target: Band I

Again the Band I is the lowest target band, 250–1000 Hz for α=63.5 mm and this target band is not well blocked by the information-based design. Unlike the former method, a new structure is regarded as non-periodic structure and its design variables vary freely without constraint of periodicity. Therefore, stopband information based on infinite periodicity is no more valid and not necessary. Once input an initial design variable, optimizer automatically finds local minimum iteratively using gradient of objective function.

Seven different optimization problem sets were carried out and their results are plotted from Figure 5.7 to 5.13. Each of subplots (a)–(d) indicates same information through those figures and after sub-sections. The subplot (a) and (b) indicate initial design variables and converged design variables respectively and numeric value above the square tip signifies its value. Variation of objective function value is plotted in subplot (c). Transmission spectra of both the initial and final design variables are plotted in (d). Blue solid line represents transmitted power spectrum of the initial and circular marks on the line are finitely selected frequency representing the Band I in order to apply to the objective function; its interval, Δf, is 5 Hz. Likewise, red solid line represents transmitted power spectrum of the final and plus marks, +, are same meaning of circular mark; its Δf is also 5 Hz. Note that the selected representative frequencies well reflect the solid-line

spectrum in most cases. Since the decreasing of Δf must cause a rise of computational cost, it is possible to claim that the selected interval, Δf=5 Hz, is fairly defined. Finally, subplot (e) represents transmission spectrum for selected frequencies that corresponds 1/3 octave band. Circular hollow and square solid marks indicate selected target frequency corresponding to 1/3 octave band of initial design and final design, respectively. Horizontal line passing through the mark is representative frequency band of 1/3 octave band.

Observing the optimization results, the multifarious final designs are obtained from different initials. Although there are some disappointing, transmission losses in most frequencies are increased compared to the initials. Among them, the case of Figure 5.11 is well designed for the lowest frequency band except the 250 Hz—there is no other fully transferred frequency.

Comparison between the information-based design and the best-optimized design for the same target band is presented in Figure 5.14. The blue-dashed line and red-solid line indicate transmitted power spectrum of the information-based design and the optimized design, respectively. For quantitative analysis, an evaluation value (*EV*) is imported, which can be fairly estimative and applicable to both design method. The evaluation value can be calculated by

$$EV = \sum_{f=f_l}^{f_u} P(\boldsymbol{\chi}; f) \quad (\Delta f = 1\,\mathrm{Hz}) \tag{5.7}$$

It is perfectly same to the objective function but frequency interval is fixed as 1 Hz. In fact, it is nothing more than a homogenization of frequency to scan.

From Figure 5.14, it may evaluate that the optimized design is better than the former design in general frequency band. Actually, the evaluation value of the optimized is about one-third of the former design.

By using optimization method, there are some improvements in designing for severe conditions. Not only the lowest part of the Band I but also the general range is relatively well prevented in comparison with the former design. This provides a beginning to expand target band including Band I such as Band I+II.

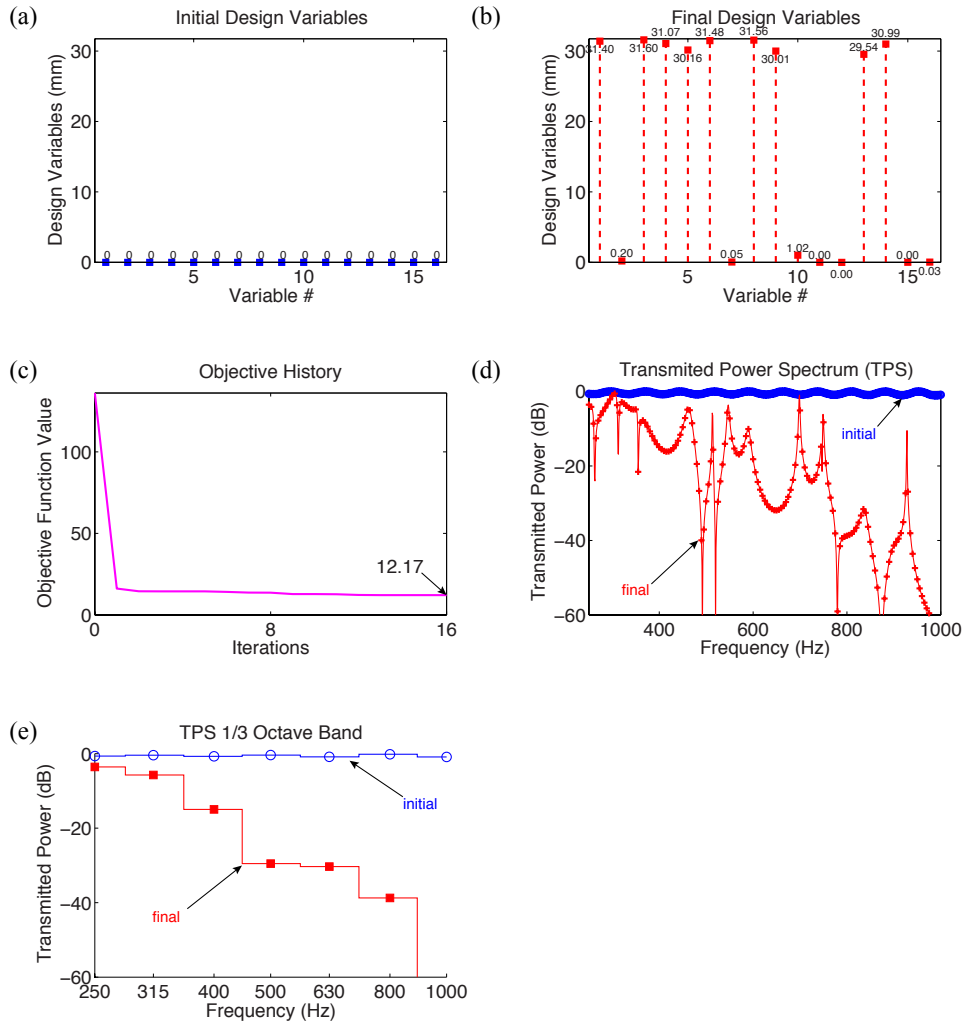

Figure 5.7 Result of design optimization for Band I with homogeneous initial design variable as 0 mm. (a) initial design variables, (b) converged design variables, (c) history of the objective function value, (d) transmission spectrum of the obtained design and the initial design, (e) transmission spectrum for one-third octave band.

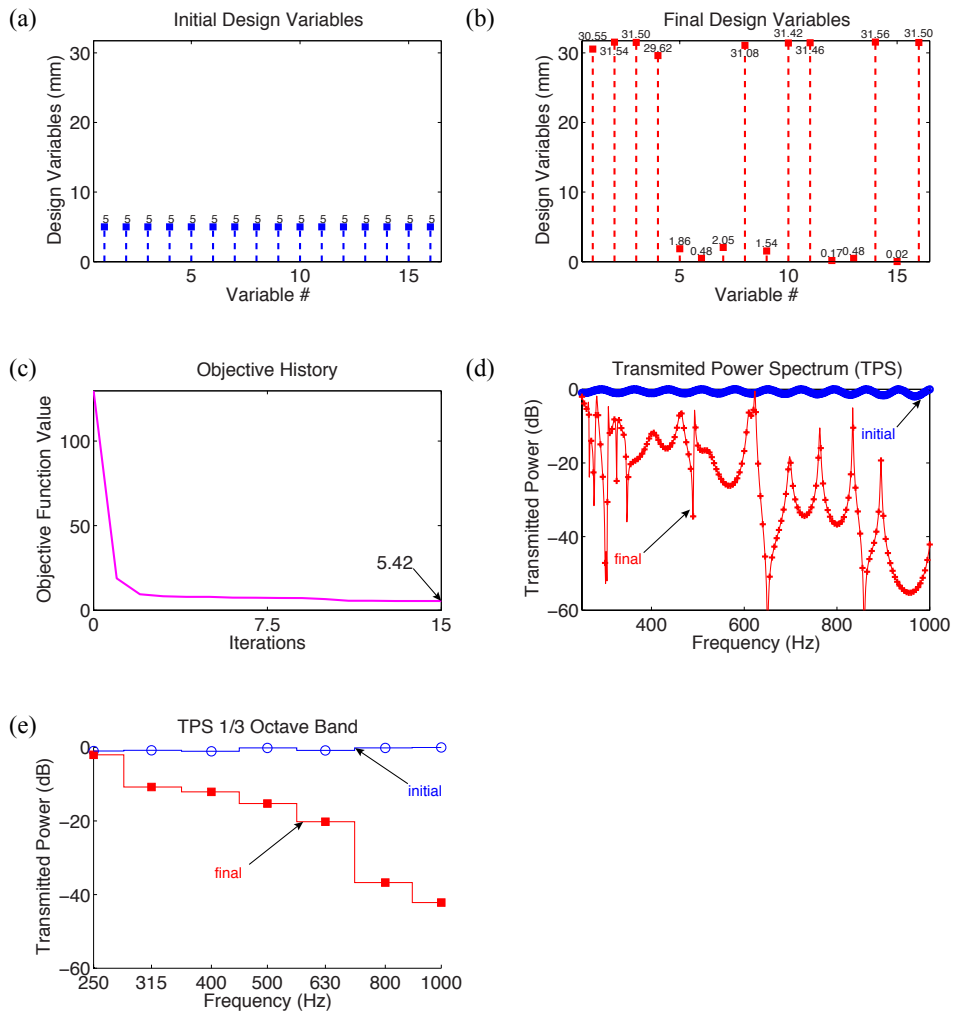

Figure 5.8 Result of design optimization for Band I with homogeneous initial design variable as 5 mm. (a) initial design variables, (b) converged design variables, (c) history of the objective function value, (d) transmission spectrum of the obtained design and the initial design, (e) transmission spectrum for one-third octave band.

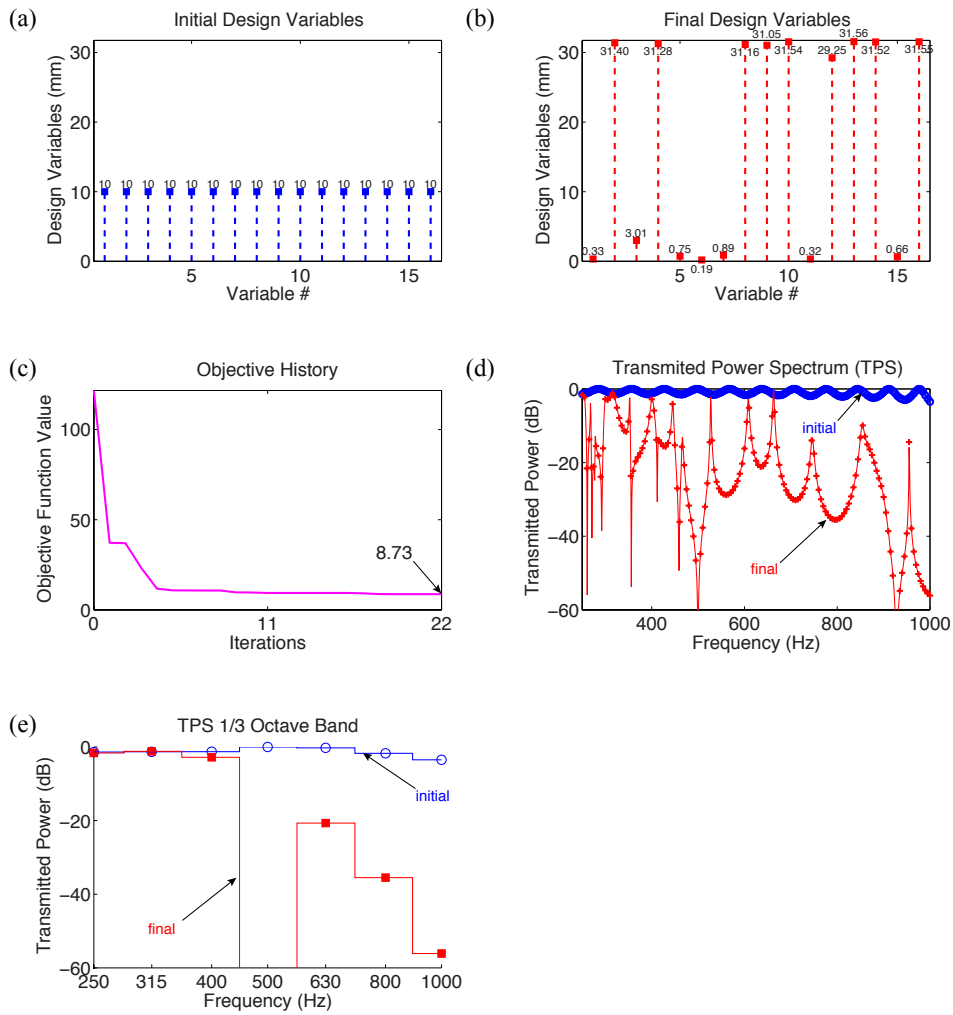

Figure 5.9 Result of design optimization for Band I with homogeneous initial design variable as 10 mm. (a) initial design variables, (b) converged design variables, (c) history of the objective function value, (d) transmission spectrum of the obtained design and the initial design, (e) transmission spectrum for one-third octave band.

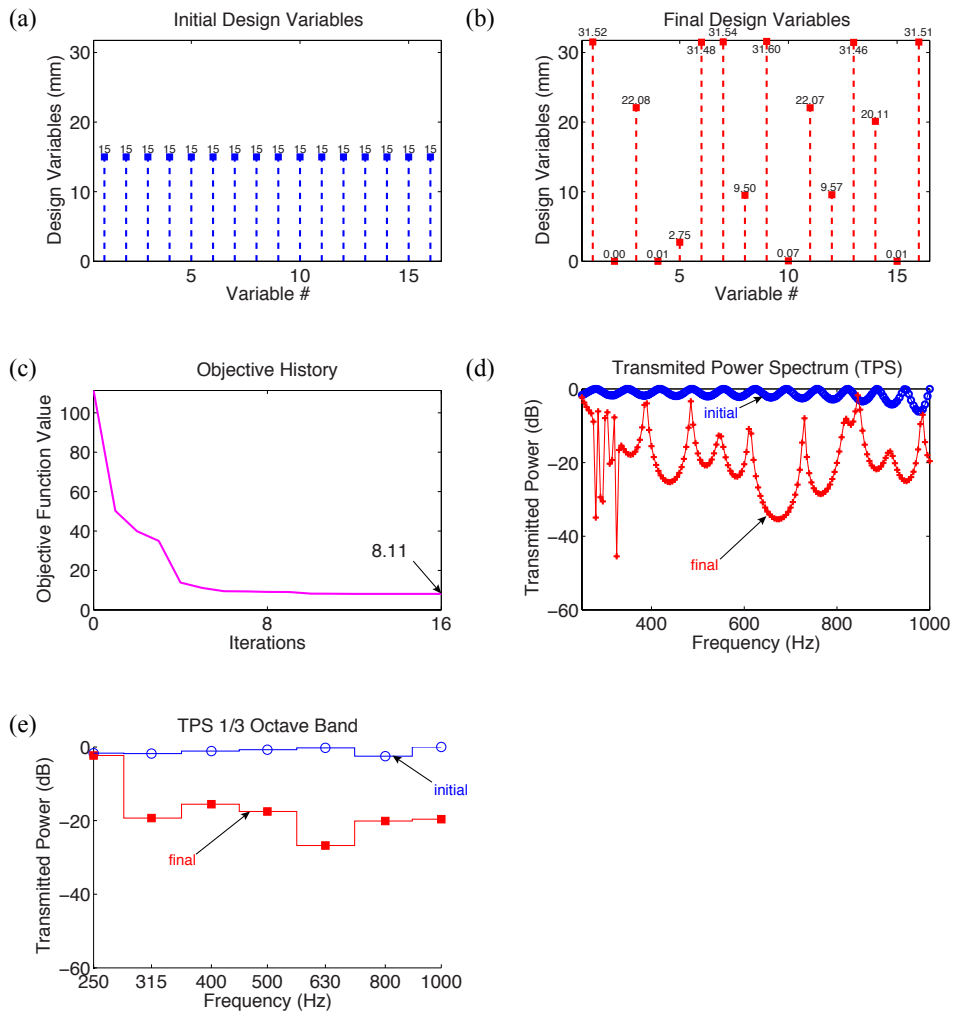

Figure 5.10 Result of design optimization for Band I with homogeneous initial design variable as 15 mm. (a) initial design variables, (b) converged design variables, (c) history of the objective function value, (d) transmission spectrum of the obtained design and the initial design, (e) transmission spectrum for one-third octave band.

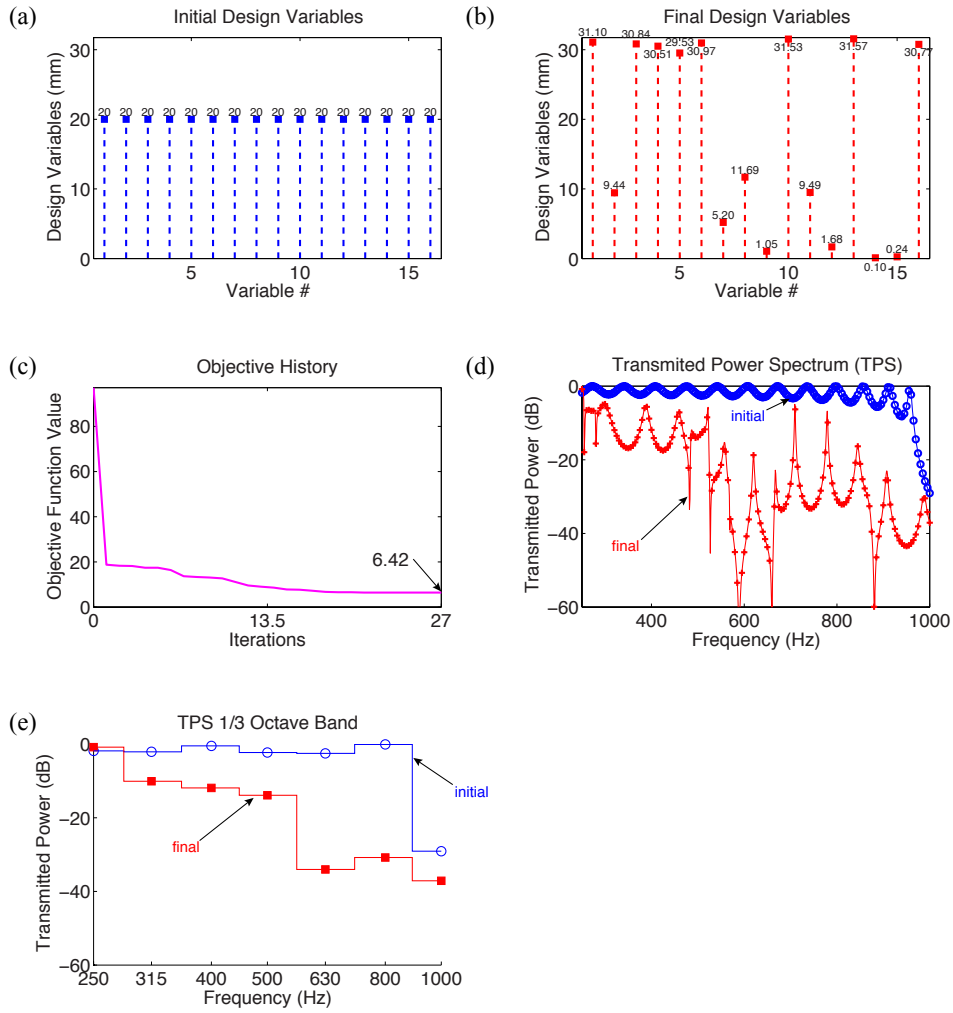

Figure 5.11 Result of design optimization for Band I with homogeneous initial design variable as 20 mm. (a) initial design variables, (b) converged design variables, (c) history of the objective function value, (d) transmission spectrum of the obtained design and the initial design, (e) transmission spectrum for one-third octave band.

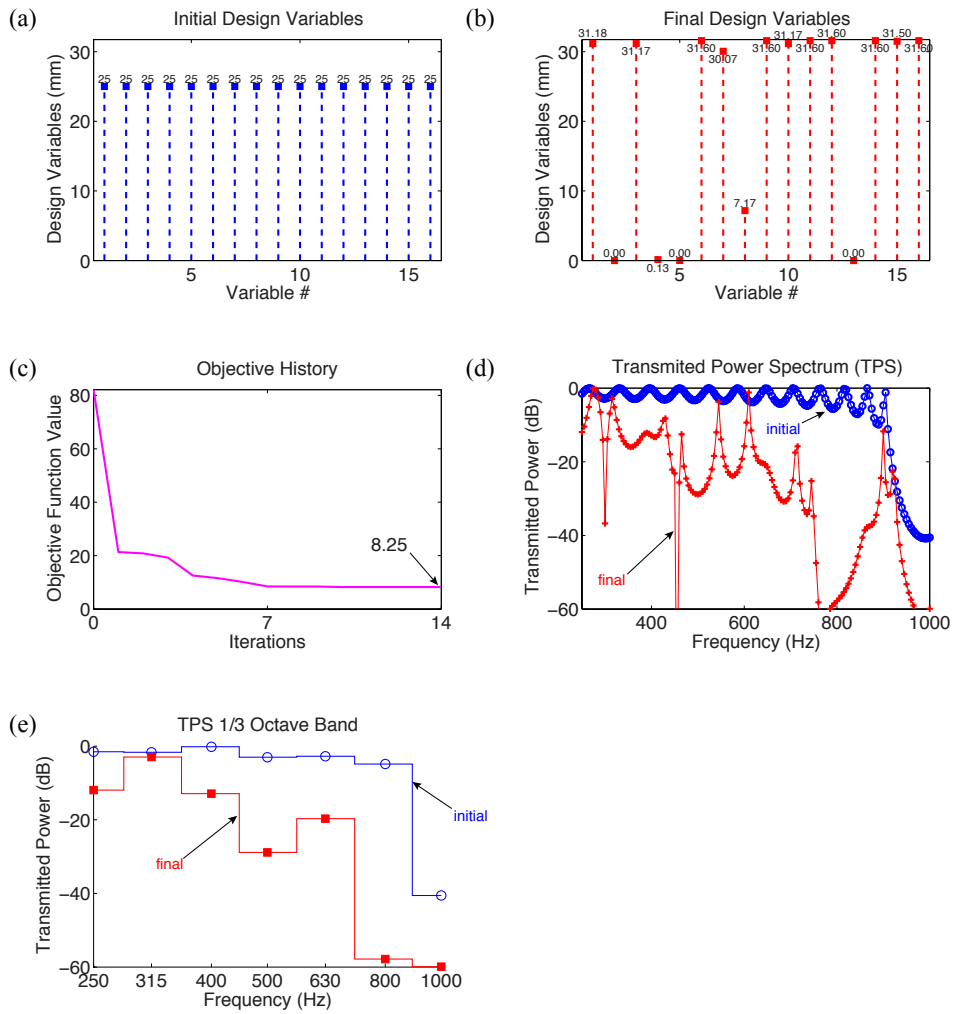

Figure 5.12 Result of design optimization for Band I with homogeneous initial design variable as 25 mm. (a) initial design variables, (b) converged design variables, (c) history of the objective function value, (d) transmission spectrum of the obtained design and the initial design, (e) transmission spectrum for one-third octave band.

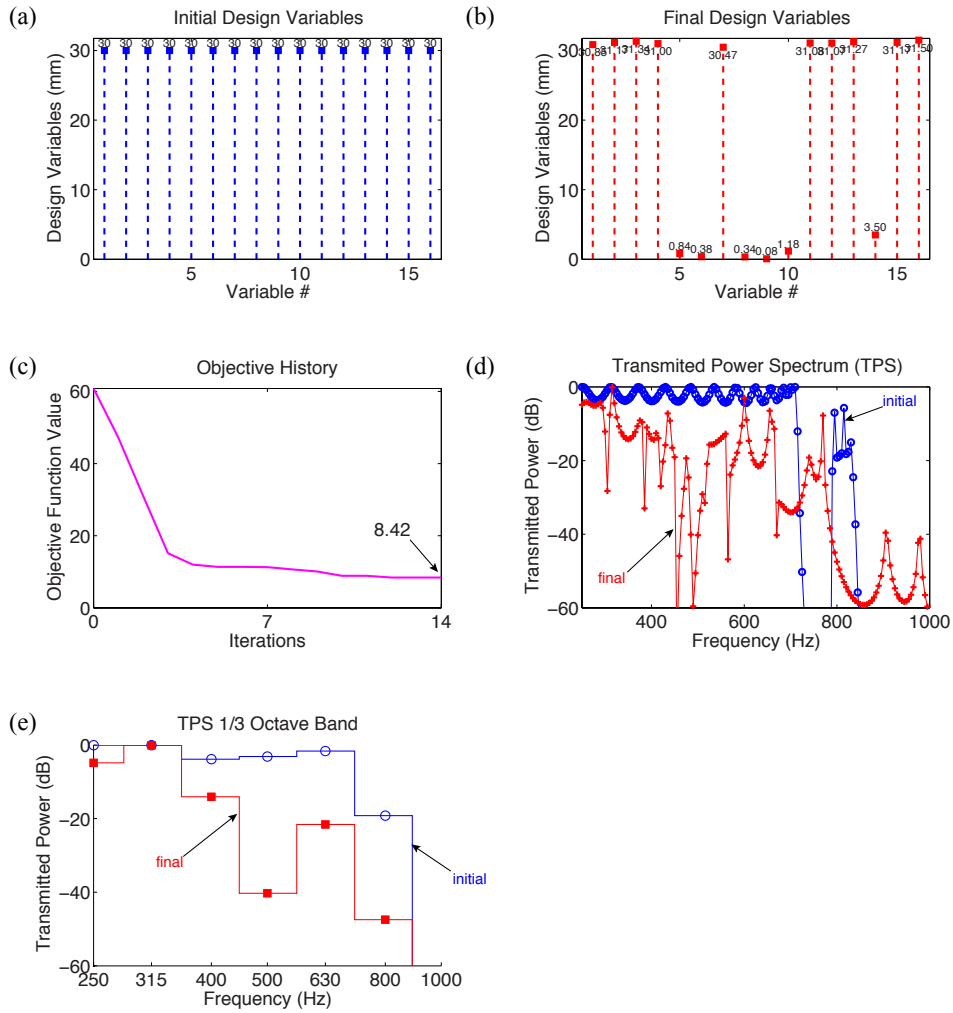

Figure 5.13 Result of design optimization for Band I with homogeneous initial design variable as 30 mm. (a) initial design variables, (b) converged design variables, (c) history of the objective function value, (d) transmission spectrum of the obtained design and the initial design, (e) transmission spectrum for one-third octave band.

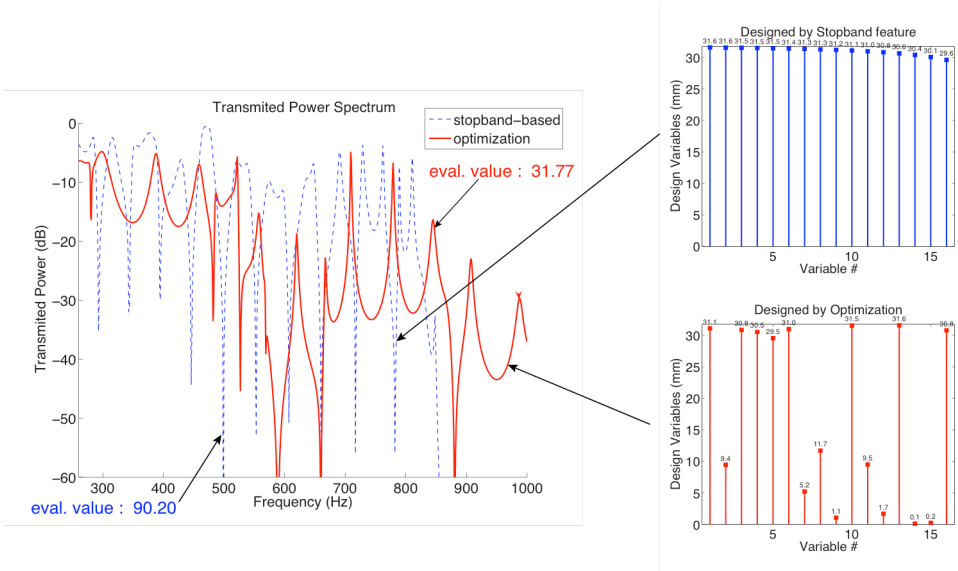

Figure 5.14 A comparison of transmission spectrum of stopband-based design and optimization design for Band I.

5.4.3 Optimization Target: Band I+II

A target band is now Band I+II, 250–2000 Hz, thanks to possibility from Band I optimization. Results are presented in Figure 5.15–18 in the same manner as the previous sub-section. Unlike the problem for Band I, relatively well-designed results are displayed only. Although the target band is more expanded than the Band I problem, spectrum result of Figure 5.17 seems to be better than Figure 5.11's; in addition, both initial design variables are all same as 20 mm. In fact, the evaluation value of Figure 5.17 is slightly larger than Figure 5.11— $EV_{5.17}$=37.9 and $EV_{5.11}$=31.8. Importing frequency average concept to the evaluation value, the superiority is reversed since bandwidth of the target band used in Figure 5.17 is almost twice larger than Figure 5.11— $EV_{5.17}$/1750=0.0217 and $EV_{5.11}$/750=0.0424.

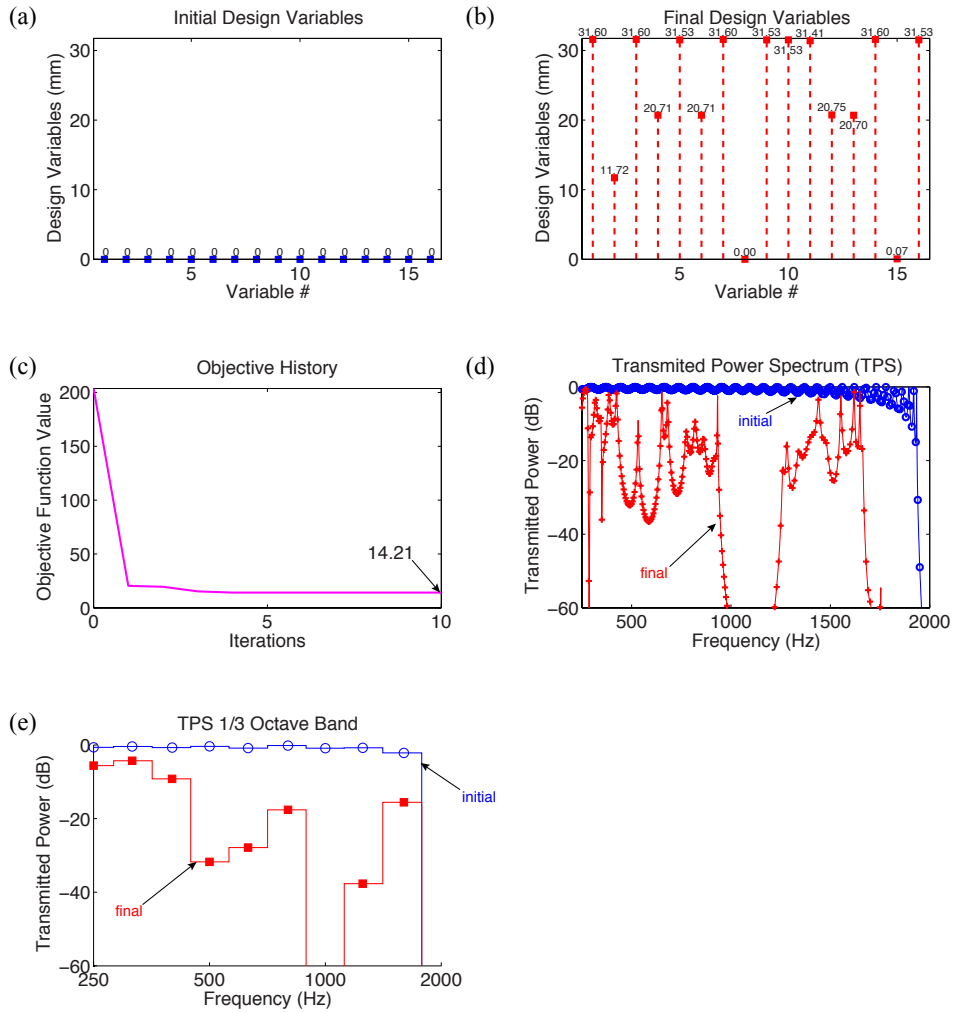

Figure 5.15 Result of design optimization for Band I+II with homogeneous initial design variable as 0 mm. (a) initial design variables, (b) converged design variables, (c) history of the objective function value, (d) transmission spectrum of the obtained design and the initial design, (e) transmission spectrum for one-third octave band.

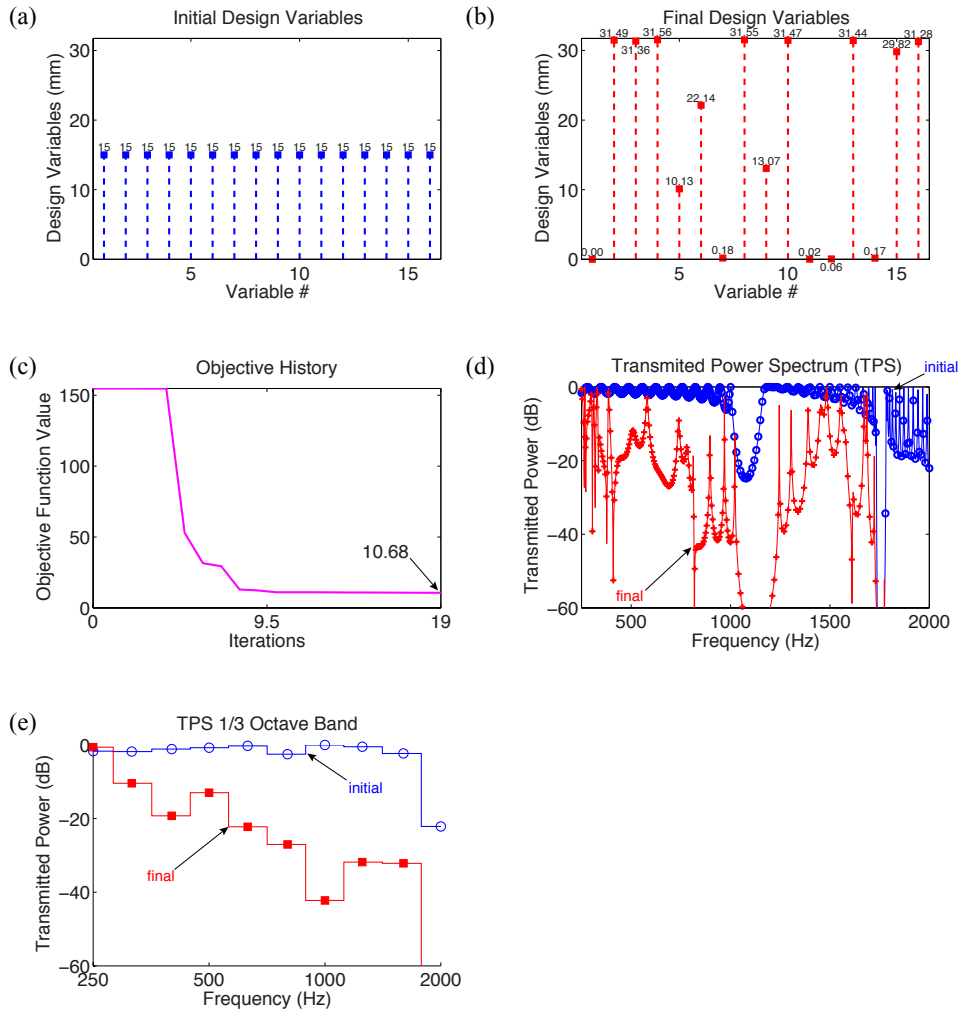

Figure 5.16 Result of design optimization for Band I+II with homogeneous initial design variable as 15 mm. (a) initial design variables, (b) converged design variables, (c) history of the objective function value, (d) transmission spectrum of the obtained design and the initial design, (e) transmission spectrum for one-third octave band.

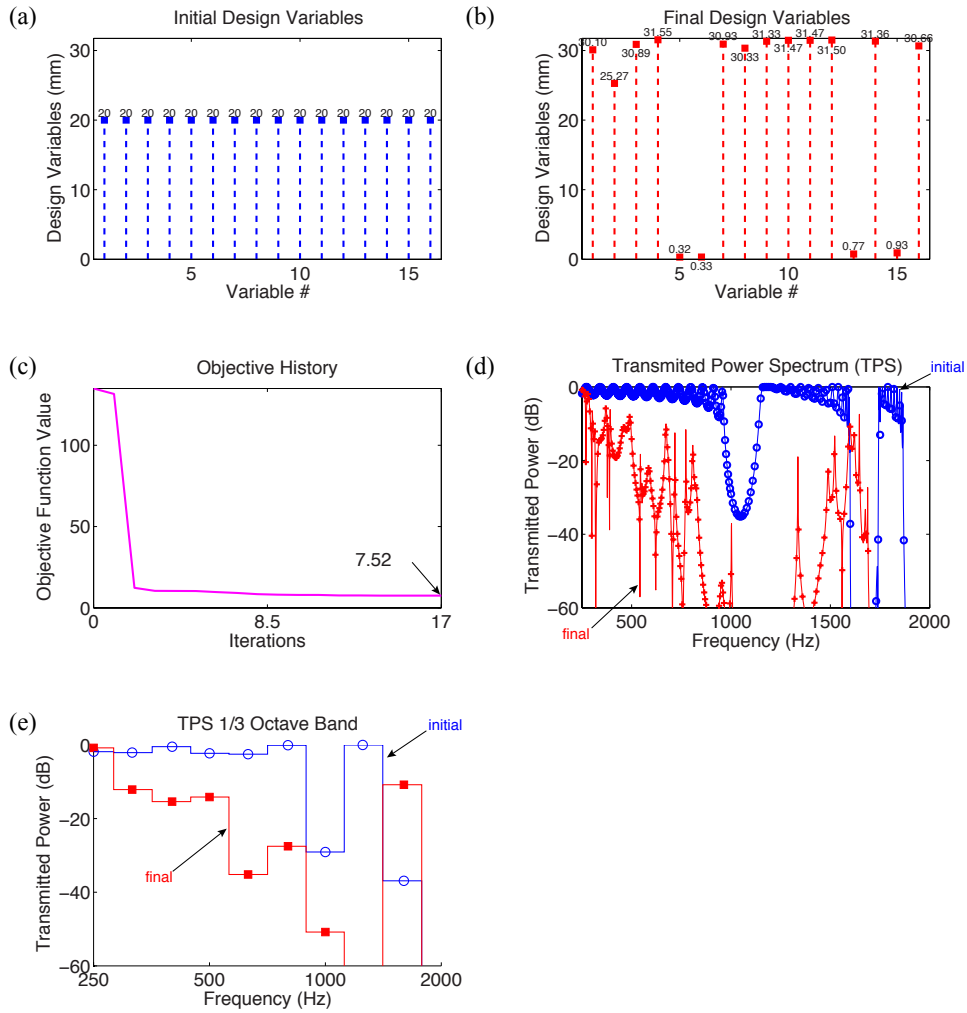

Figure 5.17 Result of design optimization for Band I+II with homogeneous initial design variable as 20 mm. (a) initial design variables, (b) converged design variables, (c) history of the objective function value, (d) transmission spectrum of the obtained design and the initial design, (e) transmission spectrum for one-third octave band.

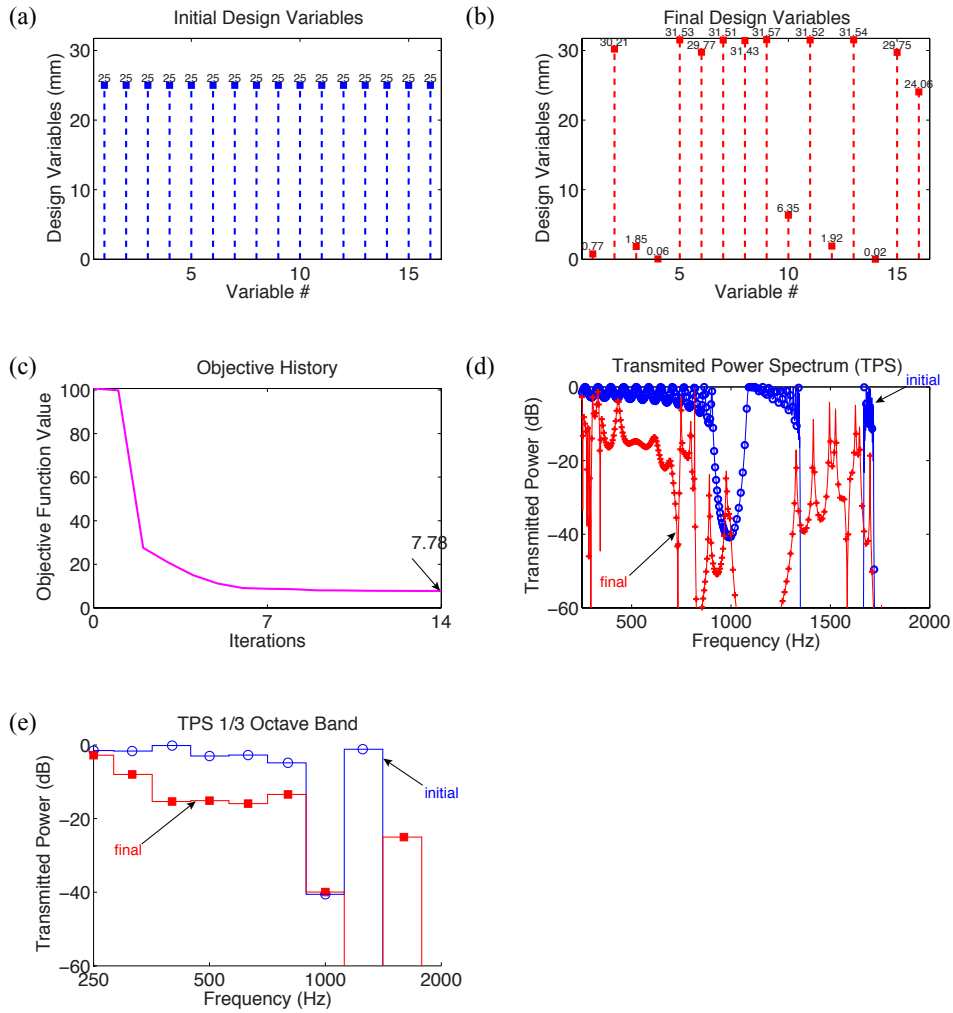

Figure 5.18 Result of design optimization for Band I+II with homogeneous initial design variable as 25 mm. (a) initial design variables, (b) converged design variables, (c) history of the objective function value, (d) transmission spectrum of the obtained design and the initial design, (e) transmission spectrum for one-third octave band.

5.4.4 Optimization Target: Band I+II+III

The most severe target band is now defined as Band I+II+III, 250–3000 Hz. As already mentioned in previous section, the Band II+III is easily handled by information-based design method. However, adding the Band I to the Band II+III maintaining the number of design variable is totally different problem and it was revealed enough by the problem for Band I+II.

Since the optimization problem is ill-conditioned, well-converged and well-minimized designing result can seldom be obtained. There are only two worth mentioning results and they are presented in Figure 5.19 and 5.20, respectively. Converged objective function values of both results are not so different but the evaluation values are quite different. Comparing their spectrums for entire frequency, one can conclude that the optimized design of Figure 5.20 is much better than Figure 5.19. For Figure 5.20, there is only one significant peak at 380 Hz, and the overall higher frequency band is blocked well comparing with Figure 5.19. Although average transmission of Figure 5.19 is lower than Figure 5.20 for the lowest band, 250–500 Hz, spectrum of Figure 5.19 has three peaks within that range and there are so many peaks after the 500 Hz comparing to Figure 5.20. Moreover, preventing performance of Figure 5.19 in range of 2400–3000 Hz is very bad considering that this frequency band was easily handled by the periodic LTPC of β=0. Therefore, it can be conclude that the structure design presented in Figure 5.20 is the most successful design even for the severest condition.

Additionally, optimization problems using relaxed frequency condition are also carried out. Target frequency for Band I+II+III is now selected as well-known 1/3 octave band frequency, which is extensively used in fieldwork. Results are presented in Figure 5.21 and 2.22 for different initial conditions. Subplots (a)–(c) in the figures are same as the previous result figures but (d) is replaced by 1/3 octave band spectrum. Comparing initial

and final spectrum, both final designs are well optimized for target frequency due to sufficient number of LTPC and few target frequency.

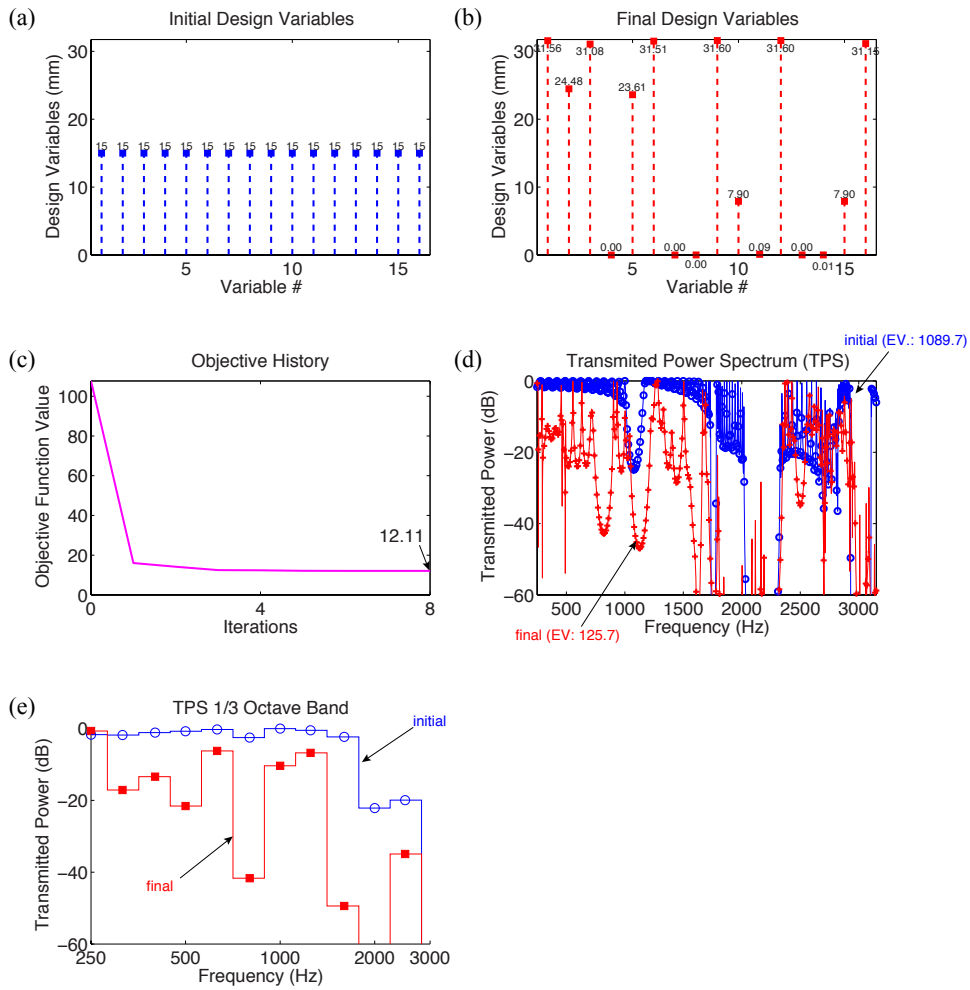

Figure 5.19 Result of design optimization for Band I+II+III with homogeneous initial design variable as 15 mm. (a) initial design variables, (b) converged design variables, (c) history of the objective function value, (d) transmission spectrum of the obtained design and the initial design, (e) transmission spectrum for one-third octave band.

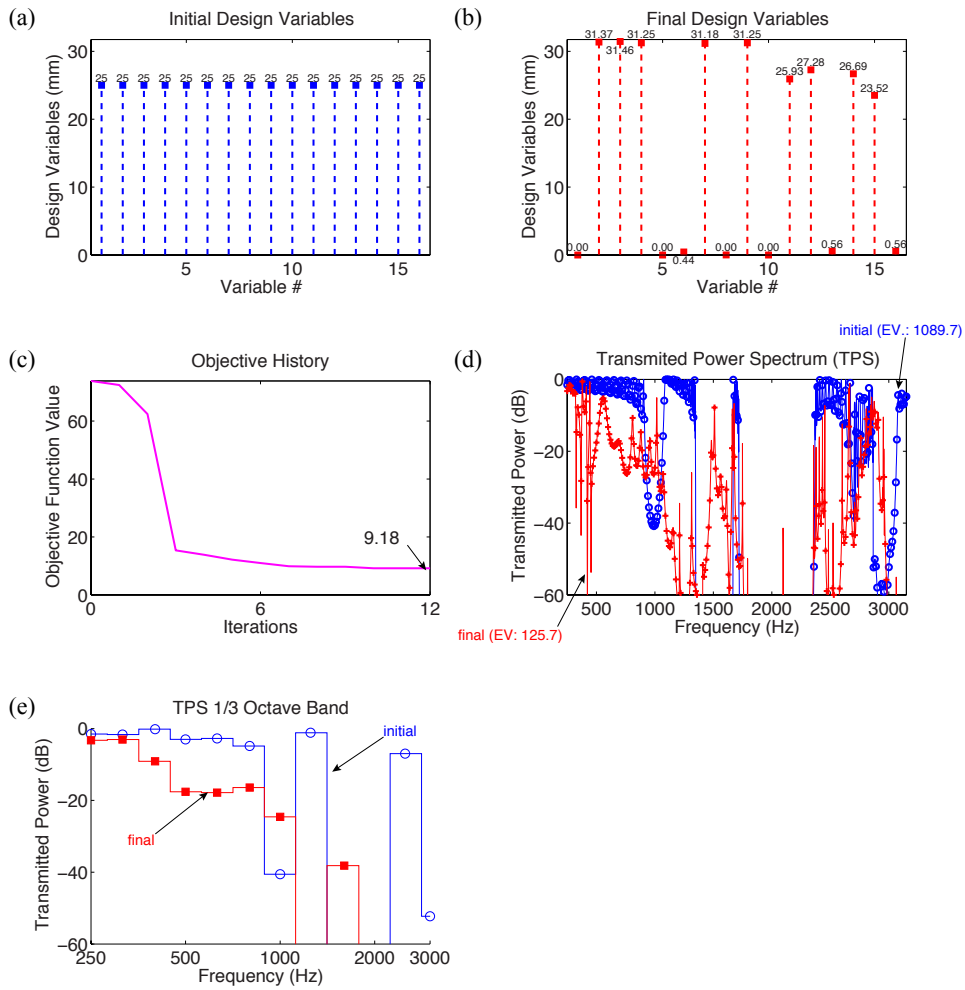

Figure 5.20 Result of design optimization for Band I+II+III with homogeneous initial design variable as 25 mm. (a) initial design variables, (b) converged design variables, (c) history of the objective function value, (d) transmission spectrum of the obtained design and the initial design, (e) transmission spectrum for one-third octave band.

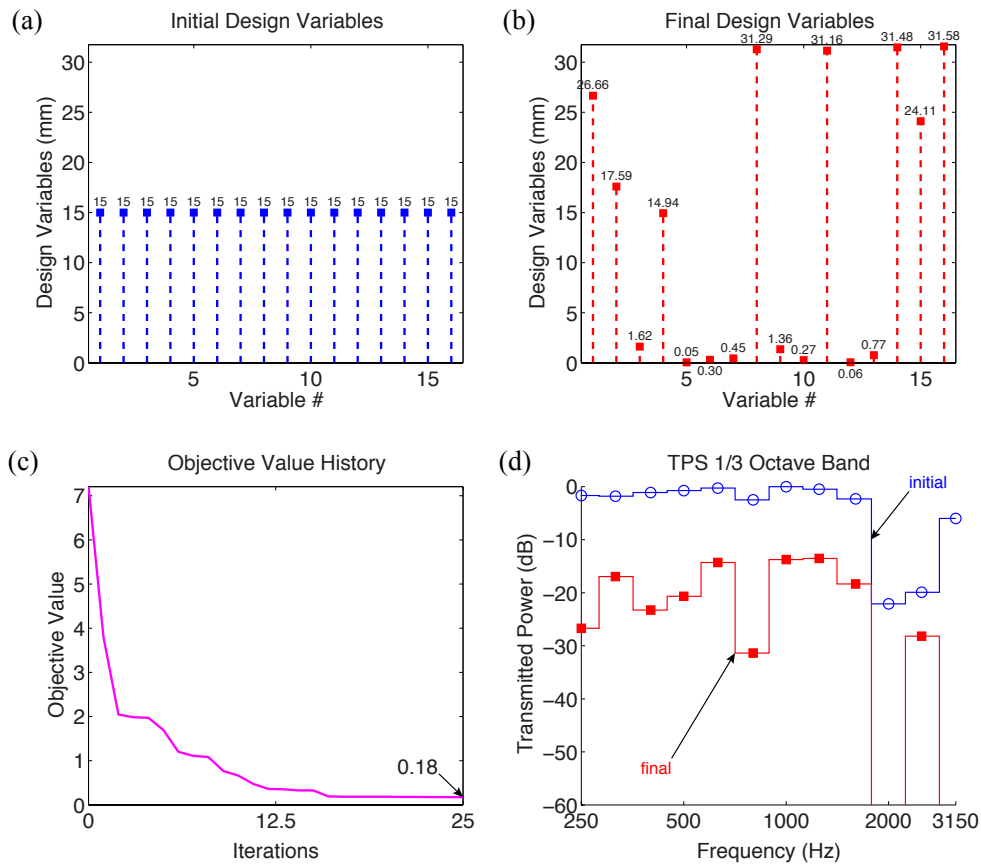

Figure 5.21 Result of design optimization for Band I+II+III with homogeneous initial design variable as 15 mm. Target frequencies are members of the one-third octave band. (a) initial design variables, (b) converged design variables, (c) history of the objective function value, (d) transmission spectrum for one-third octave band.

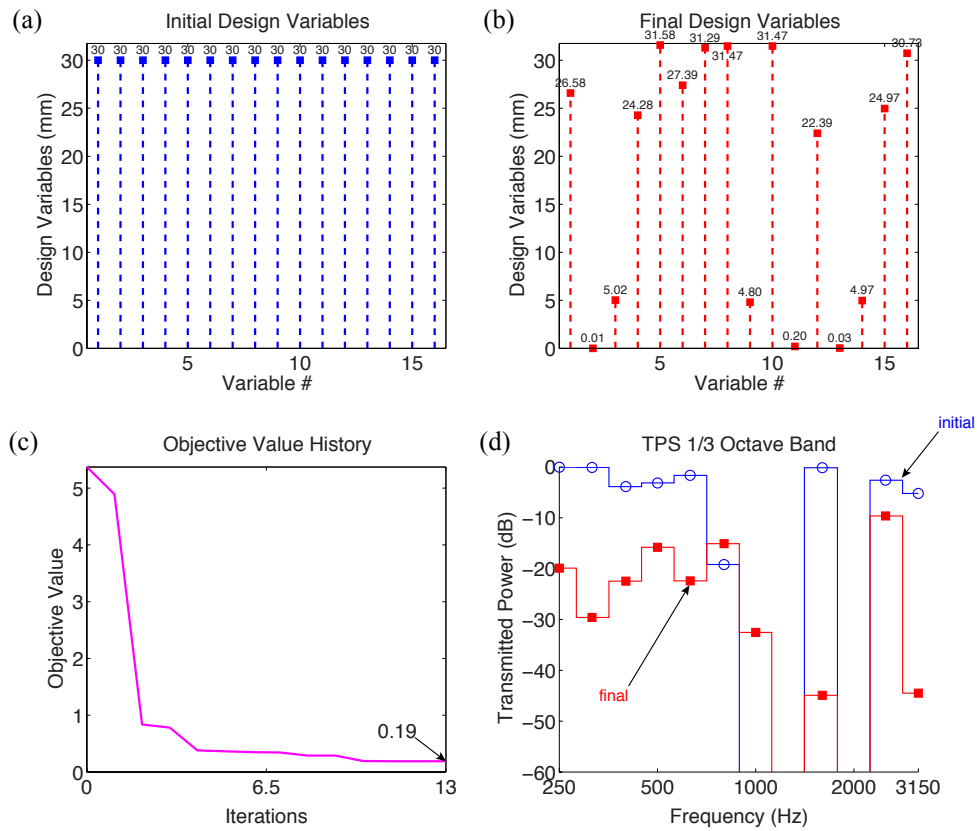

Figure 5.22 Result of design optimization for Band I+II+III with homogeneous initial design variable as 30 mm. Target frequencies are members of the one-third octave band. (a) initial design variables, (b) converged design variables, (c) history of the objective function value, (d) transmission spectrum for one-third octave band.

5.5 Summary

Unlike the Bragg gap, an individual resonance gap of the LTPC is quite narrow and it becomes narrower by decreasing resonance frequency. Even the Bragg gap, there is wide passband between the 1st and 2nd Bragg gap, which is major trouble to make stopband wide and seamless. To overcome these limitations of stopband of an individual LTPC, finitely arranged phononic crystal structures were designed by two different approaches. First approach is based on stopband information obtained in previous chapter and the second one is using numerical optimization algorithm. The information based intuitive design method, the first approach, is under an assumption that stopband of the corresponding design variable is revealed to prevent the acoustic wave, *i.e.*, the structure is an assembly of DTPCs selected for desired stopband. On the other hand, the optimization method regards the structure as a just normal acoustic structure and updates its design variables upon structural acoustic response without any considering of individual stopband.

Information-based intuitive method is very useful to design for the Bragg gap. Only three types of DTPCs could attenuate the entire tunable range of the Bragg gap, 1000-3000 Hz, at once. On the other hand, an attempt to prevent entire tunable resonance gap, 250-1000 Hz, using the same number of LTPC as the Bragg gap problem was not enough to claim successful design. Assigning only one LTPC per desired stopband is too severe condition to reveal its resonance gap. Increasing number of the LTPC per stopband is not a good solution because it makes the structure larger than a new structure that consists of new bigger lattice whose 1st Bragg gap is same as the entire tunable range of the resonance gap.

To achieve wave attenuation in range of the entire tunable resonance gap within the limited number of DTPS, iterative and gradient-based optimization was carried out. The results were obtained by various initial design variables and some designs successfully attenuated transmission of their target band. Although its attenuation intensity of the resonance gap region was not good as the Bragg gap's

attenuation, optimization method achieved attenuation of the target band that was unable to prevent sufficiently by the information-based method. From the success of the optimization, target band was expanded including the Bragg gap region. The optimization was successful even for the widest target band, which is same as the entire tunable range of the LTPC including both the Bragg gap and resonance gap.

Chapter 6.

Conclusions

In this thesis, a new tunable phononic crystal the so-called lattice-tunable phononic crystal (LTPC) was proposed and its performance was verified by numerical analyses. The design objective was to enlarge a tunable range of stopband with LTPC's as wide as possible while actual realization aspects were also considered. The stopbands of the LTPC were shown to consist of the Bragg gap and the resonance gap. A wide tunable range was achieved by the lattice size variation and also the formation of resonance cavities inside of each unit cell. Since the Bragg gap is influenced dominantly by its lattice size, the enlarging of the Bragg gap can be achieved by doubling of the lattice size. The tunable range of the resonance gap lies within the Bragg gap region so that the same tuning method can be applied to control the Bragg and resonance gaps. As a result, a seamless tunable range encompassing the Bragg gap and the resonance gap was obtained.

To investigate the acoustic characteristics of the LTPC, the finite element method (FEM) with the imposed periodic boundary condition was carried out and the dispersion diagram was found. Also, the transmission analysis was performed to complement the dispersion diagram. The transmission analysis based on a FEM model of the actual phononic crystal structure, which consists of a finite number of phononic crystal units, showed a virtually non-transmission band undetected in the dispersion diagram.

The resonance gap is another kind of a stopband independent of periodicity. We showed that the resonance gap could be located much below the Bragg gap if the cavity-like inclusion is properly designed. In fact, this finding was used to form an LTPC. In the interpretation of the resonance phenomenon in the proposed LTPC, a unit cell of the phononic crystal is viewed to have an inclusion working as a

Helmholtz resonator. In fact, it was shown that the proposed analysis model based on the Helmholtz resonator accurately predicts the center frequency of the resonance gap.

To see the transmission characteristics of the proposed LTPC, a map of transmitted power spectra was obtained. The results revealed how the tuning parameters affect the stopbands. It was shown that the whole tunable range of interest was seamlessly continuous. Furthermore, the map provides specific tuning values for a given frequency. Since the LTPC guarantees blocking any single frequency of an acoustic wave within the tunable range, it may be useful in a situation requiring dynamic tunability for varying single frequencies or frequency ranges of narrow bandwidths.

The problem to stop or minimize transmission of acoustic waves of bandwidth is extremely wider than the individual stopbands of the LTPC was considered. Two methods were proposed. The first method was to use stopbands of the LTPC. If a structure consists of several LTPCs, then each LTPC can cover different stopbands and as a whole, the structure can yield a stopband range covering the target frequency range. Sufficient repetitions of selected LTPCs were required to reveal the stopband of the phononic crystals. This condition is not favorable especially when the resonance gap is to be utilized because of it has a very narrow bandwidth. If the target band falls with a frequency range entirely covered by the tunable range by the Bragg gap, the resulting design became very successful. On the other hand, if the target band includes the entire tunable range including the resonance gap, the resulting design may not be easy to realize. This calls for the use of an optimization method.

The second method is to use a systematic optimization algorithm. The local minimum of the objective function was reached iteratively by using the gradient of the objective function. From an optimizational perspective, the structure is no longer a combination of multiple phononic crystals but a single structure having its own acoustic response under an external excitation. The optimization, therefore,

does not require acoustic information of the LTPC. Only an initial design layout was needed to proceed the optimization. As results of the optimization, many poorly-performing bands including the entire resonance gaps became bands of good attenuation.

The wide tunable sound attenuation features realized by the proposed LTPC suggest that the LTPC can be used as an acoustic filter or a sound attenuation shield for unwanted noise. The sensitive, narrow and continuous tunability of the resonance gap region may be especially favorable in filter applications. Besides, the proposed structure consisting of various LTPCs may be also applicable to attenuate stationary broadband noise. Although the attenuation intensity of the designed LTPC structure may be lower than an ideal periodic LTPC for a specific frequency band, it can attenuate a broader band sound that the uniform LTPC cannot.

References

[1] Sanchez-Perez J, Caballero D, Martinez-Sala R, Rubio C, Sánchez-Dehesa J, Meseguer F, Llinares J and Galvez F 1998 Sound attenuation by a two-dimensional array of rigid cylinders *Phys Rev Lett* **80** 5325–8

[2] Sanchez-Perez J, Rubio C, Martinez-Sala R, Sanchez-Grandia R and Gomez V 2002 Acoustic barriers based on periodic arrays of scatterers *Appl Phys Lett* **81** 5240–2

[3] Kushwaha M S, Halevi P, Dobrzynski L and Djafari-Rouhani B 1993 Acoustic Band-Structure of Periodic Elastic Composites *Phys Rev Lett* **71** 2022–5

[4] Kushwaha M S 1997 Stop-bands for periodic metallic rods: Sculptures that can filter the noise *Appl Phys Lett* **70** 3218–20

[5] Pennec Y, Vasseur J O, Djafari-Rouhani B, Dobrzyński L and Deymier P A 2010 Two-dimensional phononic crystals: Examples and applications *Surface Science Reports* **65** 229–91

[6] Laude V, Achaoui Y, Benchabane S and Khelif A 2009 Evanescent Bloch waves and the complex band structure of phononic crystals *Phys Rev B* **80** 092301

[7] Bavencoffe M, Morvan B, Izbicki J-L and Hladky-Hennion A C 2009 Characterization of evanescent ultrasonic waves in a band gap of a 1D phononic crystal *Ultrasonics Symposium (IUS), 2009 IEEE International* 1024–7

[8] Romero-García V, Sanchez-Perez J V, Castiñeira-Ibáñez S and Garcia-Raffi L M 2010 Evidences of evanescent Bloch waves in phononic crystals *Appl Phys Lett* **96** 124102-3

[9] Sigalas M M 1997 Elastic wave band gaps and defect states in two-dimensional composites *J Acoust Soc Am* **101** 1256–61

[10] Li X and Liu Z 2005 Coupling of cavity modes and guiding modes in two-dimensional phononic crystals *Solid State Commun* **133** 397–402

[11] Khelif A, Choujaa A, Djafari-Rouhani B, Wilm M, Ballandras S and Laude V 2003 Trapping and guiding of acoustic waves by defect modes in a full-band-gap ultrasonic crystal *Phys Rev B* **68** 214301

[12] Khelif A, Choujaa A, Benchabane S, Djafari-Rouhani B and Laude V 2004 Guiding and bending of acoustic waves in highly confined phononic crystal waveguides *Appl Phys Lett* **84** 4400

[13] Miyashita T 2005 Sonic crystals and sonic wave-guides *Meas. Sci.*

Technol. **16** R47–R63

[14] Hwan Oh J, Kyu Lee I, Sik Ma P and Young Kim Y 2011 Active wave-guiding of piezoelectric phononic crystals *Appl Phys Lett* **99** 083505

[15] Romero-García V, Lagarrigue C, Groby J-P, Richoux O and Tournat V 2013 Tunable acoustic waveguides in periodic arrays made of rigid square-rod scatterers: theory and experimental realization *J Phys D Appl Phys* **46** 305108

[16] Sánchez-Morcillo V J, Staliunas K, Espinosa V, Pérez-Arjona I, Redondo J and Soliveres E 2009 Propagation of sound beams behind sonic crystals *Phys Rev B* **80** 134303

[17] Martinez-Sala R, Sancho J, Sanchez J V, Gomez V, Llinares J and Meseguer F 1995 Sound attenuation by sculpture *Nature* **378** 241–1

[18] Liu Z 2000 Locally Resonant Sonic Materials *Science* **289** 1734–6

[19] Anderson C M and Giapis K P 1996 Larger Two-Dimensional Photonic Band Gaps *Phys Rev Lett* **77** 2949–52

[20] Anderson C M and Giapis K P 1997 Symmetry reduction in group 4mm photonic crystals *Phys Rev B* **56** 7313–20

[21] Caballero D, Sánchez-Dehesa J, Rubio C, Martinez-Sala R, Sanchez-Perez J V, Meseguer F and Llinares J 1999 Large two-dimensional sonic band gaps *Phys. Rev. E* **60** R6316–9

[22] Wang R, Wang X-H, Gu B-Y and Yang G-Z 2001 Effects of shapes and orientations of scatterers and lattice symmetries on the photonic band gap in two-dimensional photonic crystals *J Appl Phys* **90** 4307–13

[23] Goffaux C and Vigneron J 2001 Theoretical study of a tunable phononic band gap system *Phys Rev B* **64** 075118

[24] Cox S J and Dobson D C 1999 Maximizing band gaps in two-dimensional photonic crystals *Siam J Appl Math* **59** 2108–20

[25] Sigmund O and Jensen J 2003 Systematic design of phononic band-gap materials and structures by topology optimization *Philos T Roy Soc A* **361** 1001–19

[26] Halkjaer S, Sigmund O and Jensen J S 2006 Maximizing band gaps in plate structures *Struct Multidiscip O* **32** 263–75

[27] Bilal O R and Hussein M I 2011 Ultrawide phononic band gap for combined in-plane and out-of-plane waves *Phys. Rev. E* **84** 065701

[28] Kao C Y, Osher S and Yablonovitch E 2005 Maximizing band gaps in

two-dimensional photonic crystals by using level set methods *Appl Phys B-Lasers O* **81** 235–44

[29] Cicek A, Kaya O A and Ulug B 2012 Impacts of uniaxial elongation on the bandstructures of two-dimensional sonic crystals and associated applications *Appl Acoust* **73** 28–36

[30] Park W and Lee J-B 2004 Mechanically tunable photonic crystal structure *Appl Phys Lett* **85** 4845

[31] Kim S and Gopalan V 2001 Strain-tunable photonic band gap crystals *Appl Phys Lett* **78** 3015

[32] Fang N, Xi D, Xu J, Ambati M, Srituravanich W, Sun C and Zhang X 2006 Ultrasonic metamaterials with negative modulus *Nat Mater* **5** 452–6

[33] Wang Z G, Lee S H, Kim C K, Park C M, Nahm K and Nikitov S A 2008 Acoustic wave propagation in one-dimensional phononic crystals containing Helmholtz resonators *J Appl Phys* **103** 064907

[34] Cheng Y, Xu J Y and Liu X J 2008 Broad forbidden bands in parallel-coupled locally resonant ultrasonic metamaterials *Appl Phys Lett* **92** 051913

[35] Hu X, Chan C T and Zi J 2005 Two-dimensional sonic crystals with Helmholtz resonators *Phys. Rev. E* **71** 055601

[36] Chalmers L, Elford D P, Kusmartsev F V and Swallowe G M 2009 Acoustic band gap formation in two-dimensional locally resonant sonic crystals comprised of helmholtz resonators *International Journal of Modern Physics B* **23** 4234–43

[37] Cui Z Y, Chen T-N, Chen H L and Su Y P 2009 Experimental and calculated research on a large band gap constituting of tubes with periodic narrow slits *Appl Acoust* **70** 1087–93

[38] Romero-García V, Sanchez-Perez J V and Garcia-Raffi L M 2011 Tunable wideband bandstop acoustic filter based on two-dimensional multiphysical phenomena periodic systems *J Appl Phys* **110** 014904

[39] Li J-B 2013 Tuning of Acoustic Bandgaps in Phononic Crystals With Helmholtz Resonators *J Vib Acoust* **135** 031015

[40] Hou Z, Liu J, Kuang W, Liu Y and Wu S 2007 Sonic crystal with open resonant cavities *Phys. Rev. E* **75** 026608

[41] Kinsler L E, Frey A R, Coppens A B and Sanders J V 2000 *Fundamentals of acoustics* (Wiley)

[42] Cook R D, Malkus D S, Plesha M E and Witt R J 2002 *Concepts and*

Applications of Finite Element Analysis (Wiley India Pvt. Limited)

[43] Givoli D and Neta B 2003 High-order non-reflecting boundary scheme for time-dependent waves *J Comput Phys* **186** 24–46

[44] Brillouin L 1953 *Wave Propagation in Periodic Structures* (Dover Pulbications)

[45] Wu L-Y and Chen L-W 2010 Wave propagation in a 2D sonic crystal with a Helmholtz resonant defect *J Phys D Appl Phys* **43** 055401

[46] Elford D P, Chalmers L, Kusmartsev F V and Swallowe G M 2011 Matryoshka locally resonant sonic crystal *J Acoust Soc Am* **130** 2746

[47] Wang P, Chen T-N, Yu K-P and Wang X-P 2012 Tunable and large gaps in a two-layer semi-ring structure *Phys. Scr.* **85** 065402

[48] Lagarrigue C, Groby J-P and Tournat V 2013 Sustainable sonic crystal made of resonating bamboo rods *J Acoust Soc Am* **133** 247

[49] Romero-García V, Krynkin A, Garcia-Raffi L M, Umnova O and Sanchez-Perez J V 2013 Journal of Sound and Vibration *J Sound Vib* **332** 184–98

[50] Bertoldi K and Boyce M 2008 Mechanically triggered transformations of phononic band gaps in periodic elastomeric structures *Phys Rev B* **77** 052105

[51] Lin S-C S and Huang T J 2011 Tunable phononic crystals with anisotropic inclusions *Phys Rev B* **83** 174303

[52] Movchan A and Guenneau S 2004 Split-ring resonators and localized modes *Phys Rev B* **70** 125116

[53] Kelley C T 1999 *Iterative methods for optimization* vol 18 (Society for Industrial and Applied Mathematics)

[54] Christensen P W and Klarbring A 2008 *An Introduction to Structural Optimization* (Springer)

[55] Nocedal J and Wright S J 2006 *Numerical Optimization* (New York: Springer)

국문초록

광대역 주파수 차단을 제어하기 위한 격자 조율형 포노닉 크리스탈의 설계와 해석

유 성 민
서울대학교 공과대학원
기계항공공학부

서로 다른 음파 차단 현상인 브래그갭(Bragg gap)과 공진갭(resonance gap)을 이용하여 넓은 주파수 대역의 음향 차단대역(stopband)을 만들어 낼 수 있는 새로운 조율형 포노닉 크리스탈을 제안하였다. 차단대역의 주파수 위치는 포노닉 크리스탈의 격자 크기에 반비례하기 때문에, 격자 크기를 2배로 증가시켜 저주파에 대한 조율성능이 향상될 수 있도록 격자조율형 포노닉 크리스탈을 설계하였다. 브래그갭 이하의 주파수에 대해서도 차단대역을 얻기 위해 음향공진 포노닉 크리스탈(acoustically-resonant phononic crystal)을 도입하였다. 헬름홀츠 공진기와 유사한 음향공진 포노닉 크리스탈은 격자크기에 관계 없이 공진에 영향을 미치는 기하학적인 요인에 의해 공진갭을 형성할 수 있다. 제안한 포노닉 크리스탈의 다양한 음향학적 성능을 조사하기 위해 무한반복구조물과 유한반복구조물에 대하여 유한요소해석을 수행 하였다. 음파통과해석은 소산도표(dispersion diagram)에서는 관찰이 불가능 했던 숨겨진 차단주파수를 찾는데 큰 역할을 한다.

차단대역을 조율함으로써 넓은 주파수 대역의 음파를 차단할 수 있지만, 개별 차단대역는 그 폭이 작으며 그 자체가 커지는데에는 물리적 한계가 분명히 존재하다. 또한 일반적으로 차단대역 사이에는 반드시 음파를 온전히 전달하는 통과대역(passband)이 존재하며 이는 넓은 주파수 대역을 한번에 차단하고자 하는데 큰 방해요소이다. 단일 포노닉 크리스탈에서 오는 이러한

한계를 극복하기, 여러 종류의 포노닉 크리스탈을 조합하여 하나의 음향 구조물을 설계하였다. 수치해석을 통해서 얻어진 격자조율형 포노닉 크리스탈의 음향정보를 바탕으로한 설계법과 격자조율형 포노닉 크리스탈을 사용하되 조율값을 최적설계기법을 활용하여 체계적으로 개선해가는 설계법 모두를 수행하였다. 두 방법의 결과로 단일 포노닉 크리스탈로는 차단이 불가능한 넓은 주파수 대역의 음향파를 성공적으로 차단, 감쇄 시킬 수 있었다. 또한 여러 수치 기반 시뮬레이션으로 모든 연구 결과를 확인하였다.